YEAST ATAXIN-2 (PBP1) CONDENSATES REGULATE TORC1 ACTIVITY AND AUTOPHAGY IN RESPONSE TO CELLULAR REDOX STATE

APPROVED BY SUPERVISORY COMMITTEE

Benjamin P. Tu, Ph.D.

Kathryn O'Donnell, Ph.D.

Ralph Deberardinis, Ph.D.

Ryan Potts, Ph.D.

I would like to thank my mentor, members of graduate committee, collaborators, colleagues, and everyone who had contributed to this project.

YEAST ATAXIN-2 (PBP1) CONDENSATES REGULATE TORC1 ACTIVITY AND AUTOPHAGY IN RESPONSE TO CELLULAR REDOX STATE

by

YU-SAN YANG

DISSERTATION / THESIS

Presented to the Faculty of the Graduate School of Biomedical Sciences

The University of Texas Southwestern Medical Center at Dallas

In Partial Fulfillment of the Requirements

For the Degree of

DOCTOR OF PHILOSOPHY

The University of Texas Southwestern Medical Center at Dallas

Dallas, Texas

December, 2018

YEAST ATAXIN-2 (PBP1) CONDENSATES REGULATE TORC1 ACTIVITY AND AUTOPHAGY IN RESPONSE TO CELLULAR REDOX STATE

Publication No. _____

Yu-San Yang, Ph.D.

The University of Texas Southwestern Medical Center at Dallas, 2018

Supervising Professor: Benjamin P. Tu, Ph.D.

Yeast ataxin-2, also known as Pbp1 (Poly(A) binding protein-binding protein 1), is an intrinsically disordered protein that has earlier been implicated in stress granule formation, RNA biology, and neurodegenerative disease. However, the normal endogenous function of Pbp1 and ataxin-2 remains poorly understood. In this dissertation, I identified Pbp1 as a dedicated regulator of TORC1 signaling and autophagy under conditions that require

mitochondrial respiration. Unlike the autophagy-deficient atg mutants that harbor severe growth defects, *pbp1* null mutants exhibited significantly increased cell growth despite lack of autophagy. I discovered that Pbp1 binds to TORC1 specifically during respiratory growth, but utilizes an additional methionine-rich, low complexity (LC) region to inhibit TORC1.

This LC region of Pbp1 forms reversible cross-β fibrils that facilitate phase transition of the protein into either liquid-like or gel-like states *in vitro* and enables self-association of full-length Pbp1 into pelletable assemblies *in vivo*. Sequence analysis revealed that Pbp1 LC region contains an unusually high frequency of methionine residues (24 methionines in 150 a.a.) compared to the rest of the yeast proteome. I showed that the phase separation of Pbp1 is mediated by these methionine residues, which are sensitive to H_2O_2-mediated oxidation and mitochondrial toxins in living cells.

I also observed that the phase separation of Pbp1 mediated by its C-terminal LC region is responsive to the activity state of mitochondria and required for TORC1 inhibition. Mutants that weaken phase separation *in vitro* exhibit reduced capacity to inhibit TORC1 and induce autophagy *in vivo*. Loss of Pbp1 leads to mitochondrial dysfunction and reduced fitness during nutritional stress. Thus, Pbp1 forms a condensate in response to respiratory status to regulate TORC1 signaling. These observations offer a mechanistic explanation describing how reversible formation of condensates formed from the LC region of Pbp1 has evolved as a sensor of cellular redox state.

TABLE OF CONTENTS

PRIOR PUBLICATIONS

- Lai, T. Y., C. J. Yen, H. W. Tsai, **Y. S. Yang**, and C. W. Chiang. The B56γ3 Regulatory Subunit Containing Protein Phosphatase 2A Outcompetes Akt to Regulate p27KIP1 Subcellular Localization by Selectively Dephosphorylating Phospho-Thr157 of p27KIP1. *Oncotarget* (2015) PMID: 26684356
- Yang, C. P., C. W. Chiang, C. H. Chen, Y. C. Lee, M. H. Wu, Y. H. Tsou, **Y. S. Yang**, C. W. Chang, D. Y. Lin. Identification and Characterization of Nuclear and Nucleolar Localization Signals in 58-kDa Microspherule Protein (MSP58). *J Biomed Sci.* 22(33): 60-72. (2015) PMID: 25981436
- Lee, T. Y., T. Y. Lai, S. C. Lin, C. W. Wu, I. F. Ni, **Y. S. Yang**, L. Y. Hung, B. Law, C.W. Chiang. The B56γ3 Regulatory Subunit of Protein Phosphatase 2A(PP2A) Regulates S phase-Specific Nuclear Accumulation of PP2A and G1 to S Transition. *J Biol. Chem.* 285(28):21567-21580. (2010) PMID: 20448040
- Kuo, Y. C., K. Y. Huang, C. H. Yang, **Y. S. Yang**, W. Y. Lee, and C. W. Chiang. Regulation of Phosphorylation of Thr308 of Akt, Cell Proliferation and Survival by the B55α Regulatory Subunit Targeting of the Protein Phosphatase 2A Holoenzyme to Akt. *J Biol. Chem.* 283(4): 1882-1892. (2008) PMID: 18042541

LIST OF FIGURES

LIST OF TABLES

LIST OF ABBREVIATIONS

Pbp1 – Pab1-binding protein 1

Pab1 – Poly (A)-binding protein 1

ATG – Autophagy-related

TORC1 – Target Of Rapamycin Complex 1

WT – Wild-type

YPL – Yeast extract and peptone and lactate

SD – Synthetic medium and glucose

SD-N – Synthetic medium and glucose without nitrogen sources

SL – Synthetic medium and lactate

ALP – Alkaline phosphatase

GFP – Green fluorescent protein

OM45 – Mitochondrial outer-membrane protein 45

IDH1 – Isocitrate dehydrogenase 1

ALS – Amyotrophic lateral sclerosis

CHAPTER ONE :

INTRODUCTION

AUTOPHAGY AND TORC1 SIGNALING

Autophagy

Macroautophagy and selective autophagy

Autophagy is an evolutionarily conserved cellular process that primarily degrades cytoplasmic contents and damaged organelles to maintain cell viability in response to cellular stresses, such as nutrient starvation, oxidative stress, infection, and inflammatory stimuli (Cuervo, 2004; Klionsky, 2007; Levine and Klionsky, 2004; Shintani and Klionsky, 2004). The term "autophagy" refers to a range of processes, including macroautophagy, microautophagy, and chaperone-mediated autophagy which exists only in mammalian cells (Mizushima et al., 2008).

Macroautophagy is the major and best characterized subtype of autophagy which primarily happens during nutrient and energy deprivation. During macroautophagy, a double-membrane compartment, termed autophagosome, forms *de novo* in the cytoplasm, which engulfs portions of cytoplasm non-selectively. The autophagosome then fuses with the lysosome (mammalian cells) or vacuole (yeast) to degrade the sequestered materials (Xie and Klionsky, 2007).

In contrast to macroautophagy, which tends to be non-selective, cells can degrade organelles or proteins selectively. Selective autophagy specifically targets a wide range of cargos including mitochondria (mitophagy), peroxisomes (pexophagy), ribosomes (ribophagy), endoplasmic reticulum (ERphagy), protein aggregates (aggrephagy), and lipid droplets (lipophagy). Each type of selective autophagy requires specific receptors, regulators, and triggers, in addition to core machinery (Johansen and Lamark, 2011; Stolz et al., 2014). The ability to selectively degrade specific cellular targets renders autophagy a role in the pathogenesis of various human diseases, such as cancers, cardiac, and neurodegenerative diseases (Levine and Kroemer, 2008).

The correlation between autophagy and various neurodegenerative diseases, such as Parkinson's disease (mutant α-synuclein), Huntington's disease (mutant huntingtin), and amyotrophic lateral sclerosis (mutant TDP-43), was established based on the observation of accumulated autophagosome vesicles in affected brains (Rubinsztein et al., 2007; Williams et al., 2006). Autophagy is thought to be an effective mechanism for degrading aggregation-prone proteins linked to these diseases. Once autophagy is inhibited, the clearance of these substrates is impeded. On the other hand, activation of autophagy may lead to enhanced clearance of those toxic proteins (Metcalf et al., 2012; Vilchez et al., 2014).

Non-nitrogen-induced autophagy

One of the fundamental questions regarding the regulatory mechanism of autophagy is how cells make decisions in response to cellular physiology and metabolism. In both yeast and

mammalian cells, deprivation of essential nutrients strongly induces autophagy to recycle cellular constituents for survival (Levine and Klionsky, 2004). Therefore, nutrient starvation is a commonly-used model for the study of the metabolic regulation of autophagy. In *Saccharomyces cerevisiae*, it is known that autophagy is induced when the cells are switched from rich to nitrogen-starvation medium in the presence of glucose (Takeshige et al., 1992). Under this condition, TORC1 activity is repressed, leading to the dephosphorylation of Atg13, and in turn promotes autophagosome formation through interacting with Atg1 and the Atg17-Atg29-Atg31 complex (Nakatogawa et al., 2009; Xie and Klionsky, 2007).

Accordingly, nitrogen starvation (SD to SD-N) is the most commonly-used condition in yeast to study many aspects of autophagy. However, in the presence of glucose, yeast cells turn off many stress response pathways, a phenomenon termed "glucose repression" (Carlson, 1999; Gancedo, 1998). To study autophagy regulation under a more physiologically relevant condition, our laboratory has adopted a condition where cells are switched from rich to amino acid starvation medium in the presence of non-fermentable carbon source, lactate. We have reported that yeast cells turn on autophagy under this condition even though they have nitrogen (Wu and Tu, 2011). The discovery of this non-nitrogen starvation induced autophagy (NNS-induced autophagy) has allowed us to identify additional autophagy regulators that become essential outside of highly glycolytic growth conditions.

Regulators of autophagy

The autophagy process along with major regulators were identified in yeast by Dr. Yoshinori Ohsumi who was awarded the Nobel Prize in 2016, and Dr. Daniel Klionsky (Harding et al., 1995; Takeshige et al., 1992; Tsukada and Ohsumi, 1993). The autophagy regulatory genes isolated were unified under the name AuTophaGy-related (*ATG*) genes (Klionsky et al., 2003). Most of the *ATG* genes encode proteins involved in autophagic membrane biogenesis in yeast (Mizushima and Klionsky, 2007). So far, 37 ATG genes that are required for macroautophagy and/or selective autophagy were identified and characterized (Meijer et al., 2007; Thumm et al., 1994; Tsukada and Ohsumi, 1993).

Since the identification of the NNS-induced autophagy, which happens under the respiratory growth condition in the presence of nitrogen and non-fermentable carbon source, our laboratory has been trying to elucidate the regulatory mechanisms of autophagy beyond the core autophagy machinery (i.e. the *ATG* genes). By using a visual screen, we have identified four genes that are specifically required for autophagy induction under the respiratory growth condition. The four genes are *NPR2*, *NPR3*, *IML1*, and *PBP1* (Wu and Tu, 2011)(unpublished data).

Npr2, Npr3, and Iml1 form a protein complex. Interestingly, unlike the autophagy-deficient *atg* mutants that have severe growth defects, *npr2*, *npr3*, or *iml1* null mutant cells exhibited significantly increased cell growth despite lack of autophagy (Wu and Tu, 2011). Subsequent studies demonstrated that this complex, termed SEACIT (Seh1-associated subcomplex inhibiting TORC1), is the ortholog of mammalian GATOR1 which functions as a negative regulator of TORC1 (Bar-Peled et al., 2013; Panchaud et al., 2013). Under nutrient-

limiting conditions, SEACIT senses the signal of amino acid insufficiency and suppresses TORC1 activity to induce autophagy.

TOR (Target of Rapamycin) Complex 1

Overview

TORC1 is a kinase complex that regulates many cellular processes such as protein translation and cellular metabolism in response to nutrient availability (Sengupta et al., 2010). In yeast, TORC1 consists of four components including Kog1 (the ortholog of mammalian Raptor), Lst8, Tco89, and either TOR1 or TOR2 (Loewith et al., 2002; Reinke et al., 2004; Wedaman et al., 2003). Studies have shown that in log-phase growing cells, TORC1 is present in cells in the dimeric form, whereas the majority of protein enters foci-like structures in stationary phase (Prouteau et al., 2017). STORM (stochastic optical reconstruction microscopy) images revealed that these foci are organized into a large cylindrical structure, which was termed "TOROID" (TORC1 organized in inhibited domains)(Prouteau et al., 2017). The assembly of TOROIDs inhibits TORC1 activity which can be reversed by replenishing of glucose.

Inhibition of TORC1 leads to the induction of autophagy (Levine and Klionsky, 2004). Dysregulation of TORC1 signaling, like autophagy deficiency, has been associated with cancer and neurodegenerative diseases (Boland et al., 2008; Nixon, 2013; Ravikumar et al., 2004). Precisely how cells sense their metabolic state to alternately regulate anabolic versus catabolic processes mediated by TORC1 has yet to be fully elucidated. Moreover, whether there might

exist additional regulators of TORC1 signaling and autophagy that function under more specialized conditions also remains unknown.

Regulation of TORC1 signaling

Since TORC1 coordinates cell growth and survival in response to metabolic cues, it requires strict regulation particularly under metabolically challenging conditions.

The upstream regulator that senses amino acid availability and passes the signal to TORC1 is the Rag GTPase complex (Binda et al., 2009). The yeast Rag GTPase complex is a heterodimer composed of Gtr1 (the ortholog of mammalian RagA and RagB) and Gtr2 (the ortholog of mammalian RagC and RagD) (Hirose et al., 1998; Nakashima et al., 1999; Schurmann et al., 1995; Sekiguchi et al., 2001). The nucleotide-binding state of Gtr1-Gtr2 is crucial for the regulation of TORC1. Under amino acid-replete condition, the $Gtr1^{GTP}$ - $Gtr2^{GDP}$ heterodimer, which has a higher binding affinity to TORC1, stimulates TORC1 activity; whereas under nutrient starvation, the $Gtr1^{GDP}$ - $Gtr2^{GTP}$ heterodimer is less capable of interacting with TORC1, leads to decreased TORC1 activity. Thus, switching of the nucleotide-binding state of the Gtr1-Gtr2 complex, and the resulting effects on TORC1 activity, are key events in cellular adaptation to amino acid fluctuations (Binda et al., 2009).

Besides amino acid availability, TORC1 also responses to many other extracellular conditions in yeast (Loewith and Hall, 2011). However, the mechanisms by which TORC1 is responsive to other conditions are not fully understood.

The metabolic function of TORC1

By dissecting the metabolic phenotypes of the cells lacking negative regulator of TORC1 (i.e. *npr2*, *npr3*, or *iml1*), our laboratory has proposed a fundamental role for TORC1 in the regulation of metabolism – switching the mitochondria from an energy production mode, to a biosynthetic mode (Chen et al., 2017; Laxman et al., 2014). Mitochondria is critical for making important metabolites, such as glutamate, glutamine, and aspartate, for making proteins. Aspartate and glutamine are also required for cells to make nucleotides. TORC1 activates mitochondria and promotes them to enter this biosynthetic mode. The negative regulators of TORC1, such as SEACIT, function to regulate key cataplerotic reactions of the mitochondrial TCA cycle in tune with the amino acid and nitrogen status of cells (Chen et al., 2017).

Pbp1 (Poly(A)-binding protein 1-binding protein 1)

Features of Pbp1

Pbp1 is one of the genes identified from the same screen for autophagy regulator in which we found *NPR2-NPR3-IML1*. Sequence analysis showed that Pbp1 is serine-rich with 83 serine residues in 722 amino acids (11.5%). In addition, Pbp1 possesses a proline and methionine-rich C-terminus. The most conserved features of Pbp1 are the two putative RNA-binding domains, Lsm and LsmAD, located close to its N-terminus. Besides these two domains, the rest of the protein has no predicted secondary structures.

In 2010, a large study of ~1000 ALS patients revealed ataxin-2, the mammalian ortholog of Pbp1, and its poly-glutamine (polyQ) repeat expansion, as one of the most prominent genetic links to ALS defined to date (Elden et al., 2010). However, the true biological functions of Pbp1/Ataxin-2 that contribute to increased risk of ALS remains poorly understood.

Pbp1 in the regulation of translation

Pbp1 was first identified as an interacting protein of Pab1 through an yeast-two-hybrid study. Deletion of *PBP1* suppresses the lethality caused by *PAB1* deletion (Mangus et al., 1998). Together with Pab1, Pbp1 functions in maintaining proper length of mRNA poly(A) tails. *PBP1* null mutant cells initially produced full-length poly(A) tails, but then they are subsequently trimmed at a faster rate, resulting in a poly(A) tail which is 15-30 nucleotide shorter than WT. Further investigation revealed that Pbp1 maintains the length of mRNA poly(A) tail through negatively regulating exonuclease (Pan2/Pan3) activity (Mangus et al., 2004b).

Besides its function in regulating the length of mRNA poly(A) tails, Pbp1 was also found to be with both the translating and non-translating pools of (Mangus et al., 1998; Mangus et al., 2004a). Pbp1 also interacts with the Pbp4 and Lsm12, all of which associate with the translation machinery (Swisher and Parker, 2010). Therefore, it is believed that Pbp1 has a function in translation regulation.

Pbp1 and stress granules

Studies in both yeast and mammalian cells implicate a role for Pbp1 and ataxin-2 in the assembly of stress granules. Deletion of Pbp1 in yeast or siRNA knockdown of ataxin-2 in mammalian cells significantly reduced stress granule formation under glucose deprivation or following arsenite treatment, respectively (Buchan et al., 2008; Nonhoff et al., 2007). Pbp1 is also reported to be involved in the P-body-dependent formation of stress granules (Buchan et al., 2008).

Another study reported that overexpression of Pbp1 inhibits TORC1 by sequestering TORC1 into stress granules at a supraphysiological temperature (46℃) (Takahara and Maeda, 2012). A follow up study claimed that the phosphorylation and activation of Pbp1 by PAS kinase (Psk1) in response to energy or nutrient deprivation enables Pbp1 to form stress granules under glucose deprivation or heat shock conditions. PAS kinase-deficient cells showed reduced amount of Pbp1 localized to cytosolic foci (DeMille et al., 2015).

Pbp1/ataxin-2 and pathogenesis of ALS

Since the report which implicated Pbp1/ataxin-2 as a risk factor for ALS, studies have focused on connecting known functions of these proteins, including RNA processing, translational regulation, and stress granule formation, to the pathogenesis of ALS. Thus far, none of the deficiencies in these previously reported functions of ataxin-2 can promisingly account for the development of ALS. Therefore, the true biological functions of Pbp1/ataxin-2 that may contribute to disease progression and how these functions may relate to other cellular pathways implicated in ALS remain to be identified.

Significance

Mutant forms of ataxin-2 have been strongly associated with certain neurodegenerative diseases. The polyQ tract and two putative RNA binding domains in Ataxin-2 have been the major focus of studies on this protein. Both gain- and loss-of-function mechanisms have been proposed to explain how these features link ataxin-2 to ALS pathogenesis; for the loss-of-function perspective, severe aggregation of ataxin-2 might interfere with the RNA metabolism and cellular stress response, whereas for the gain-of-function perspective, aggregated ataxin-2 might sequester interacting proteins, or enhance the aggregation of other proteins. However, up to now none of the aforementioned hypotheses were confirmed to be the definitive disease-driving mechanism, and the true biological functions of ataxin-2 that contribute to ALS pathogenesis remain to be determined.

Recent evidence demonstrates autophagy as the most prominent pathway to clear protein aggregates and protect motor neurons, and pharmacological activation of autophagy has neuroprotective effects in certain neurodegeneration diseases including Huntington's disease, Parkinson's disease, and Alzheimer's disease (Sarkar et al., 2008). However, in various ALS experimental models, different strategies to induce autophagy showed paradoxical outcomes in terms of their effects on motor neuron protection or protein aggregates clearance. Induction of autophagy by genetic manipulation or ER-stress has been shown to delay the ALS progression, but induction of autophagy by rapamycin accelerates motor neuron degeneration (Hetz et al., 2009; Zhang et al., 2011). These seemingly contradictory results

suggest that it is crucial to understand the mechanism through which autophagy is regulated under specific conditions in order to optimize therapies targeting autophagy. My work on the yeast ortholog will guide subsequent studies of ataxin-2 and provide new insights into how loss- or gain-of-function of this protein could cause neurodegenerative diseases.

CHAPTER TWO :

AN UNFORESEEN ROLE OF PBP1 IN TORC1 REGULATION

PBP1 IS REQUIRED FOR AUTOPHAGY THROUGH INHIBITING TORC1 SIGNALING

Introduction

A previous study in our laboratory has shown that when prototrophic yeast cells are switched from a rich (YP) to a minimal (S) medium using a non-fermentable carbon source (lactate), they induce autophagy despite the presence of nitrogen (Wu and Tu, 2011). This autophagy-inducing regimen that forces cells to heavily utilize mitochondria enabled us to identify additional autophagy regulators that become essential outside of highly glycolytic growth conditions. Using a visual screen, our laboratory has identified genes encoding a complex of three proteins (Iml1-Npr2-Npr3) specifically required for the induction of autophagy following the switch from YPL to SL medium, but not for autophagy triggered by the complete nitrogen starvation in high glucose (SD-N medium) (Wu and Tu, 2011). This complex has emerged as the more evolutionary conserved negative regulator of TORC1 that functions in response to amino acid insufficiency (Bar-Peled et al., 2013; Panchaud et al., 2013).

Since our first report of this screen, we have sequenced additional transposon mutants that compromise autophagy following the switch from YPL to SL medium. In this chapter, I show that Pbp1, the yeast ortholog of mammalian ataxin-2, is also a previously unrecognized regulator of autophagy. Pbp1 and ataxin-2 are intrinsically disordered proteins that had earlier been implicated in stress granule assembly and RNA biology (Buchan et al., 2008; Nonhoff et al., 2007; Ralser et al., 2005). Triplet repeat expansions in ataxin-2 are strongly linked to neurodegenerative diseases such as spinocerebellar ataxia and amyotrophic lateral sclerosis (Alves-Cruzeiro et al., 2016; Elden et al., 2010). However, the normal endogenous function of Pbp1/ataxin-2 and the resulting impact of expanded glutamine tracts are not well understood. In this chapter, I will address the mechanisms by which Pbp1 regulates autophagy.

Results

Pbp1 regulates autophagy and cell growth under conditions that require mitochondrial respiration

To interrogate a possible role for Pbp1 in the regulation of autophagy, we assayed autophagy in wild-type (WT) and *pbp1*Δ cells under a growth condition that requires mitochondrial respiration (Figure 2-1). In the presence of the non-fermentable carbon source lactate, cells lacking Pbp1 were unable to induce autophagy following the switch from rich (YPL) to minimal (SL) medium as determined by three different assays: appearance of Mito-DsRed reporter in vacuoles (Figure 2-1A), the GFP-cleavage assay that is indicative of mitophagy (Figure 2-1B), and the alkaline phosphatase (ALP) reporter assay as a quantitative

measure of general autophagy (Figure 2-1C). In contrast, *pbp1*Δ mutants showed no deficit in autophagy induction upon switch to the more commonly utilized high glucose, nitrogen starvation condition (SD-N medium) (Figure 2-2). These data suggest that the function of Pbp1 is selectively required when cell growth is restricted by non-fermentable carbon sources that require an increased dependency on mitochondria for energy.

Suppression of autophagy by deletion of core autophagy machinery components severely impedes cell growth following the switch to SL medium (Wu and Tu, 2011). Surprisingly, *pbp1*Δ cells exhibited a significantly increased growth rate in SL medium despite the lack of autophagy (Figure 2-3A), indicative of dysregulation of cellular growth control pathways. This increased growth phenotype of *pbp1*Δ was not observed when glucose was present as the carbon source (Figure 2-3B). Taken together, the lack of autophagy and abnormal growth phenotypes of *pbp1*Δ mutant cells in SL medium indicate the protein is involved in the regulation of cell growth under conditions that require mitochondrial respiration.

Multiple directions were explored to identify the signaling involved in Pbp1's autophagy regulation function

To elucidate the mechanisms by which Pbp1 regulates autophagy and cell growth, I looked into some possible phenotypes of *pbp1*Δ mutant cells.

pbp1Δ cells can undergo metabolic cycles

Since the function of Pbp1 is specifically required under respiratory growth conditions, I examined whether *pbp1*Δ cells can undergo yeast metabolic cycles similar to WT cells. During continuous growth in a chemostat, *pbp1*Δ cells can undergo complete metabolic cycles with a shorter cycling period (3.15 h, compared to ~4 h for WT cells) (Figure 2-4A), and the expression of Pbp1 protein remained constant throughout the cycle (Figure 2-4B).

Pbp1 has indistinguishable interactome between different conditions

Another strategy I undertook to elucidate the mechanisms behind Pbp1's function was to compare the interacting proteins of Pbp1 between non-autophagy-inducing (YPL) and autophagy-inducing (SL) conditions, as well as different phases of the yeast metabolic cycle. Silver staining of Pbp1 precipitants from cells grown in YPL and SL medium, respectively, showed no significant, reproducible differences in associating proteins (Figure 2-5). Similarly, there were no significant differences between the interacting proteins of Pbp1 immunoprecipitated from cells collected from different stages of the yeast metabolic cycle (Figure 2-6).

The reported functions of Pbp1 in mRNA stability regulation and stress granule formation do not account for its role in autophagy regulation

Pbp1 was reported to maintain the appropriate length of mRNA poly(A) tails by negatively regulating the poly(A) exoribonuclease, Pan2 (Mangus et al., 2004b). *pbp1*Δ cells

initially produced normal length poly(A) tails which were then trimmed at a much faster rate. This accelerated poly(A) trimming was not observed in *pbp1*Δ /*pan2*Δ cells (Mangus et al., 2004b). To figure out whether the dysregulation of poly(A) length in *pbp1*Δ mutant is relevant to the phenotype of interest, I knocked out *PAN2* along with *PBP1*. Deletion of *PAN2* did not rescue the autophagy of *pbp1*Δ cells (Figure 2-7), suggesting that the dysregulation of autophagy is not due to the abnormal poly(A) length of mRNAs.

In 2015, Demille et al. reported that under stressful conditions such as glucose deprivation or heat shock, PAS kinase (Psk1) phosphorylates Pbp1, which allows Pbp1 to form stress granules and sequester TORC1 (DeMille et al., 2015). Since the activity of TORC1 is directly correlated with autophagy, I examined autophagy in *psk1*Δ or *psk2*Δ cells following YPL to SL switch. The GFP cleavage assay clearly showed that deletion of either *psk1* or *psk2* did not affect autophagy (Figure 2-8), suggesting that the regulatory mechanisms proposed by Demille et al. under glucose-deprived conditions did not fully explain the loss of autophagy phenotype of *pbp1*Δ cells under the respiratory growth condition.

Pbp1 functions by negatively regulating TORC1 signaling

The autophagy-deficiency and rapid growth phenotypes of *pbp1*Δ cells were reminiscent of mutants lacking the function of a three-protein complex (Iml1-Npr2-Npr3) previously identified to be required for autophagy under these conditions (Sutter et al., 2013; Wu and Tu, 2011). Subsequent work revealed that this complex, termed SEACIT or GATOR1, acts as a negative regulator of TORC1 (Bar-Peled et al., 2013; Panchaud et al., 2013).

Interestingly, *iml1*Δ, *npr2*Δ, and *npr3*Δ mutants all bypass autophagy and exhibit an increased growth rate in SL medium (Laxman et al., 2013; Wu and Tu, 2011), just like *pbp1*Δ mutants. These similarities suggest that the autophagy and growth phenotypes of *pbp1*Δ mutants might also be due to hyperactive TORC1 signaling.

In addition, the *pbp1*Δ*npr2*Δ double knockouts showed exactly the same phenotype as single *pbp1*Δ or *npr2*Δ knockouts (Figure 2-9), suggesting that Pbp1 and Npr2 functions in the same pathway.

I therefore tested whether Pbp1 might induce autophagy via negative regulation of TORC1 signaling. Treatment with rapamycin completely restored autophagy (Figure 2-10A) and reversed the increased growth of Pbp1-deficient cells in SL medium (Figure 2-10B), suggesting that these phenotypes are indeed mediated through TORC1.

***pbp1*Δ cells exhibit features of hyperactive TORC1 signaling**

Hyperphosphorylation of TORC1 substrates

To assess whether the rapamycin-reversible phenotypes of *pbp1*Δ cells are due to increased TORC1 activity, we examined phosphorylation of TORC1-dependent substrates, Sch9, Atg13, Gln3, and Npr1. Each protein exhibited increased phosphorylation in *pbp1*Δ cells compared to WT following the switch to SL medium (Figure 2-11).

Increased anabolic metabolism and ribosome biogenesis

We next performed a proteomic survey to investigate the basis of the increased growth of *pbp1*Δ mutants in SL medium. Using a SILAC (Stable-Isotope Labelling by Amino acids in Cell culture) experiment to compare protein abundances in *pbp1*Δ mutant and WT, we found the proteins that were most significantly increased in *pbp1*Δ cells in SL medium were enzymes involved in anabolic metabolism and biosynthesis (Figure 2-12A-highlighted in red, 2-12B, and Table 2-1). In particular, proteins involved in ribosome biogenesis were significantly increased in abundance in *pbp1*Δ cells (Figure 2-12C and Table 2-2).

Thus, the increased abundance of proteins involved in translation and anabolic biosynthesis was also consistent with the reporters of increased TORC1 activity in *pbp1*Δ cells. Taken together, these data suggest that *pbp1*Δ cells have hallmarks of hyperactive TORC1 signaling, and that Pbp1 is therefore a negative regulator of TORC1.

Pbp1 interacts with TORC1 specifically during respiratory growth

We next tested whether Pbp1 might interact with components of TORC1 as a possible mechanism of regulation. Taking into account growth conditions in which Pbp1 is required for autophagy, we observed that endogenous Kog1, the yeast ortholog of RAPTOR, co-immunoprecipitated with Pbp1 exclusively in the minimal lactate medium (SL), but not in minimal glucose medium (SD) (Figure 2-13A). Moreover, this interaction between Pbp1 and Kog1 in SL medium was substantially decreased following switch back to glucose medium (SD) (Figure 2-13B). In *pbp1*Δ cells, more TORC1 appeared associated with vacuolar

membranes as assessed by imaging of Kog1-GFP expressed at an endogenous level (Figure 2-14). Note the Kog1 level did not change in *pbp1*Δ cells in SL medium over the time period observed (Figure 2-15).

Therefore, the association between Pbp1 and Kog1 is responsive to cellular metabolic conditions and is more prominent when cells are grown in a non-fermentable carbon source. Increased association between Pbp1 and TORC1 under these conditions is consistent with inhibition of TORC1 and reduced vacuolar localization.

The interaction between Pbp1 and Kog1 is mediated through a.a. 338-442 on Pbp1

To identify the region within Pbp1 required for binding to TORC1, we constructed a series of deletion mutants of Pbp1 (Figure 2-16) and tested their ability to co-immunoprecipitate Kog1. Pbp1 possesses two putative RNA-binding domains, Like SM (Lsm) and Lsm Associated Domain (LsmAD), near its N-terminus, with the remainder of the protein having no predicted secondary structure (Figure 2-16). Pbp1 mutants lacking one or both RNA binding domains (Figure 2-16, mutant 3, 4, 5) retained the ability to interact with Kog1 (Figure 2-17A). The addition of RNase A to lysates also did not affect the interaction between Pbp1 and Kog1 (Figure 2-17B). The mutants lacking the RNA-binding domains also did not affect autophagy or growth (Figure 2-17C, D).

We then tested the ability of other Pbp1 truncation mutants to co-immunoprecipitate Kog1 (Figure 2-18). We observed that the interaction between Pbp1 and Kog1 is mediated through a ~100 amino acid region (a.a. 338-442) downstream of the two putative RNA binding

domains (Figure 2-18 – mutant 6, 8, 9, 12, 13 and 2-19A). Pbp1 mutants lacking this region exhibited the same increased growth and defective autophagy phenotype as the *pbp1*Δ null mutant (Figure 2-19B, C), as well as increased phosphorylation of the TORC1-responsive substrate Atg13 (Figure 2-19D). These data demonstrate that an interaction between Pbp1 and Kog1 is required for the inhibition of TORC1 during respiratory growth.

Pbp1 inhibits TORC1 independent of the SEACIT-Gtr1/2 pathway

The SEACIT complex (Npr2-Npr3-Iml1) functions as a GAP (GTPase Activating Protein) to negatively regulate the activity of the heterodimeric Rag GTPase complex, Gtr1 and Gtr2, which acts as an activator for TORC1 in response to nutrient signals (Binda et al., 2009). Since my data so far indicated that Pbp1 and SEACIT complex function in the same pathway as bona fide negative regulators of TORC1, I next tested for possible epistasis between Pbp1 and SEACIT-Gtr1/2.

First of all, to test whether Pbp1 functions upstream of SEACIT and Gtr1/2, I examined the activity of Npr2 in *pbp1*Δ cells as indicated by its phosphorylation. Deletion of *pbp1* did not significantly alter the dynamics of Npr2 phosphorylation when switching the cells from YPL to SL medium (Figure 2-20), suggesting that Pbp1 does not function upstream of the SEACIT complex. Cells lacking Gtr1 exhibited a growth defect, and further deletion of its upstream regulator, *npr2*, did not show any additive effect (Figure 2-21A). To investigate the relationship between Pbp1 and the Gtr1/2 complex, I made *pbp1*Δ*gtr1*Δ double knockouts. Deletion of *pbp1* in *gtr1*Δ cells increased the growth rate of *gtr1*Δ cells to a level similar to

WT. This additive effect suggests that Pbp1 negatively regulates TORC1 independent of Gtr1 (Figure 2-21B).

Pbp1 might compete with Gtr1-Gtr2 heterodimer for TORC1 binding

The Gtr1-Gtr2 heterodimer is asymmetrically loaded with GTP (guanosine 5′-triphosphate) and GDP (guanosine diphosphate) in response to amino acid availability (Binda et al., 2009). The nucleotide-binding state of Gtr1-Gtr2 determines its binding affinity to TORC1. The binding of Gtr1-Gtr2 heterodimer is important for TORC1 activity. Under amino acid-replete condition, the $Gtr1^{GTP}$ - $Gtr2^{GDP}$ heterodimer, which has a higher binding affinity to TORC1, stimulates TORC1 activity; whereas under nutrient starvation, the $Gtr1^{GDP}$ - $Gtr2^{GTP}$ heterodimer is less capable of interacting with TORC1, leading to decreased TORC1 activity. Consistent with these reports, I observed that Gtr1 primarily binds to the TORC1 component, Kog1, in SD compared to SL condition (Figure 2-22).

The aforementioned genetic epistasis studies between Pbp1, Npr2, and Gtr1 (Figure 2-21) have led us to a hypothesis regarding how Pbp1 inhibits TORC1 activity. The hypothesis is that Pbp1 competes with Gtr1/2 for TORC1 binding. Under conditions where the Gtr1/2 heterodimer is unable to interact with TORC1, the majority of TORC1 is bound by the negative regulator, Pbp1, resulting in TORC1 inactivation. Under this circumstance, removing the negative regulator Pbp1 should increase TORC1 activity.

To test this hypothesis, I made a mutant strain expressing the GDP-locked Gtr1 (Gtr1-S20L), which is known to have low affinity to TORC1 (Boguski and McCormick, 1993; Gao

and Kaiser, 2006; Nakashima et al., 1999). The TORC1 activity of this strain, which is indicated by the growth rate, was very low compared to WT (Figure 2-23). Further deletion of *pbp1* in this $Gtr1^{GDP}$-expressing strain significantly increased TORC1 activity (Figure 2-23), supporting our hypothesis.

In addition, I examined the binding affinity between Pbp1 and TORC1 in the presence of WT Gtr1, GTP-locked Gtr1 (Gtr1-Q65L), which strongly interacts with TORC1, or GDP-locked Gtr1 (Gtr1-S20L), which has reduced ability to interact with TORC1. Immunoprecipitation revealed that the binding affinity of Pbp1 to TORC1 is the highest in the presence of GDP-locked Gtr1, decreased in the presence of WT Gtr1, and lowest in the presence of GTP-locked Gtr1 (Figure 2-24). These data are consistent with the model of competition between Pbp1 and Gtr1 for binding to TORC1. In this competition model, both Pbp1 and Gtr1 are expected to show a stronger interaction with TORC1 in the absence of one another. However, immunoprecipitation showed that WT Gtr1 pulled down less TORC1 in the absence of Pbp1 (Figure 2-25), suggesting a more complicated regulation beyond the competition model proposed.

Discussion

Growth phenotypes of *pbp1*Δ and *npr2*Δ cells vary with carbon sources and amino acid availability.

In this chapter, I focused on the phenotypes of *pbp1*Δ cells after switching from YPL to SL medium. Compared to WT, *pbp1*Δ cells exhibited increased growth in SL medium like

*npr2*Δ (Figure 2-3A, 2-26A), and *pbp1*Δ*npr2*Δ double knockouts showed the same growth rate as *pbp1*Δ or *npr2*Δ single knockout (Figure 2-26A). It is worth mentioning that these mutants showed different growth phenotypes in YPL, SD, or YPD medium. In YPL medium, *npr2*Δ cells still grow faster than WT as they do in SL medium; however, *pbp1*Δ cells grow slower than WT. The *pbp1*Δ*npr2*Δ double knockouts grow the same as *pbp1*Δ cells (Figure 2-26B). In YPD medium, all three mutants grow the same as WT (Figure 2-26D). In SD medium, while *pbp1*Δ cells grow comparably to WT, *npr2*Δ cells and *pbp1*Δ*npr2*Δ double knockouts grow slower than WT (Figure 2-26C). These phenotypes suggest that there might be multiple regulatory mechanisms involving TORC1 regulation depending on the carbon source and nutrients.

For example, it has been shown that in high glucose (SD medium), *npr2Δ* mutants have hallmarks of increased TORC1 signaling, but grow slowly unless amino acids are supplemented (Chen et al., 2017). Compared to WT, *npr2Δ* showed reduced metabolic activities that are required to achieve the amino acid- and nitrogen-replete state. Therefore, each inhibitor of TORC1 signaling could play a distinct role in cell growth regulation. Pbp1 and Npr2 might be responsible for sensing different carbon sources, nutrients, or even mitochondrial status in SD, YPL, and SL, in order to properly regulate TORC1 activity.

Model of Pbp1-Gtr1 competition requires further testing

Through genetic epistasis studies between Pbp1, Npr2, and Gtr1, I hypothesize that one of the mechanisms by which Pbp1 regulates TORC1 is to compete with Gtr1/2 complex for

TORC1. The differential binding affinities of Pbp1 to TORC1 in the presence of $Gtr1^{WT}$, $Gtr1^{GTP}$, or $Gtr1^{GDP}$ support this hypothesis (Figure 2-24). Based on the hypothesis, $Gtr1^{WT}$ should have a stronger interaction with TORC1 in *pbp1*Δ cells compared to that in WT cells. However, contrary to our expectations, the interaction between $Gtr1^{WT}$ and TORC1 is decreased in *pbp1*Δ cells (Figure 2-25). These data indicate that Pbp1 is required for the interaction between Gtr1 and TORC1 for a reason yet to be elucidated.

I also tried to examine if deletion of *PBP1* enhances the interaction between $Gtr1^{GDP}$ and TORC1 since $Gtr1^{GDP}$ can barely bind to TORC1 in WT cells. However, $Gtr1^{GDP}$ was very unstable, and I was unable to pull down a significant amount of $Gtr1^{GDP}$ to detect its interacting proteins (Figure 2-24). In addition, I observed that the protein level of Kog1 was significantly decreased in $Gtr1^{GDP}$/ *pbp1*Δ cells (Figure 2-24), hinting that binding to either Gtr1/2 or Pbp1 might protect Kog1 or the entire TORC1 from degradation, perhaps through modulation of distinct conformational or oligomeric states of TORC1 (Prouteau et al., 2017).

Materials and Methods

Yeast Strains

The prototrophic Saccharomyces cerevisiae CEN.PK strain was used in all experiments. Gene deletions were carried out using standard PCR-based strategies to amplify resistance cassettes with appropriate flanking sequences, and replacing the target gene by homologous recombination (Longtine et al., 1998). C-terminal tags were similarly made using PCR to amplify resistance cassettes with flanking sequences. The diploid strain was constructed by

standard mating procedures. Pbp1 mutants with various domain deletion or point mutations were first made using PCR and then integrated into the PBP1 locus in a *pbp1*Δ strain with different selection markers.

Yeast Growth Media and Procedures

Media used in this study

YPL (0.5% yeast extract (Bio Basic), 2% peptone (BD Biosciences) and 2% lactate (Sigma L1375)); SL (0.17% yeast nitrogen base without amino acids (BD Biosciences), 2% lactate); SD (0.17% yeast nitrogen base without amino acids, 2% glucose); SD-N (0.17% yeast nitrogen base without amino acids and ammonium sulfate (BD Biosciences), 2% glucose); SCL-Lys-Arg (0.17% yeast nitrogen base without amino acids, CSM-Lys-Arg (Sunrise science), 2% lactate).

Media switch

Cells from overnight YPL culture were inoculated into fresh YPL to 0.1 optical density (OD_{600})/ml and grown for a few generations in log phase. The log-phase cells were then diluted again to very low OD_{600}, grown overnight till the OD_{600} reached ~1. The cells were then spun down, washed, and re-suspended to OD_{600} = 0.7 in SL, SD or SD-N. Samples were collected at indicated times. Growth curves for different cells grown in SL, SD, or SD-N were performed by starting cultures at OD_{600} ~0.15, and then measuring OD_{600} periodically until saturation.

Assays to monitor autophagy

Imaging

A dual-color reporter strain expressing mitochondrial-localized DsRed (Mito-DsRed) and GFP-tagged vacuolar membrane protein Vph1 (Vph1-GFP) was constructed to visualize mitophagy. An increase in the signal of Mito-DsRed in the vacuole indicates the induction of mitophagy. Images were taken under a 100X oil-immersion objective lens with a Deltavision DVRT microscope. Cells grown under indicated conditions were visualized after directly mounting under a coverslip. Images were deconvolved, then processed using ImageJ.

GFP cleavage assay

A mitochondrial matrix protein, Idh1, was tagged with GFP. When mitophagy is induced, this protein accumulates in the vacuole and is degraded. The more stable GFP is detected by immunoblotting with anti-GFP monoclonal antibody (Roche, clone 7.1 and 13.1) as semi-quantitative evidence for mitophagy (Kanki et al., 2009).

ALP activity assay

*pho8*Δ60/*pho13*Δ cells with or without Pbp1 were subject to ALP activity assay before and 8 h after media switch to measure the level of general autophagy. The protocol for ALP assay essentially followed previously described methods (Noda et al., 1995) with some modifications. Briefly, cell pellets were resuspended in 400 µl of lysis buffer (250 mM Tris-HCl pH 9, 25 mM $MgSO_4$, 1% Triton, 2X EDTA-free protease inhibitor cocktail (Roche). After adding ~100

μl of glass beads (Sigma), cells were lysed by three rounds of bead beating: 1 min of beating, then 1 min of cooling on ice. Cell debris and glass beads were separated from the cell extracts by centrifugation at maximum speed for 10 min at 4°C. For each sample, 70 μl of cell extracts were added to triplicate wells in 96-well, flat bottom plates. Plates were kept on ice before the substrate was added. Lysis buffer (70 μl) was added to the blank well. 70 μl of substrate solution (250 mM Tris-HCl pH 9, 25 mM $MgSO_4$, 1% Triton, 2.7 mM p-nitrophenyl phosphate (MP Biomedicals Life Sciences)) was then added to each well. The plate was incubated at room temperature for 5 min before the reaction was stopped with 140 μl of stop buffer (1 M glycine, pH 11). The plate was read at 400 nm to measure the production of p-nitrophenol.

TCA-precipitated whole cell extracts preparation

Cell pellets were resuspended in 250 μl 8% TCA. After adding ~100 μl glass beads, cells were lysed by five rounds of bead-beating: 30s beating/30s cooling on ice. The lysates were then centrifuged at maximum speed for 10 min at 4°C. The pellets were then washed with 100% ice-cold acetone and resuspended in 2X SDS sample buffer (400 mM Tris-HCl pH 7.5, 4% SDS, 20% glycerol), boiled for 5 min, and briefly centrifuged. The supernatant was then separated, and the protein concentration was measured using BCA protein assay kit (Thermo Scientific). Bromophenol blue and 2-mercaptoethanol were added to the lysates after concentration measurement.

TORC1 substrate phosphorylation

At the indicated time points, 5 OD of cells expressing Sch9-HA, HA-Atg13, Gln3-Flag, or Npr1-Flag were quenched by mixing with TCA to a final concentration of 10% and incubated on ice for 20 min before centrifugation. Cell pellets were then subject to whole cell TCA extraction and analyzed by Western immunoblotting. Sch9-HA samples were analyzed by phos-tag SDS-PAGE (Wako chemical laboratory) immunoblot with anti-HA antibody (Cell Signaling, C29F4). HA-Atg13, Gln3-Flag, or Npr1-Flag samples were analyzed by SDS-PAGE immunoblot with anti-HA and anti-Flag (Sigma, M2) antibodies, respectively. The loading control was immunoblotted with rabbit anti-G6PD Ab2 (Sigma). For cells treated with rapamycin and cycloheximide, 200 ng/ml rapamycin (Sigma) or 25 μg/ml cycloheximide (Sigma) was added to cells grown in YPL and grown for 30 min before harvesting.

SILAC and GO term analysis

Culture preparation

WT or *pbp1*Δ strains auxotrophic for lysine and arginine (*lys1*Δ/*arg4*Δ) were grown in YPL for several generations and then diluted to OD_{600} 0.01 in SCL-Lys-Arg media supplemented with 50 μg/ml lysine and 50 μg/ml arginine (Lys^0+Arg^0 for *pbp1*Δ cells, Lys^{+8}+Arg^{+10} for WT cells). For efficient labeling, cells were grown for ~22 h (7-8 complete generations) until OD_{600} ~1. 20 OD of cells at this point were collected as SCL samples, and the rest of cultures were washed with SL and resuspended to OD_{600} = 0.7 in SL supplemented with 50 μg/ml lysine and 50 μg/ml arginine (Lys^0+Arg^0 for *pbp1*Δ cells, Lys^{+8}+Arg^{+10} for WT cells). SL samples were collected after 6 h.

Protein Extraction

Cell pellets from WT cells grown in heavy SILAC media were lysed (lysis buffer: 50 mM Tris-HCl pH 8.0, 75 mM NaCl, 50 mM NaF, 50 mM B-glycerophosphate, 1 mM sodium orthovanadate, 5 mM EDTA, 8 M urea, lysis procedures as described earlier for TCA extraction), mixed in 1:1 ratio with *pbp1*Δ cell lysates grown in light media. Proteins in the mixed lysates were separated by SDS-PAGE and stained with Coomassie Blue. Excised gel bands were chopped into 1 mm^3 cubes for in-gel digestion.

In-gel digestion

Coomassie blue stain was removed from gel pieces by incubating for 30 min at 37°C in 50 mM triethylammonium bicarbonate (TEAB)/acetonitrile (1:1, v/v). Gel pieces were then dehydrated with acetonitrile at room temperature, followed by reduction/alkylation using DTT and iodoacetamide. Gel pieces were dehydrated by ACN and rehydrated by a 10 μg/mL solution of trypsin in 0.05% HOAc. The digestion was carried out at 37°C overnight. Peptides were extracted at 37°C for 15 min using the extraction buffer (50% acetonitrile and 3.3% TFA). All the steps above were carried out on a thermomixer shaker (Eppendorf) unless stated otherwise. Extracts were then dried using a speed vacuum concentrator and re-suspended in 2% ACN, 0.1% TFA. Salts were removed using Oasis HLB μElution plate (Waters) before LC-MS/MS analysis.

LC-MS/MS detection of peptides

Reverse phase chromatography was performed on an Ultimate 3000 nano HPLC system (Dionex), equipped with a 75 μm i.d. x 50 cm EasySpray column (Thermo). Separation of peptides was carried out at 250 ml/min by a 60min linear gradient of 1%-28% buffer B. Buffer A contained 2% (v/v) ACN and 0.1% formic acid in water, and buffer B contained 80% (v/v) ACN, 10% (v/v) trifluoroethanol, and 0.1% formic acid in water.

Mass spectrometric analyses were performed on an Orbitrap Elite Instrument (Thermo Electron). The mass spectrometer operated in positive ion mode with a source voltage of 2.4 kV and a capillary temperature of 255°C. MS scans were acquired at 240,000 resolution in the Orbitrap and up to 14 MS/MS spectra were obtained for each full spectrum acquired using collisionally-induced dissociation (CID) for ions with charges 2 or higher. The charge exclusion was applied to exclude the unassigned and charge 1 species, and dynamic exclusion was used with a duration of 15 sec.

SILAC data analysis

RAW data files were analyzed using MaxQuant (version 1.5.0.30) (Cox and Mann, 2008). Peptide and protein identification were performed against the UniProtKB yeast whole proteome sequence database. Default parameters were used for the MaxQuant analysis, with the exception that Ile-leu equivalence was disabled to ensure reported peptide and protein sequences were identical to those in the original sequence database. Precursor mass tolerances

were automatically determined by MaxQuant during processing, while MS/MS mass tolerance was 20 ppm. Peptide and protein identifications were filtered to a 1% false discovery rate (FDR). Quantitation of a protein required the presence of at least two quantified peptide features for that protein.

GO term analysis

Proteins with expression level highly increased in *pbp1*Δ cells in SL ($0.5 < (pbp1\Delta/WT)_{SCL} < 1.5$, $(pbp1\Delta/WT)_{SL} > 2$) were analyzed for GO enrichments for biological processes using the GO term finder interface on the Saccharomyces Genome Database, including a p-value cutoff for significant shared GO terms of 0.01 (Ashburner et al., 2000; Boyle et al., 2004).

Immunoprecipitation

At the indicated time points, 50 OD of cells were harvested, flash frozen with liquid nitrogen, and stored at -80°C until cell lysis. The cell pellet was resuspended with 350 µl of lysis buffer A (50 mM HEPES pH 7.5, 150 mM NaCl, 10 mM $MgCl_2$, 0.5% NP-40, 2X protease inhibitor cocktail, 1 mM PMSF, 1mM sodium orthovanadate, 5 mM NaF, 10 nM leupeptin, 5 nM pepstatin A). After adding ~300 µl of glass beads, cells were lysed by bead beating 6 times: 30s of beating / 2 min of cooling on ice. The lysed cells were then separated from glass beads by centrifugation at 6000 rpm for 2 min at 4°C, and diluted with 525 µL of lysis buffer B devoid of NP-40 (50 mM HEPES pH 7.5, 150 mM NaCl, 10 mM $MgCl_2$, 2X

protease inhibitor cocktail, 1 mM PMSF, 1 mM sodium orthovanadate, 5 mM NaF, 10 nM leupeptin, 5 nM pepstatin A). The crude cell extracts were then clarified by two successive centrifugations at maximum speed for 10 min at 4°C (Panchaud et al., 2013).

The protein concentration of the cleared lysates was then measured using Bradford assay (Bio-Rad), and adjusted to be equal among all samples in 800 µl reaction volume. For input samples, 8 µl of the reactions were taken and mixed with SDS sample dye and denatured for 5 min at 95°C. For each co-immunoprecipitation reaction, 25 µl of dynabeads protein G (Life technologies) were washed with the IP lysis buffer and incubated with 3 µg of anti-Flag antibody (Sigma, M2) for 1 h at 4°C. The unbound antibodies were then removed by centrifugation at 500 g for 1 min at 4°, and the conjugated dynabeads-antibody were then added to the cleared lysates. If indicated, ribonuclease A (Sigma) was added to the lysates. After incubating for 2h at 4°C, the dynabeads were washed 3 times with wash buffer (50 mM HEPES pH 7.5, 150 mM NaCl, 10 mM $MgCl_2$, 2X protease inhibitor cocktail, 0.2% NP-40), resuspended in 2X SDS sample dye, and denatured for 5 min at 95°C.

Image analysis

Pbp1 distribution

To estimate the heterogeneity of Pbp1 distribution in individual cells, GFP intensity of every pixel in a cell was determined using ImageJ. The pixels with intensity lower than background were removed and the standard deviation of all the remaining pixels was calculated to display

the variability of GFP intensity between pixels. Accordingly, the standard deviation of the GFP intensity between pixels in a cell is correlated with the heterogeneity of the GFP distribution.

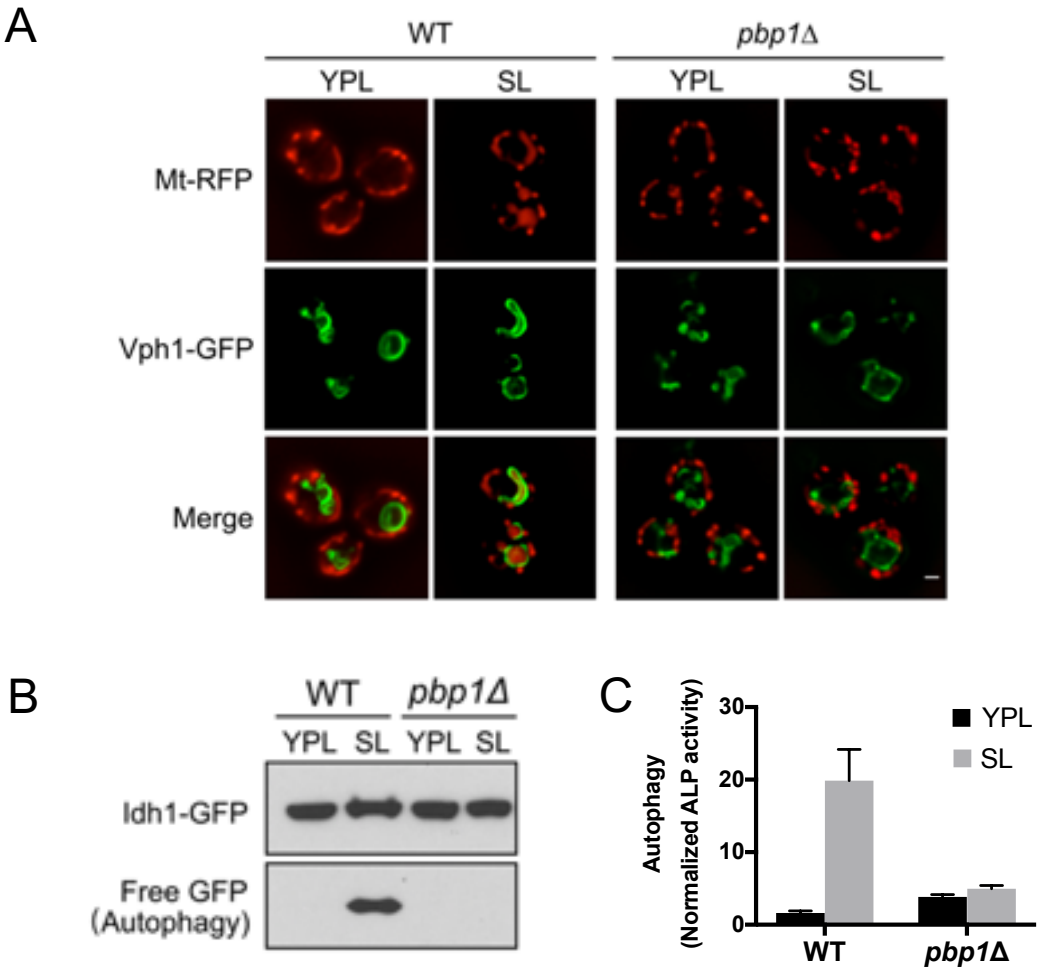

Figure 2-1. Pbp1 is required for autophagy under the respiratory growth condition.

(A) Images of WT and *pbp1*Δ cells before and after switching from YPL to SL medium for 8 h. The accumulation of the mitochondria-targeted RFP (Mito-DsRed) reporter in the vacuole (Vph1-GFP) indicates mitophagy. *pbp1*Δ mutant cells were unable to induce mitophagy following switch to SL medium. Scale bar = 1 μm. (B) GFP cleavage assay. The accumulation of free GFP following switch to SL medium indicates mitophagy. *pbp1*Δ cells were unable to induce mitophagy following switch to SL medium. (C) ALP activity assay. Using a cytosolic alkaline phosphatase reporter, general autophagy was monitored using the alkaline phosphatase assay as described previously (Noda et al., 1995) and in Methods. *pbp1*Δ cells were unable to induce general autophagy following switch to SL medium. Data were mean ± s.d. from 5 independent experiments.

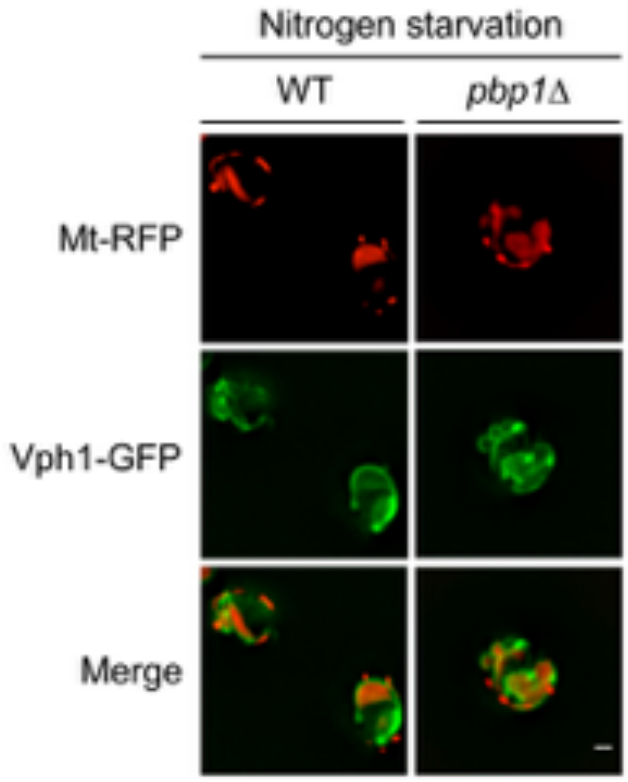

Figure 2-2. *pbp1*Δ cells were able to induce mitophagy after switching from SD to SD-N.

Images of WT and *pbp1*Δ cells after switching from YPL to SD–N medium for 8 h. *pbp1*Δ mutant cells were able to induce mitophagy following switch to SD-N medium. Scale bar = 1 μm.

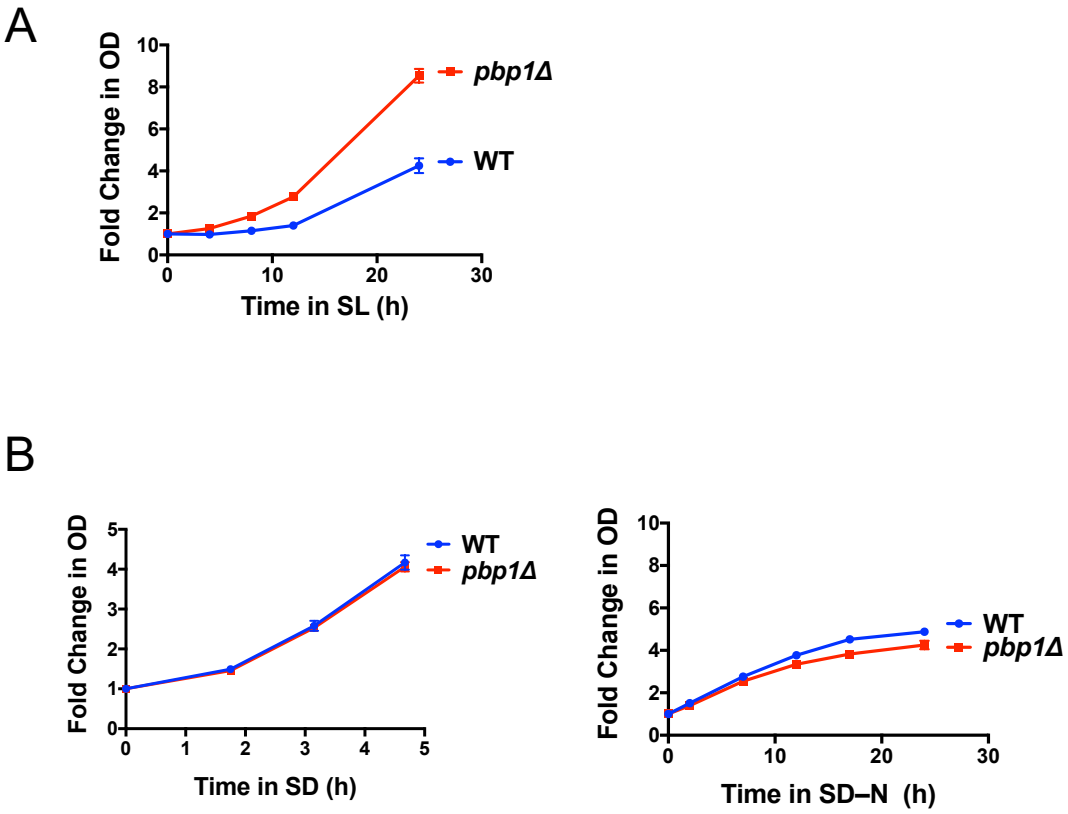

Figure 2-3. *pbp1*Δ cells exhibited increased growth rate in SL medium but not in the presence of glucose.

Growth of WT and *pbp1*Δ cells in (A) SL medium or SD and SD-N medium (B). *pbp1*Δ cells exhibited increased cell growth in SL medium and comparable cell growth to WT in the presence of glucose. Data were mean ± s.d. from 3 independent experiments.

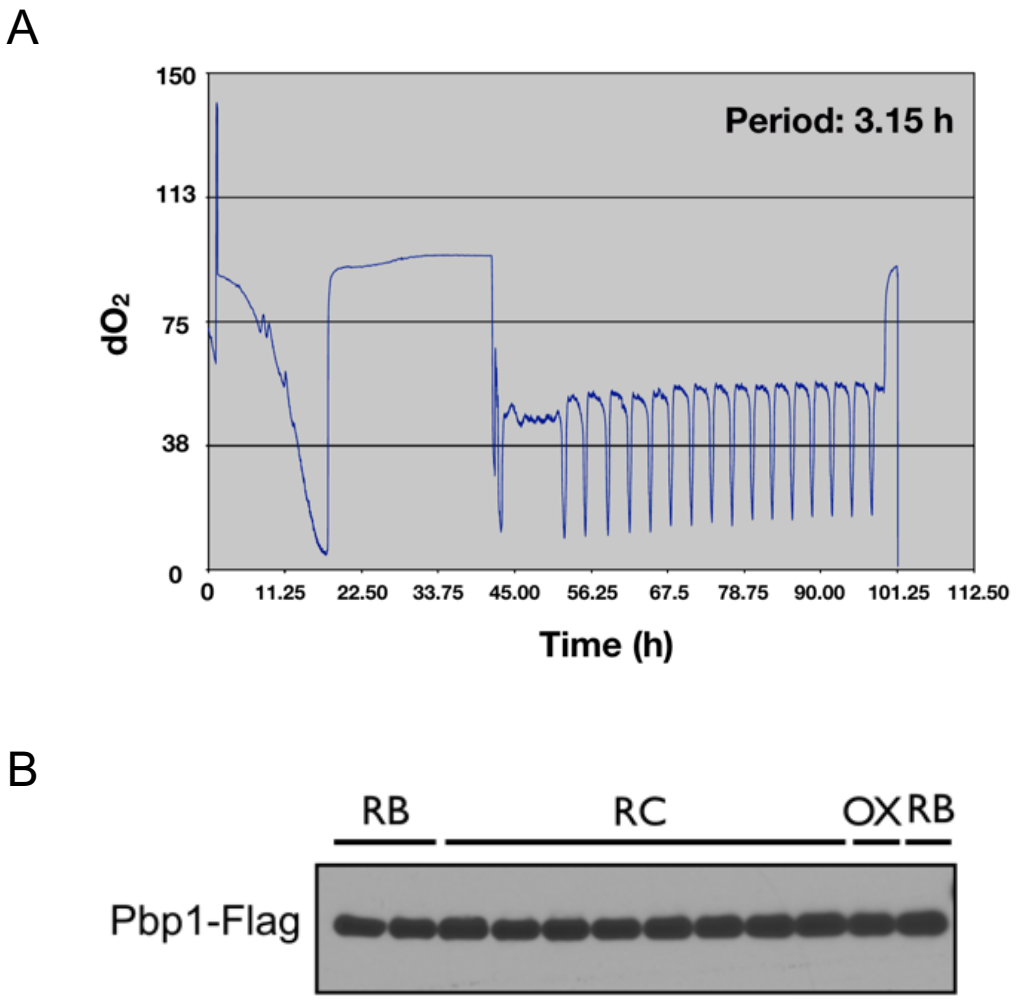

Figure 2-4. *pbp1*Δ cells undergo complete metabolic cycles but with a shorter period, and the level of Pbp1 expression did not change significantly during the cycle.

(A) Metabolic cycles exhibited by *pbp1*Δ cells. dO_2 refers to dissolved oxygen concentrations (% saturation) in the media. (B) Western blot showing the protein level of Pbp1 throughout a complete cycle. Cells were collected from the fermentor every 20 min for 12 time points within a cycle covering RB (reductive, building), R/C (reductive, charging), and Ox (oxidative) phase.

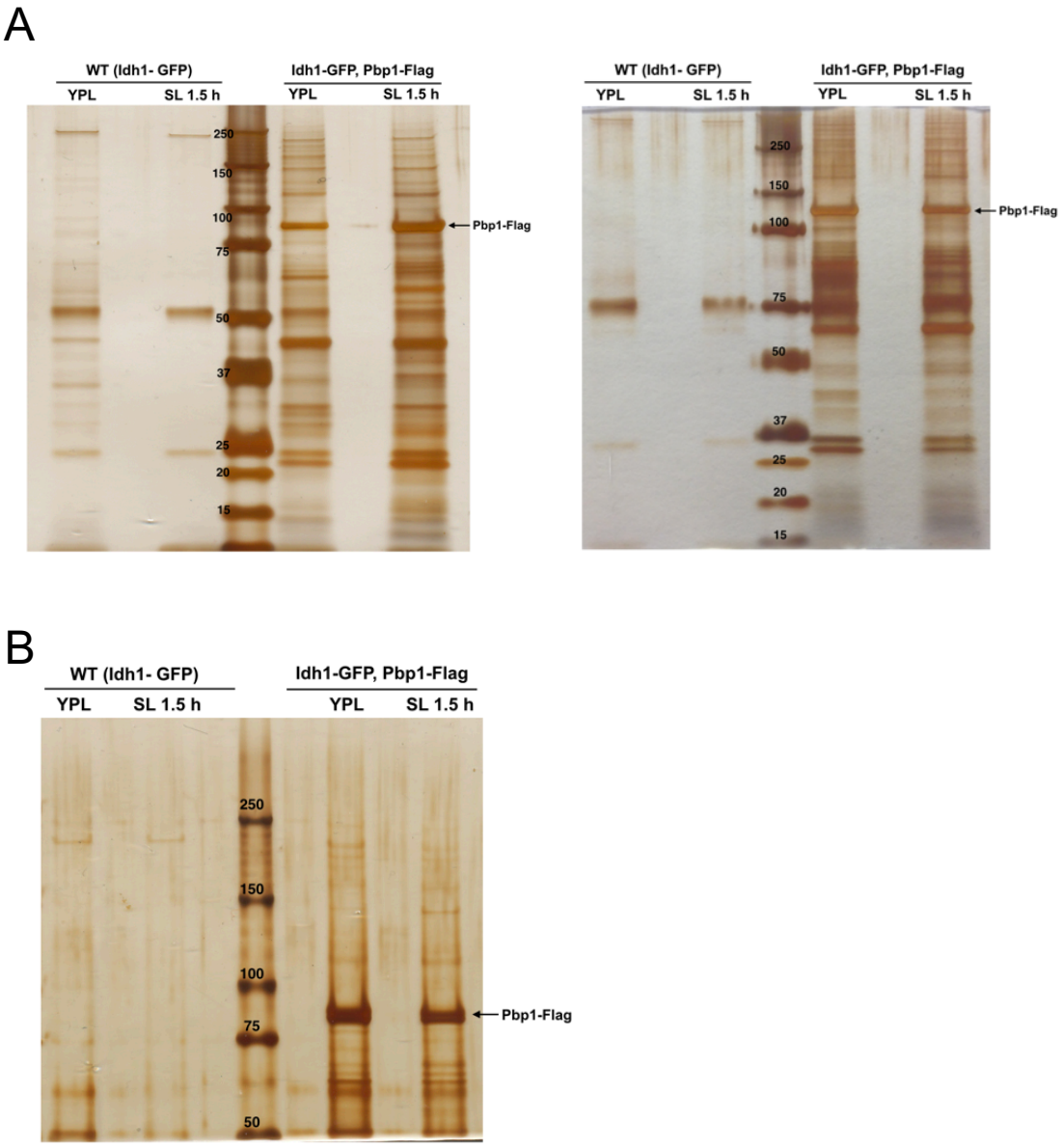

Figure 2-5. Pbp1 in YPL and SL medium has similar interactomes.

Pbp1and its interacting proteins immunoprecipitated from the extracts of cells grown in YPL and SL medium. Flag-tagged Pbp1in cell lysates was immunoprecipitated with an anti-Flag antibody. Precipitants were separated on a 4-12% Bis-Tris SDS-PAGE (A) or 3-8% Tris-Acetate SDS-PAGE (B) and visualized with silver staining. The two gels shown in (A) are two biological repeats.

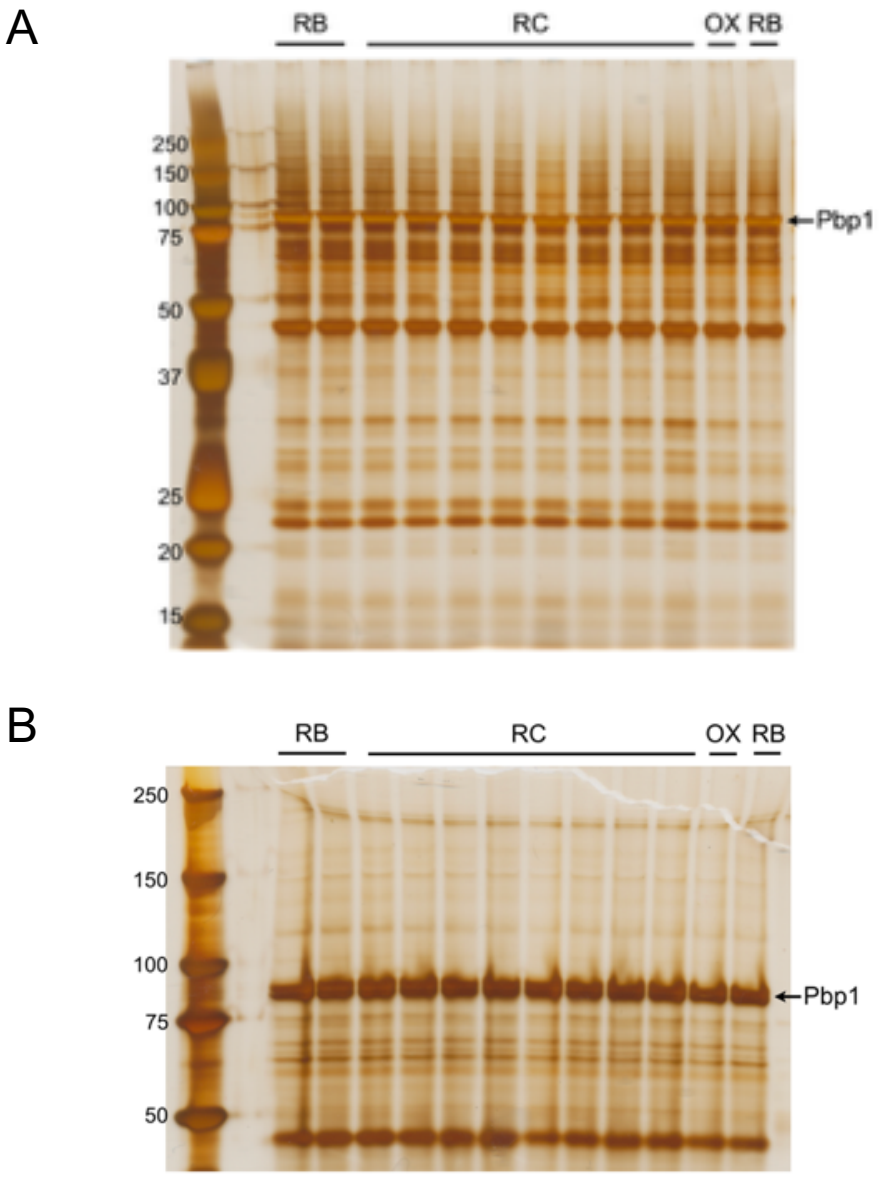

Figure 2-6. Pbp1 has comparable interactomes throughout the metabolic cycle.

Pbp1and its interacting proteins immunoprecipitated from the extracts of cells collected from RB (reductive, building), R/C (reductive, charging), or OX (oxidative) phase across one metabolic cycle. Samples were collected every 20 min. Flag-tagged Pbp1in cell lysates was immunoprecipitated with an anti-Flag antibody. Precipitants were separated on a 4-12% Bis-Tris SDS-PAGE (A) or 3-8% Tris-Acetate SDS-PAGE (B) and visualized with silver staining.

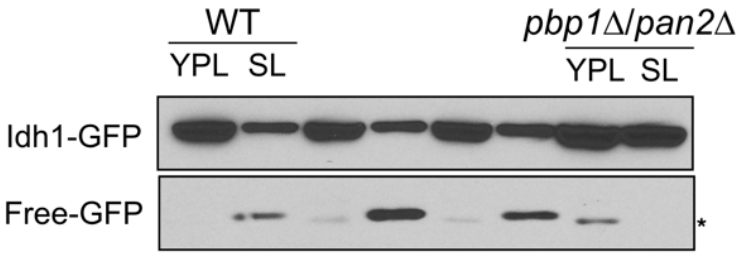

Figure 2-7. Deletion of *PAN2* in *pbp1*Δ cells did not rescue autophagy.

GFP cleavage assay showing *pbp1*Δ*/pan2*Δ cells were unable to induce mitophagy following switch to SL medium. * denotes a non-specific band.

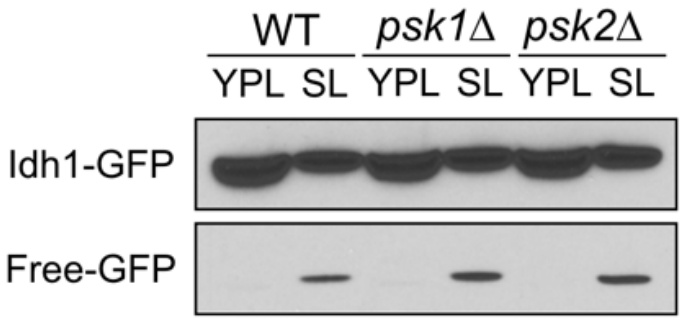

Figure 2-8. Psk1 or Psk2 is not involved in autophagy induction in SL medium.

GFP cleavage assay showing autophagy induction in *psk1*Δ or *psk2*Δ cells following switch to SL medium.

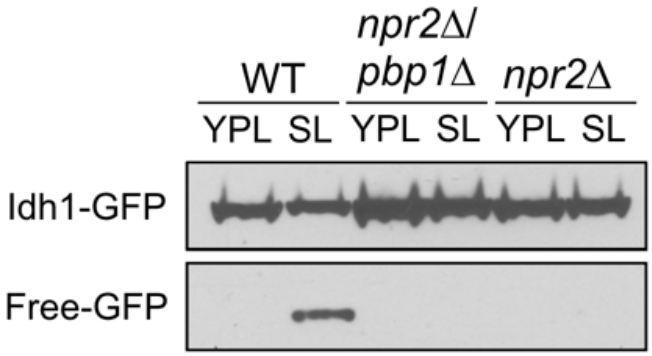

Figure 2-9. *npr2*Δ/*pbp1*Δ showed the same loss of autophagy as single *npr2*Δ.

GFP cleavage assay showing that both *npr2*Δ/*pbp1*Δ double knockouts or *npr2*Δ single knockout cells were unable to induce autophagy following switch to SL medium.

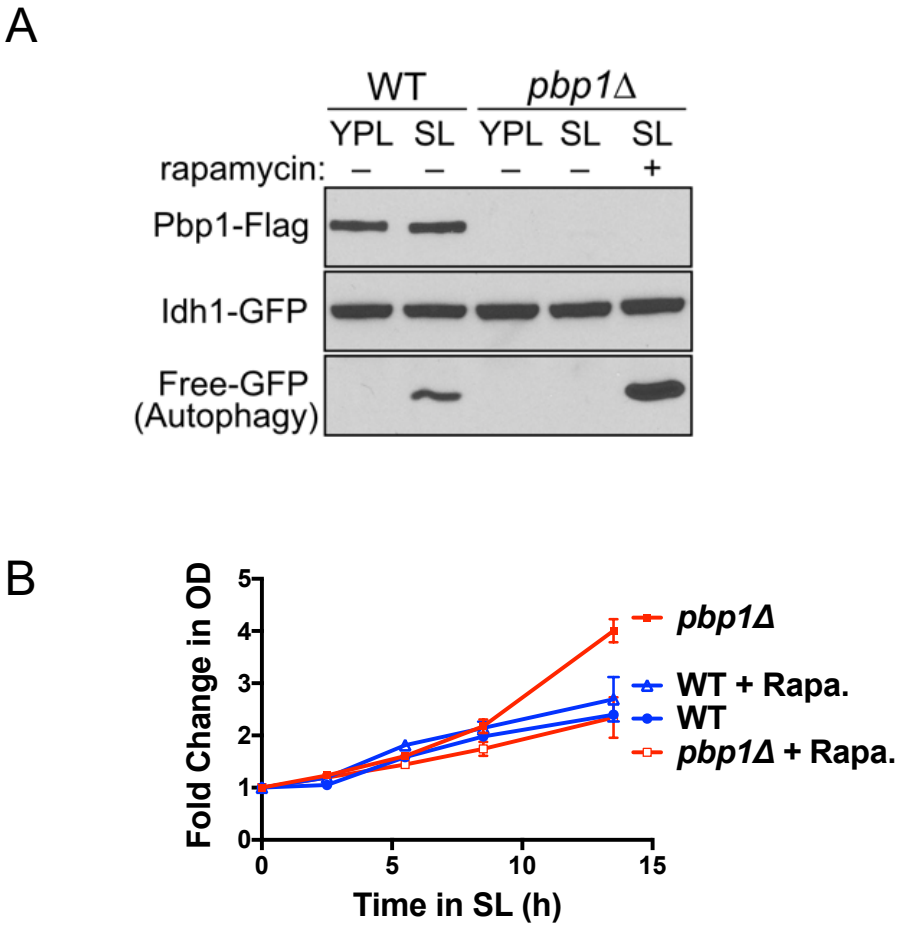

Figure 2-10. Rapamycin reverses the phenotype of *pbp1*Δ cells.

(A) GFP cleavage assay reflecting autophagy amounts in *pbp1*Δ cells in SL medium with or without rapamycin (200 nM). Treatment with rapamycin completely restored autophagy in *pbp1*Δ cells. (B) Growth of WT and *pbp1*Δ cells in SL medium containing 2 nM rapamycin. Treatment of rapamycin reversed the increased growth of *pbp1*Δ cells. Data were mean ± s.d. from 3 independent experiments. Rapa. : rapamycin.

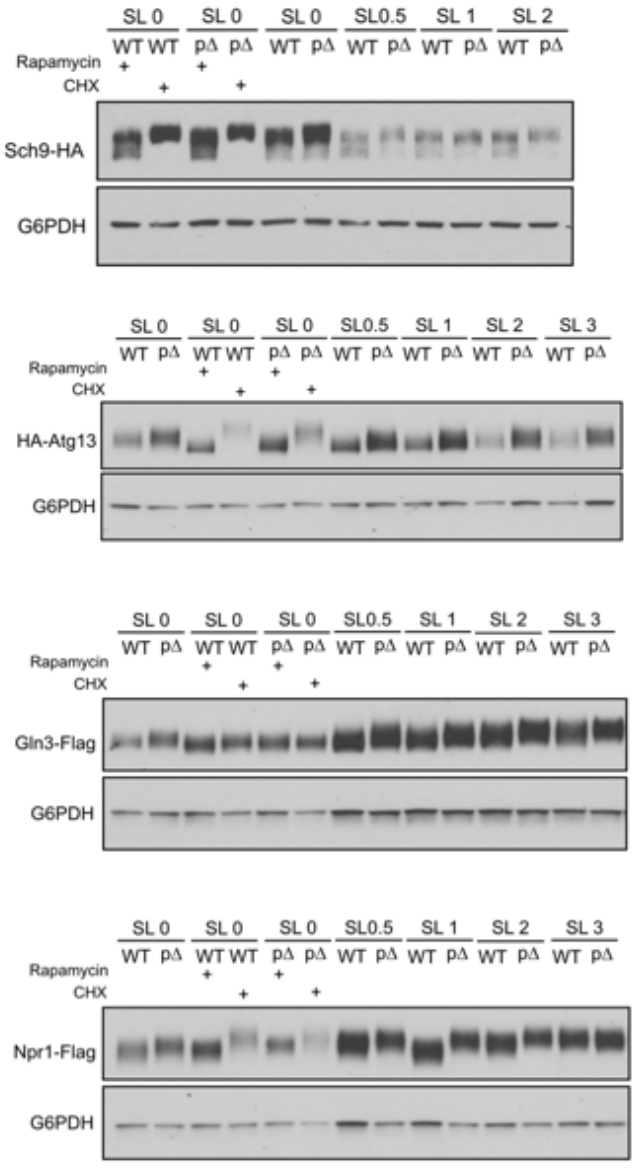

Figure 2-11. TORC1-dependent substrates are hyperphosphorylated in *pbp1*Δ cells.

Phosphorylation of endogenously tagged Sch9, Atg13, Gln3, and Npr1 at the indicated time points before and after switch to SL medium. Phosphorylated species exhibit reduced migration during SDS-PAGE. Sch9 samples were analyzed using phos-tag SDS-PAGE. Rapamycin (200 ng/ml) and cycloheximide (CHX)(25 ug/ml) treatment were used to assess the migration of low and high phosphorylated states of these substrates. *pbp1*Δ mutant cells exhibited increased phosphorylation of TORC1 substrates following switch to SL medium.

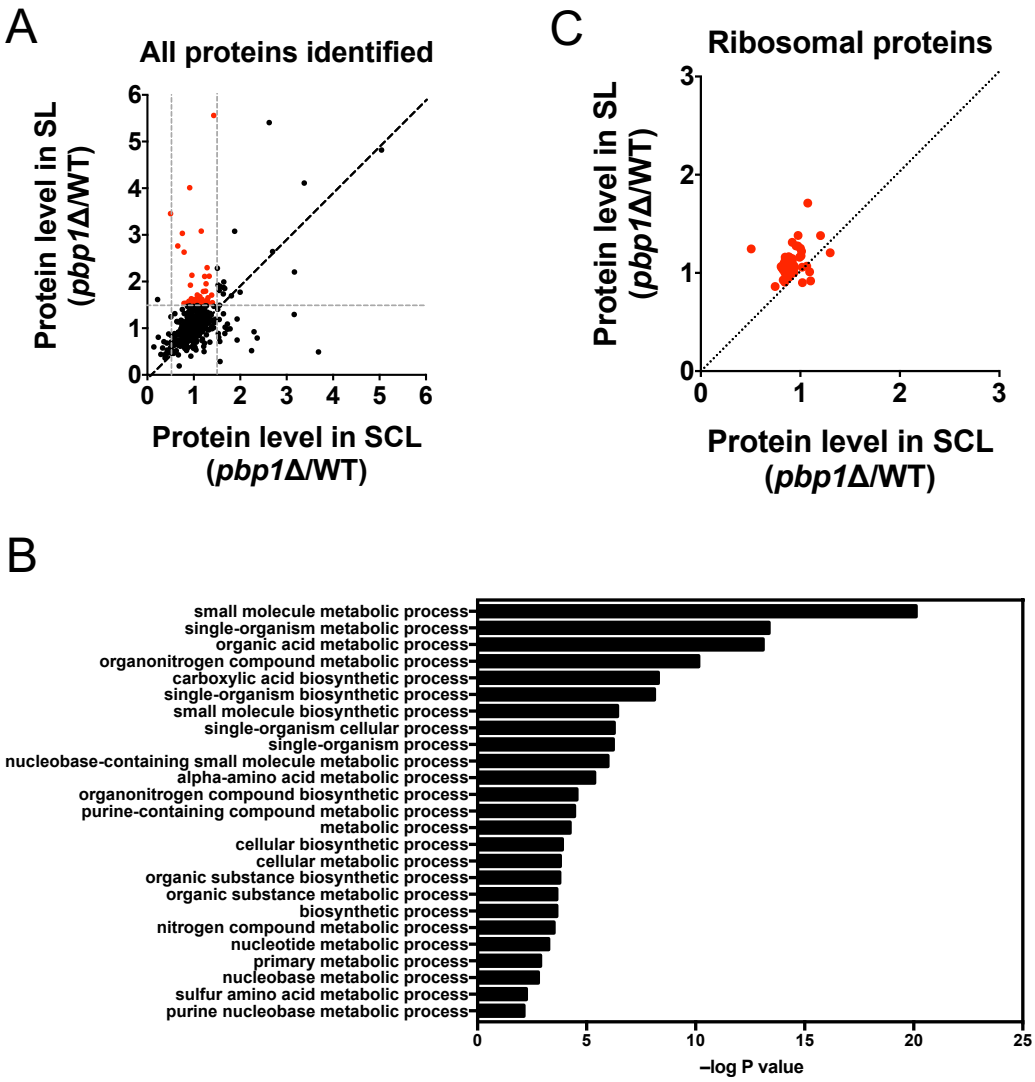

Figure 2-12. *pbp1*Δ cells have increased anabolic metabolism and ribosome biogenesis.

SILAC quantitative proteomic approach for assessing global changes in protein levels in *pbp1*Δ versus WT cells. The ratio of the expression amounts of all 608 proteins detected in *pbp1*Δ versus WT cells was plotted. Proteins present at increased amounts in *pbp1*Δ in SL ($(pbp1\Delta / WT)_{SL} > 1.5$), but not in SCL ($0.5 < (pbp1\Delta / WT)_{SCL} < 1.5$) are highlighted in red, and listed in Table 2-1. (B) Gene ontology analysis for proteins that exhibit increased abundance in *pbp1*Δ cells in SL medium (proteins highlighted in red in (A)). (C) Correlation plot comparing the amounts of ribosomal proteins in *pbp1*Δ versus WT cells in SCL (X-axis) and SL (Y-axis). Ribosomal proteins were increased in abundance in pbp1Δ cells in SL medium. Protein identities are listed in Table 2-2.

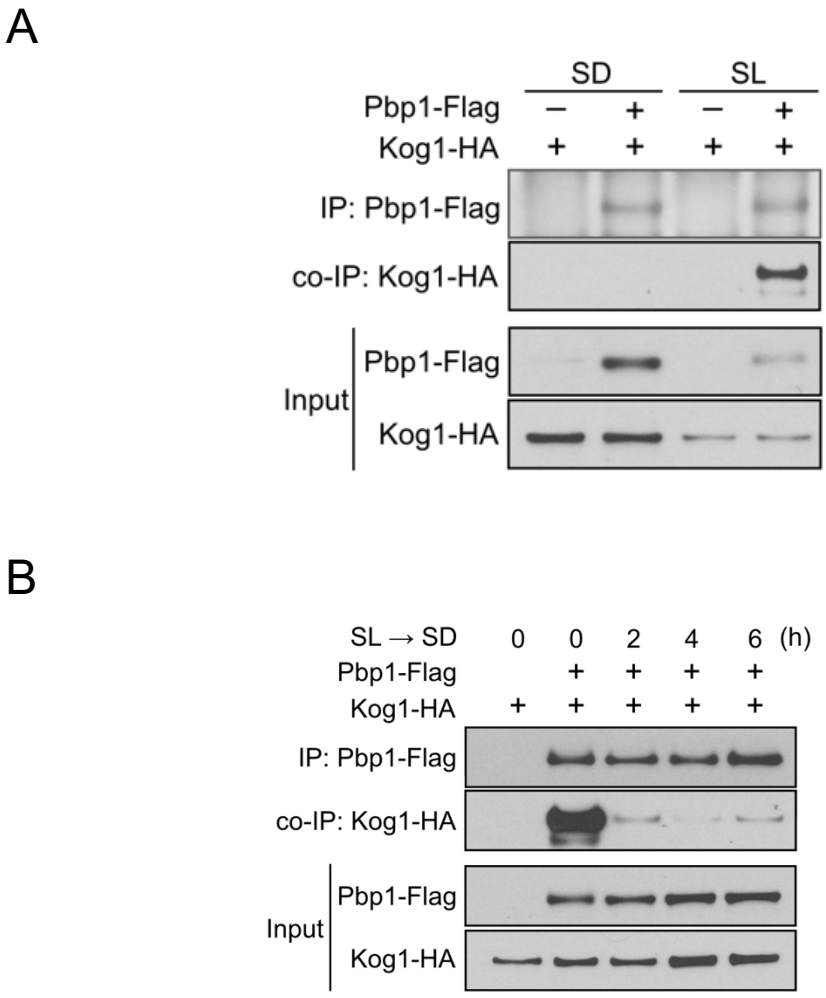

Figure 2-13. Pbp1 interacts with TORC1 specifically during respiratory growth.

(A) Pbp1 interacts with TORC1 component Kog1 in cells grown in SL, but not SD medium. Cells with endogenously tagged Pbp1 and Kog1 grown in YPL medium were switched to SD or SL medium for 3 h. Flag-tagged Pbp1 in cell lysates was immunoprecipitated with an anti-Flag antibody. Co-immunoprecipitation of Kog1-HA was detected by immunoblotting with anti-HA antibody. (B) Reduced interaction between Pbp1 and Kog1 following glucose repletion. Cells with endogenously tagged Pbp1 and Kog1 were switched from YPL to SL medium for 3 h and then switched back to SD medium for the indicated times. Immunoprecipitation was performed as described in (A).

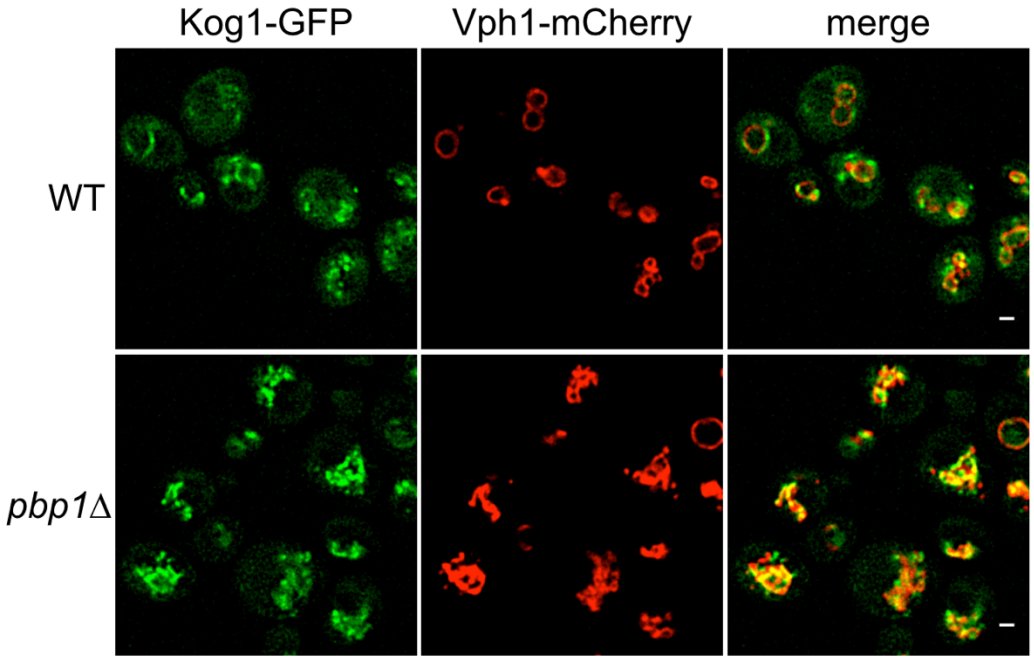

Figure 2-14. More TORC1 appeared associated with vacuole membranes in *pbp1*Δ cells.

Images of Kog1-superfolderGFP expressed at endogenous levels in WT and *pbp1*Δ cells in SL medium. Vph1: vacuolar membrane protein. Scale bar = 1 um.

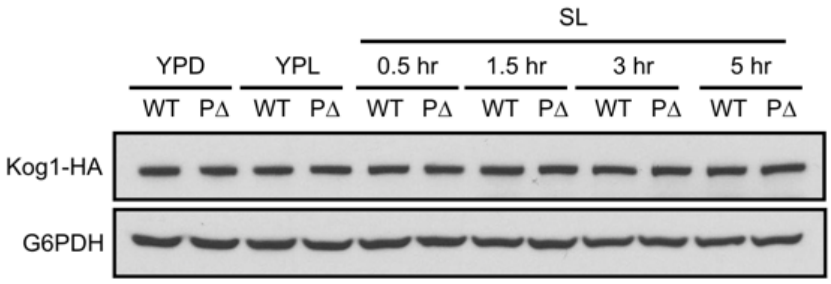

Figure 2-15. The protein level of Kog1 did not change in *pbp1*Δ cells in SL medium.

Western blot showing the protein level of Kog1 in YPD, YPL and various time points after switching to SL medium. pΔ: *pbp1*Δ.

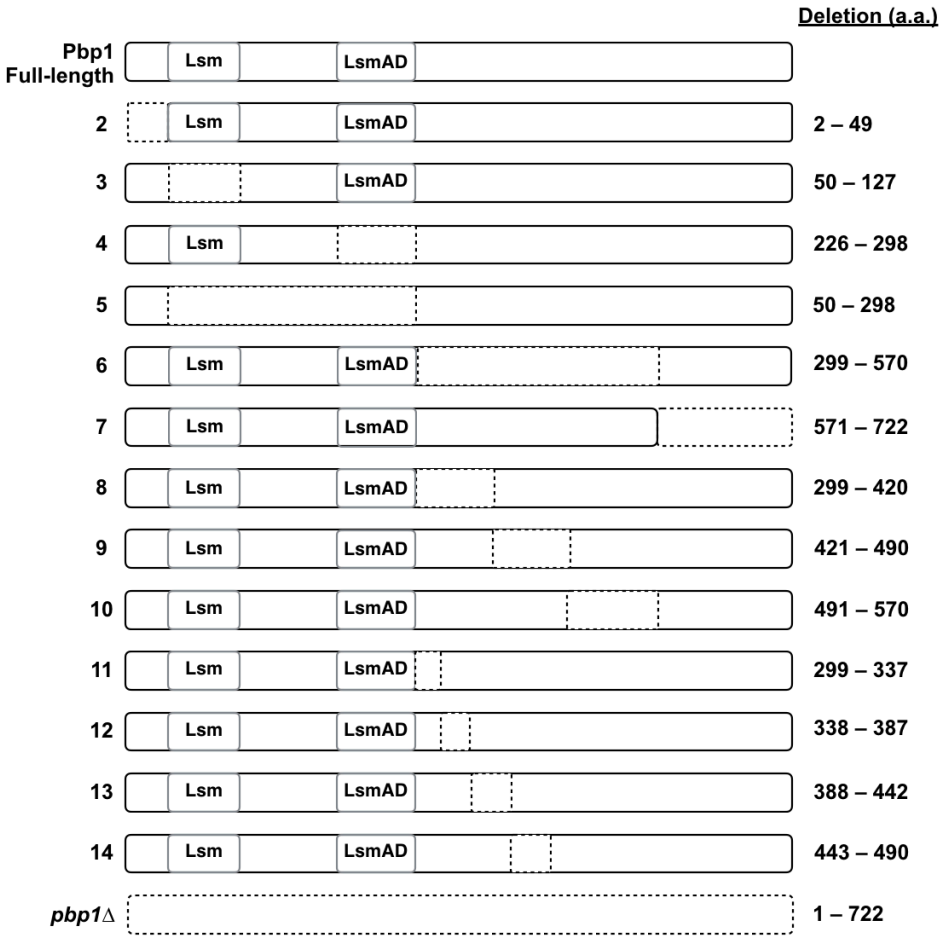

Figure 2-16. Schematic representation of Pbp1 deletion mutants.

Dotted lines indicate the deleted region. These deletion mutants were assayed for their ability to interact with Kog1 (Figure 2-17 and 2-18)

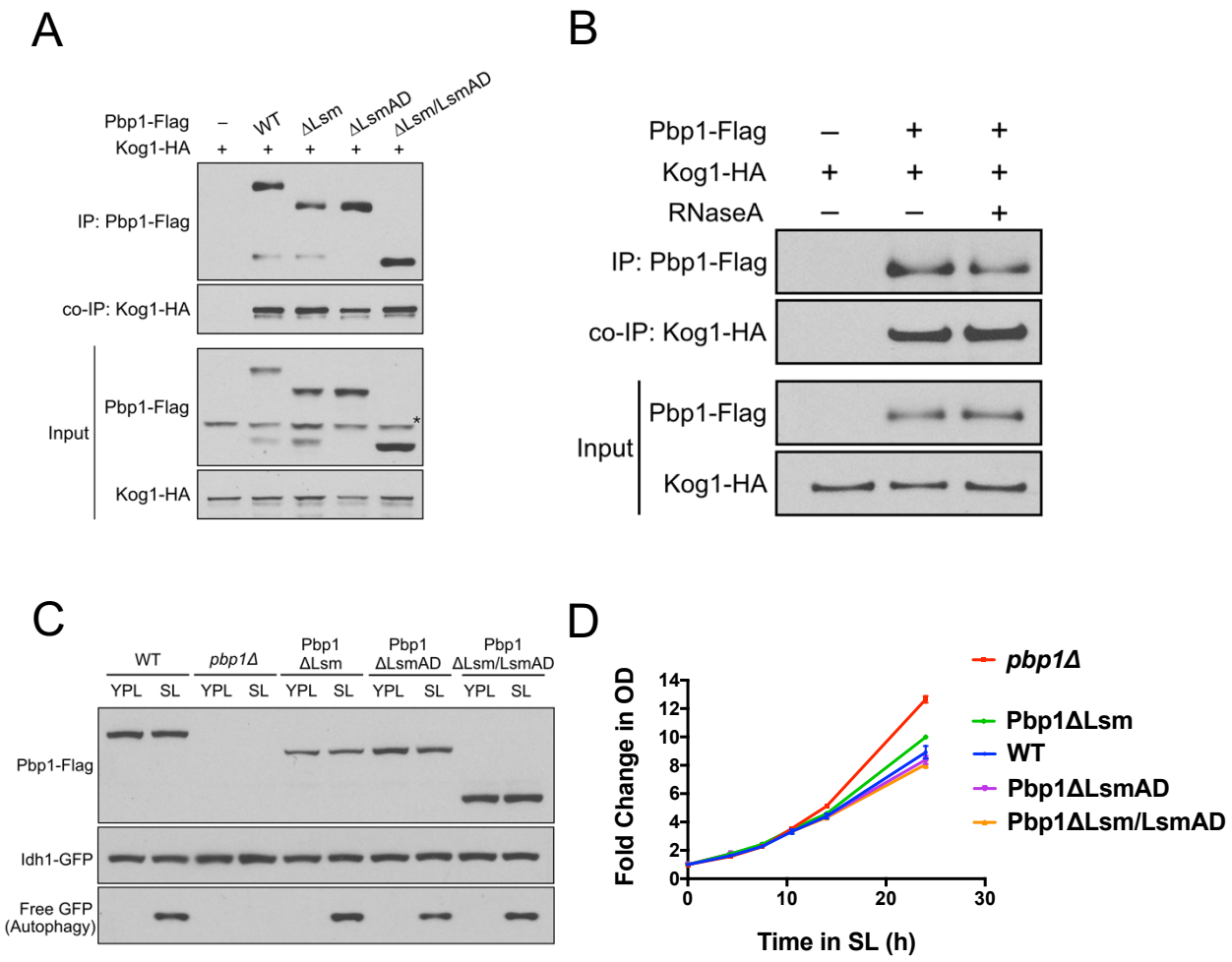

Figure 2-17. The ability of Pbp1 to self-associate and inhibit TORC1 is independent of RNA binding.

(A) Pbp1 variants lacking individual or both RNA-binding domains could still interact with Kog1. Cells were switched from YPL to SL medium for 3 h and immunoprecipitation was performed as described in Figure 2-13(A). *non-specific band. (B) RNase A treatment did not affect the interaction between Kog1 and Pbp1. 200 µg/ml RNase A was added to cell lysates before immunoprecipitation of Pbp1. (C) GFP cleavage assay showing autophagy in cells expressing Pbp1 mutants lacking the putative RNA-binding domains alone or in combination. Deletion of these domains did not affect autophagy. (D) Growth curves of cells expressing the indicated variants of Pbp1. Data were mean ± s.d. from 3 independent experiments.

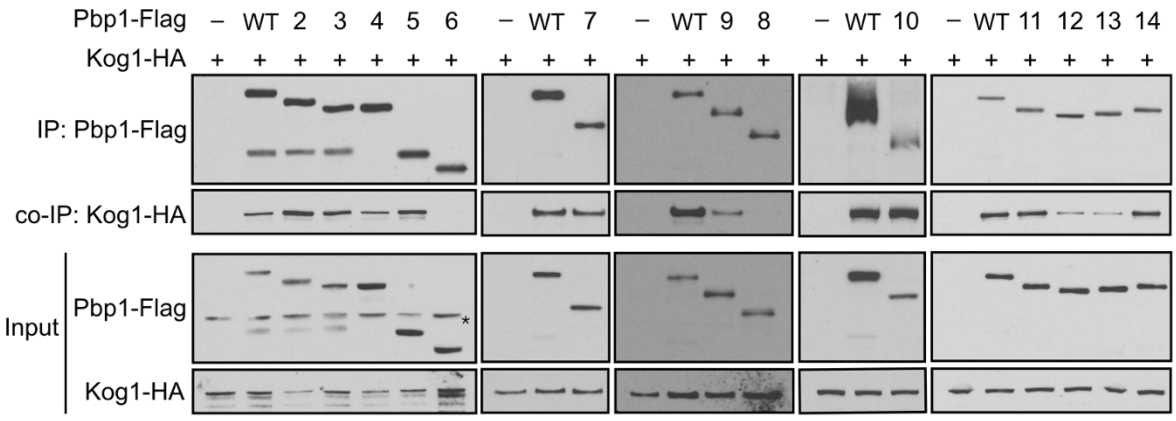

Figure 2-18. Pbp1 interacts with Kog1 via a.a. 338-442.

Immunoprecipitation assessing the interaction between Kog1 and various Pbp1 deletion mutants shown in Figure 2-16. Cell culture and immunoprecipitation were performed as described in Figure 2-13(A). Note that the Pbp1 mutants lacking a.a.338-442 (mutant 6, 8, 9, 12, 13) showed reduced interaction with Kog1. *non-specific signal

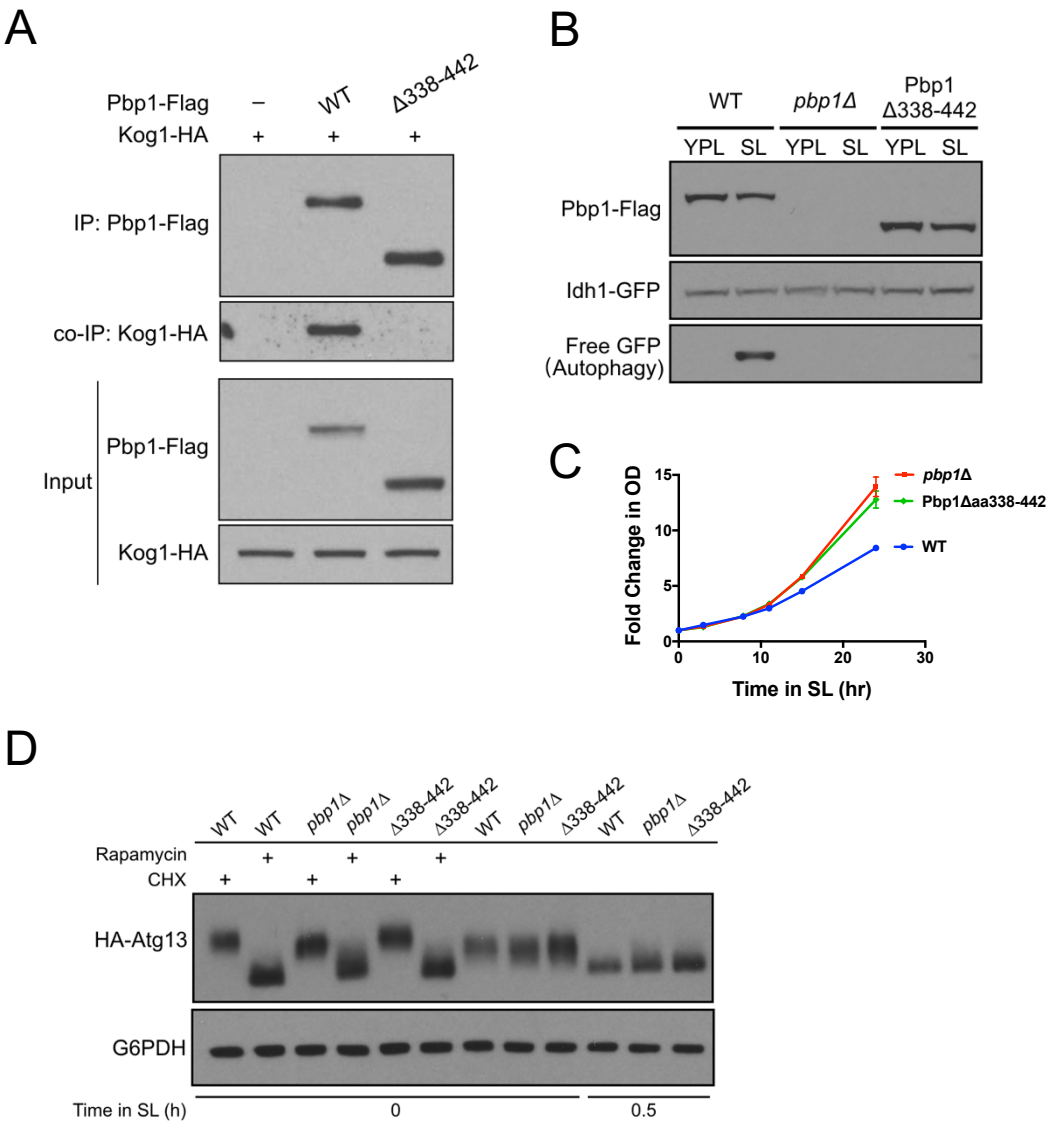

Figure 2-19. a.a. 338-442 on Pbp1 is required for TORC1 regulation.

(A) Pbp1 mutant lacking a.a.338-442 (Pbp1Δ338-442) was unable to interact with Kog1. Cells were switched from YPL to SL medium for 3 h and immunoprecipitation was performed as described in 2-13 (A). (B) GFP cleavage assay. Cells expressing Pbp1Δ338-442 exhibited reduced autophagy after switching to SL medium. (C) Pbp1Δ338-442 exhibited similar growth compared to *pbp1*Δ cells in SL medium. Data were mean ± s.d. from 3 independent experiments. (D) Pbp1Δ338-442 showed increased phosphorylation of endogenously tagged Atg13 similar to *pbp1*Δ cells.

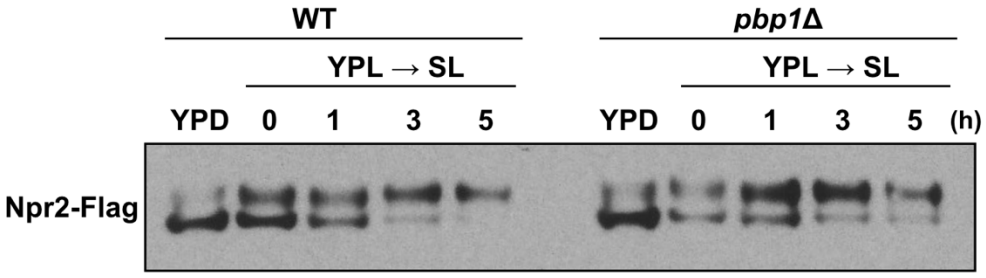

Figure 2-20. Deletion of *pbp1* does not affect Npr2 phosphorylation.

Western blot showing the phosphorylation of Npr2 in YPD, YPL, and various time points after switching to SL medium. Phosphorylated species exhibit reduced migration on SDS-PAGE.

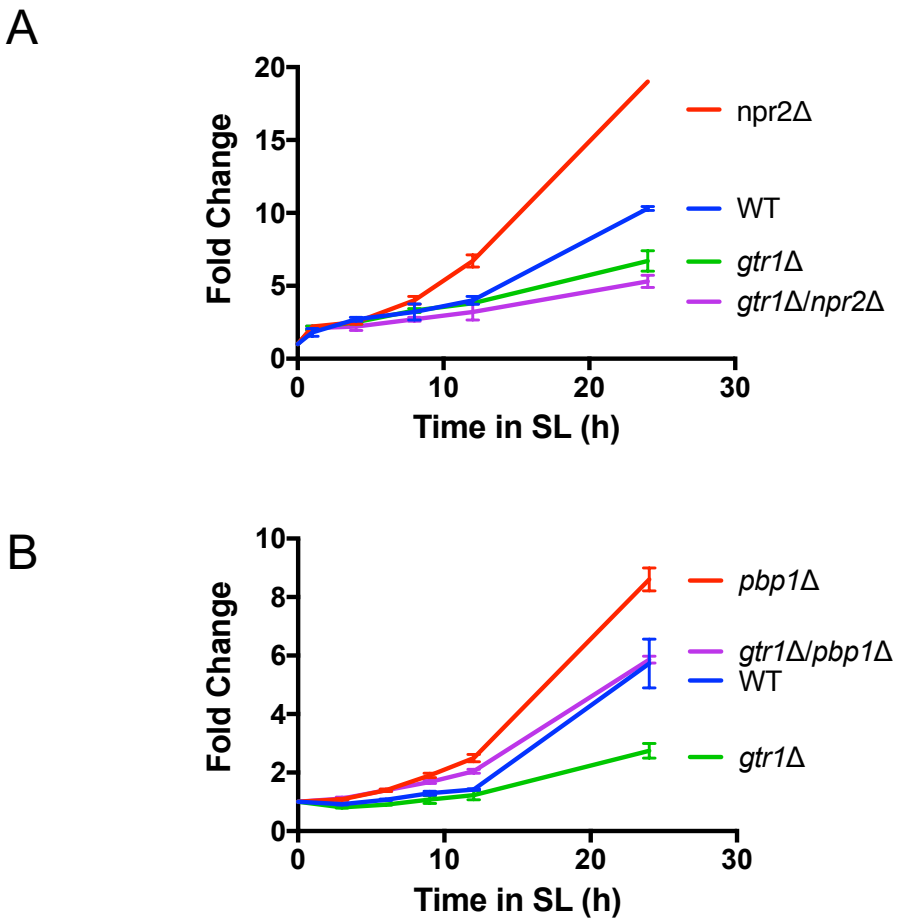

Figure 2-21. *pbp1* knockout and *gtr1* knockout have an additive effect on cell growth.

Growth of WT, *npr2*Δ, *gtr1*Δ, and *npr2*Δ/*gtr1*Δ cells (A) or WT, *pbp1*Δ, *gtr1*Δ, and *pbp1*Δ/*gtr1*Δ cells (B) in SL medium. Deletion of *gtr1* greatly reduced cell growth. Further deletion of the upstream regulator, *npr2*, showed a similar growth phenotype. Further deletion of *pbp1* instead rescued the growth of *gtr1*Δ cells. Data were mean ± s.d. from 3 independent experiments.

Note: The growth rates shown in (A) were measured by Lei Shi, Ph.D.

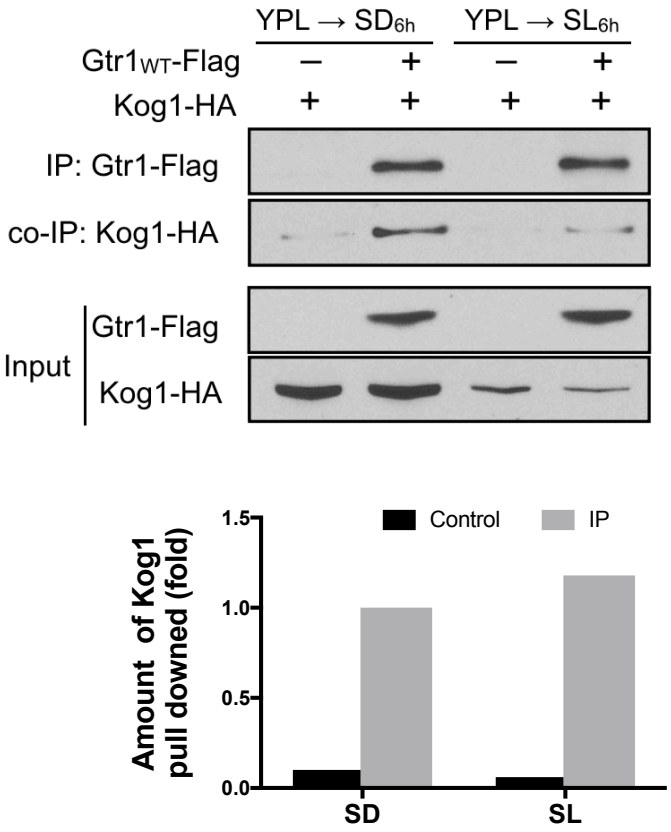

Figure 2-22. Gtr1 primarily interacts with Kog1 in SD.

Gtr1 interacts with TORC1 component Kog1 in cells grown in SD, but this interaction is reduced in cells grown in SL medium. Cells with endogenously tagged Gtr1 and Kog1 grown in YPL medium were switched to SD or SL medium for 6 h. Flag-tagged Gtr1 in cell lysates was immunoprecipitated with an anti-Flag antibody. Co-immunoprecipitation of Kog1-HA was detected by immunoblotting with anti-HA antibody. The band intensity of co-immunoprecipitated Kog1 was quantified using ImageJ and normalized with input.

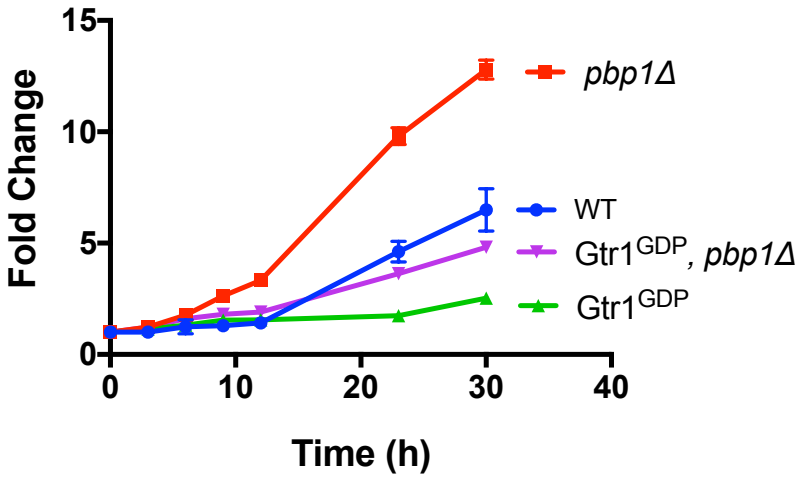

Figure 2-23. Deletion of *pbp1* significantly rescued the growth defect of cells expressing GDP-locked Gtr1.

Growth of WT, *pbp1*Δ, Gtr1^{GDP} (Gtr1 S20L)-expressing, and Gtr1^{GDP} -expressing *pbp1*Δ cells in SL medium. Gtr1^{GDP} was expressed from the original chromosomal locus. Expression of Gtr1^{GDP} limited cell growth, which can be partially rescued by *pbp1* knockout. Data were mean ± s.d. from 3 independent experiments.

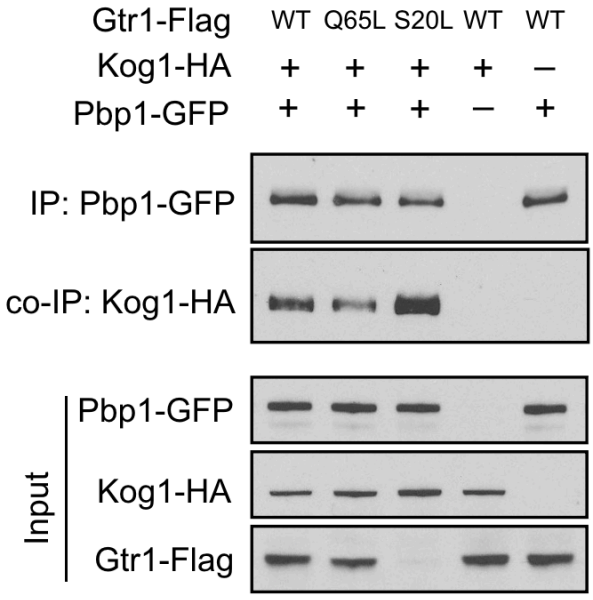

Figure 2-24. The nucleotide-binding state of Gtr1 affected the binding affinity between Pbp1 and Kog1.

Immunoprecipitation showing the binding affinity between Pbp1 and TORC1 component Kog1 in cells expressing $Gtr1^{WT}$, $Gtr1^{GTP}$ (Gtr1 Q65L), or $Gtr1^{GDP}$ (Gtr1 S20L). Cells with endogenously tagged Pbp1, Kog1, and Gtr1 grown in YPL medium were switched to SL medium for 3 h. GFP-tagged Pbp1 in cell lysates was immunoprecipitated with an anti-GFP antibody. Co-immunoprecipitation of Kog1-HA was detected by immunoblotting with anti-HA antibody. Note that the interaction between Pbp1 and Kog1 is the strongest in the presence of $Gtr1^{GDP}$. The expression level of $Gtr1^{GDP}$ was low due to the instability of this protein.

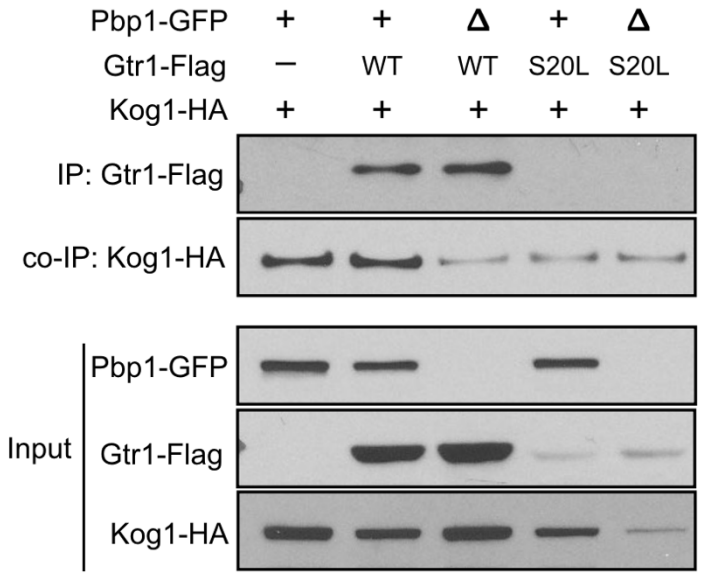

Figure 2-25. The interaction between Gtr1^{WT} and Kog1 decreased in the absence of Pbp1.

Immunoprecipitation showing the binding affinity between Gtr1^{WT} or Gtr1^{GDP} (Gtr1 S20L) and TORC1 component Kog1 in the presence or absence of Pbp1. The indicated strains were grown in YPL medium and then switched to SL medium for 3 h. Flag-tagged Gtr1 in cell lysates was immunoprecipitated with an anti-Flag antibody. Co-immunoprecipitation of Kog1-HA was detected by immunoblotting with anti-HA antibody. The expression level of Gtr1^{GDP} was too low to be immunoprecipitated.

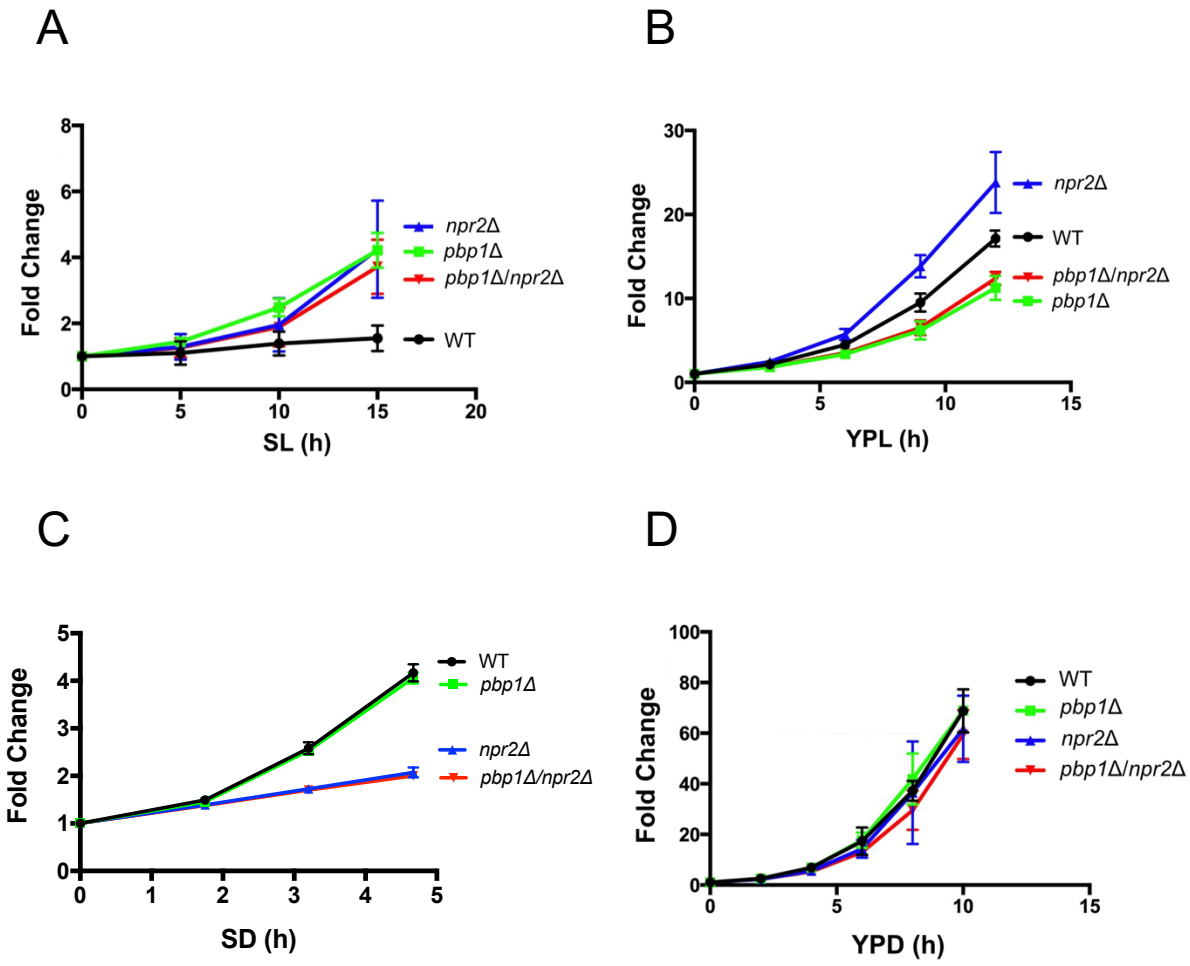

Figure 2-26. Growth phenotypes of *pbp1*Δ and *npr2*Δ cells vary with carbon sources and amino acid availability.

Growth of WT, *pbp1*Δ, *npr2*Δ, and *pbp1*Δ/*npr2*Δ cells in SL (A), YPL (B), SD (C), or YPD (D) medium. Data were mean ± s.d. from 3 independent experiments.

Table 2-1. List of proteins detected in SILAC experiment in *pbp1*Δ versus WT cells.

Only the proteins present at increased amounts in pbp1Δ in SL ((pbp1Δ / WT)SL > 1.5), but not in SCL (0.5 < (pbp1Δ / WT)SCL < 1.5) are listed.

Gene	(WT/*pbp1*Δ)$_{SCL}$	(WT/*pbp1*Δ)$_{SCL}$ Normalized	(WT/*pbp1*Δ)$_{SL}$	(WT/*pbp1*Δ)$_{SL}$ Normalized
GDH1	1.524181134	1.429408654	8.287063893	5.55771689
YHR033W	0.991473329	0.911327805	5.633168094	4.00930158
STL1	0.54062821	0.500225101	4.983057604	3.454231434
SRO9	1.201085782	1.161723533	4.331066742	3.080524921
JEN1	0.791452315	0.752105897	4.373305344	3.031772981
DLD3	0.700623555	0.655823715	3.972352427	2.762965214
SHM2	0.861549065	0.79001422	3.806188863	2.629848784
SAM1	1.36299204	1.285380087	3.214607175	2.297952524
MET6	1.033762689	0.958313368	3.19284802	2.133970679
NDE1	1.438041962	1.331557923	3.035361967	2.115059222
RNR1	1.289075089	1.234476459	2.942041777	2.110506099
ICL1	1.342263862	1.262945188	2.933927943	1.953239448
ILV5	1.005560751	0.926354794	2.869522798	1.922078921
ARO8	1.33336889	1.253808443	2.593293742	1.795009873
SAM2	1.292156609	1.205342076	2.603420895	1.787150389
YEF3	1.16623516	1.074402364	2.503881016	1.710893257
HOR2	1.441586899	1.384542962	2.578116943	1.70943093
HIS7	1.202848345	1.130799588	2.418496662	1.676811375
TRP5	1.400364095	1.305176329	2.495694926	1.653029176
ADE12	1.063433828	0.945984297	2.440750775	1.632359903
QCR6	1.07752815	1.057954762	2.263672582	1.628240198
GLN1	1.189867092	1.178369843	2.231594921	1.617651817
URA7	1.070904593	0.993936984	2.326934264	1.610902589
ILV3	0.993739442	0.96255655	2.365576136	1.605110672
ADE5,7	1.172841678	1.076855152	2.335139174	1.600051202
XRN1	1.345116554	1.278167619	2.299749327	1.591393743
ZEO1	1.403134603	1.291338989	2.133788542	1.584007857
ALD6	1.230224147	1.132413059	2.322179133	1.57713781
DED1	0.981450584	0.895014768	2.273192244	1.575994452
KRS1	1.345587147	1.25524063	2.274743523	1.567078808
PRE9	1.289257903	1.178592054	2.056978299	1.551566306
THS1	1.498037571	1.402878707	2.209407658	1.546551191
ADE3	1.064622591	1.010111213	2.075291578	1.543996171
NEW1	1.034928849	1.023604316	2.219558752	1.539219308
GUK1	1.186014517	1.10799641	2.223309173	1.535956747
CYS3	0.898795614	0.825695649	2.214103841	1.533436585
ADE6	0.863483292	0.787525595	2.215722769	1.53313096
ARO2	1.005338347	0.946611132	2.23588597	1.533013445
LEU1	1.458512609	1.357330944	2.267059624	1.529917537
ADO1	1.144649337	1.054874575	2.238538682	1.522371245

Table 2-2. List of ribosomal proteins detected in SILAC experiment in *pbp1*Δ/WT cells.

Gene	(*pbp1*Δ/WT)$_{SCL}$ Normalized	(*pbp1*Δ/WT)$_{SL}$ Normalized	Gene	(*pbp1*Δ/WT)$_{SCL}$ Normalized	(*pbp1*Δ/WT)$_{SL}$ Normalized
AIM21	0.506816684405251	1.24404413868604	**RPL6B**	0.853825136612022	1.08493994857385
ARB1	1.02043940120616	0.901306894997747	**RPL7A**	0.889917237696894	1.01020305081321
ASC1	0.858295425285383	1.02213954249034	**RPL8A**	0.854627809588924	1.08649594193766
CDC48	1.29962960556241	1.20506609787547	**RPL8B**	0.934841544358231	1.07350273206445
EFT1	1.09381665445238	1.01151099512452	**RPL9B**	0.862663906142167	1.0334635497406
FUN12	0.85426277122843	0.9379103357719	**RPP0**	0.936592675845275	1.06382978723404
GCN1	1.1026330878137	0.918189330639978	**RPS10A**	0.869716472429988	1.02314350610817
HYP2	1.01222771074581	1.22019669570735	**RPS11A;RPS11B**	0.871991628880363	1.02597775680223
NOP1	0.827746047512623	0.927471712112781	**RPS12**	0.874584572328144	1.08168916580132
PAB1	1.00765820233777	1.17336462305661	**RPS13**	0.887390185464549	1.03834612229641
RLI1	0.934142923867352	1.03323930855625	**RPS14A;RPS14B**	0.848032564450475	1.16133228039207
RPL10	0.878734622144113	1.13174662456569	**RPS15**	0.831186102568365	1.08800905223531
RPL11A;RPL11B	0.846238470000846	0.998801438274071	**RPS16A;RPS16B**	0.874508089199825	1.13840759545548
RPL12A;RPL12B	0.878657411475266	1.12247303258539	**RPS17A;RPS17B**	0.896860986547085	1.12436613858937
RPL13A;RPL13B	0.893974611121044	1.14492454947219	**RPS18A;RPS18B**	0.867227473766369	1.07502606938218
RPL14A;RPL14B	0.86095566078347	1.11870588103682	**RPS19A;RPS19B**	0.916926462497708	1.14678899082569
RPL15A	0.878271561566836	0.960061443932412	**RPS1A**	0.887390185464549	0.95565749235474
RPL16B	0.838926174496644	1.09761050193728	**RPS1B**	0.867754251995835	0.950931913275009
RPL17A	0.842176183257538	1.10821743226021	**RPS2**	0.840265523905554	1.04558762024258
RPL17B	0.825218682950982	1.05079545215728	**RPS20**	0.889600569344364	1.04891070623158
RPL18A;RPL18B	0.872981230903536	1.00500492452413	**RPS22A;RPS22B**	0.92910898448388	1.04625493047636
RPL19A;RPL19B	0.806451612903226	1.06398825356968	**RPS23A;RPS23B**	0.829393713195654	1.0294526400313
RPL1A;RPL1B	0.935366195865681	1.00158250035055	**RPS24A;RPS24B**	0.908843042806507	1.13636363636364
RPL20A;RPL20B	0.881600987393106	1.11563563340213	**RPS25A;RPS25B**	0.814796708221299	1.04948312955869
RPL23A;RPL23B	0.879816998064403	1.07247806782351	**RPS26A;RPS26B**	0.878117316473481	1.09780329560549
RPL24A;RPL24B	0.884173297966401	1.05002310050821	**RPS27A;RPS27B**	0.880049282759835	1.13379970294448
RPL25	0.919540229885058	1.12875735103225	**RPS28A;RPS28B**	0.91869545245751	1.31157861602224
RPL26B	0.884173297966401	1.12875735103225	**RPS3**	0.891981090000892	1.01032552688476
RPL27A;RPL27B	0.880824451686779	1.11599669664978	**RPS4A;RPS4B**	0.894934669769107	1.04257892322449
RPL28	0.857118368046627	1.05852589683607	**RPS5**	0.91844232182219	1.0663368131458
RPL29	0.849617672047579	1.09808055518953	**RPS6A;RPS6B**	0.907441016333938	1.08504589744146
RPL2A;RPL2B	0.893655049151028	1.11918165437432	**RPS7A**	0.873820342537574	1.13193878475052
RPL3	0.864154856550294	0.98135426889107	**RPS7B**	0.957395883197702	1.27437237160698
RPL30	0.991866693116445	1.15993133206514	**RPS8A;RPS8B**	0.862366333218351	1.06455459035939
RPL31A;RPL31B	0.879120879120879	1.16268254115896	**RPS9B**	0.870397771781704	1.1016491688057
RPL32	0.84573748308525	1.07842291433008	**SUI2**	0.909173561232839	1.01428107757222
RPL33A	0.886367665307569	1.16276365665915	**TEF1**	1.01801893515219	1.05784284686667
RPL34A;RPL34B	0.854116843184148	1.07538444994085	**TEF4**	1.06508749693787	1.06772585071057
RPL35A;RPL35B	0.849112677252271	1.14004286561175	**TIF3**	0.977517106549365	1.38108193959148
RPL36A;RPL36B	0.847960654625625	1.09638303237619	**TIF5**	0.746380056724884	0.861252260787185
RPL38	0.853096741170449	1.08218081076986	**TMA19**	0.884329678103997	1.15195429045375
RPL43A;RPL43B	0.974848898420745	1.27347978350844	**YEF3**	1.0744023636852	1.71089325736967
RPL4A	0.867453157529493	1.09841827768014	**YGR054W**	0.843810648890389	0.905961224859576
RPL5	0.888967908258512	1.01766669380445	**YMR31**	1.2028338766133	1.3802241484017
RPL6A	0.875120329045244	1.12598664579838	**ZUO1**	1.0014821936466	1.25140783381304

CHAPTER THREE :

THE LOW COMPLEXITY REGION OF PBP1 AND ITS PHYSIOLOGICAL ROLE

PBP1 PHASE SEPARATES TO INHIBIT TORC1 DURING RESPIRATORY GROWTH

Introduction

In chapter two, I have demonstrated that Pbp1 is required for TORC1 inhibition specifically under amino acid-deprived respiratory condition when cells are heavily dependent on mitochondria.

Under stressful conditions such as heat shock, TORC1 is regulated by stress granules(Takahara et al., 2006). Ectopic formation of stress granules by Pbp1 overexpression in unstressed cells sequesters TORC1 in this compartment, thereby reducing TORC1 signaling (Takahara and Maeda, 2012). However, whether this is the mechanism through which TORC1 is inhibited by Pbp1 in SL medium is not clear.

Phase separation of proteins to form membrane-free intracellular compartments is thought to perform diverse functions in a variety of cellular processes, including the stress response, and the control of signal transduction. The molecular determinants of protein phase separation are widely studied. One well-accepted feature of the proteins that phase separate is

the presence of intrinsically disordered regions (IDRs) or low complexity (LC) domains (Banani et al., 2017; Kato et al., 2012; Lin et al., 2015).

Pbp1 possess long intrinsic disordered and low complexity regions outside of the two putative RNA-binding domains. It has been noted that the C-terminus of Pbp1 is methionine- and proline-rich (Mangus et al., 1998). Using yeast-two-hybrid, this previous study showed that this region mediates the binding of Pbp1 to Pab1 (Poly(A)-binding protein 1). Whether this low complexity region has other functions beyond Pab1-binding, remains to be elucidated.

In this chapter, I will provide evidence to demonstrate that Pbp1 self-associates into intracellular assemblies in response to the metabolic state. The low complexity region of Pbp1 forms labile fibrils with cross-β structure *in vitro* and mediates Pbp1 self-association *in vivo*. Mutants that weaken phase separation *in vitro* exhibit reduced capacity to inhibit TORC1 and induce autophagy.

Many low complexity domains are characterized by enriched numbers of tyrosine and/or phenylalanine residues, and phase separation of these low complexity domains is impeded upon mutational change of these aromatic residues to serine (Han et al., 2012; Kato et al., 2012). Moreover, many subsequent studies have confirmed the importance of these aromatic residues widely distributed among many LC domains that are subject to phase separation into either liquid-like droplets or hydrogels (Lin et al., 2017; Wang et al., 2018; Xiang et al., 2015). Instead of the aromatic amino acids, the LC region of Pbp1 contains many methionines. In this chapter, I will also discuss the importance of these methionines in TORC1 inhibition and autophagy regulation.

Results

The regulation of TORC1 by Pbp1 does not involve stress granule formation

To investigate how Pbp1 regulates TORC1 signaling, I examined a possible link to Pbp1 as a component of stress granules (Buchan et al., 2008). Under severe heat stress, Pbp1 was reported to sequester TORC1 in foci-like stress granules, which prevent TORC1 activation (Takahara and Maeda, 2012). However, in cells expressing normal amounts of Pbp1-GFP, Pbp1 did not form any structures reminiscent of defined, foci-like granules in SL medium (Figure 2-26). Two other stress granule markers, Pab1 and Pub1, also did not localize to foci-like granules in SL medium as compared to the glucose deprivation medium (Figure 3-2). Instead, Pbp1 exhibited a non-uniform distribution, and the protein appeared to be present in the form of nebulous assemblies throughout the cell, reminiscent of a condensate (Banani et al., 2017) (Figure 3-1). Cycloheximide, which reportedly inhibits stress granule formation by depleting the pool of non-translating mRNAs (Mangus et al., 1998; Mangus et al., 2004b), did not change the distribution pattern of Pbp1 within cells (Figure 3-2). Interestingly, in glucose medium, Pbp1 exhibited a more uniform distribution throughout the cytoplasm (Figure 3-1).

To better define the subcellular localization of Pbp1, I tested for possible co-localization with various organelle markers. Pbp1 did not co-localize with membrane-bound organelles, such as vacuole, endoplasmic reticulum, and mitochondria (Figure 3-3). Using live-cell imaging, we further observed that the Pbp1 assemblies were very dynamic in SL medium.

To better visualize the nebulous assemblies of Pbp1 in cells, I adopted two strategies – increasing the resolution of Pbp1-GFP images, or overexpressing Pbp1.

Pbp1-yoEGFP showed a clearer pattern of non-homogenous distribution

The resolution of fluorescence images is determined by multiple factors including the light source of the microscope, the numerical aperture of the lens, the refractive index of the specimen medium, and the quantum yields of the fluorophore used. yoEGFP (yeast optimized enhanced GFP) is reported to be brighter and more photostable compared to the conventional GFP (Lee et al., 2013). Indeed, when imaged under the same conditions as Pbp1-GFP, Pbp1-yoEGFP showed a more distinct nebulous pattern – the distribution of Pbp1 is clearly not homogenous, it was highly enriched at certain regions within a cell (Figure 3-4).

Overexpressing Pbp1 driving by TEF promoter did not significantly change the distribution pattern in SL medium

Pbp1 is a component of stress granules (Buchan et al., 2008). It has been shown that overexpression of Pbp1 induces stress granule formation, where TORC1 is sequestered (Takahara and Maeda, 2012). In addition, when the overexpression of Pbp1 was induced by galactose, Pab1, a binding protein of Pbp1, formed aggregate-like structures that appeared to be strung together into a fibrillary morphology (Swisher and Parker, 2010). Consistent with my observation, the Pab1 aggregates seen when Pbp1 was over-expressed was not as severely affected by cycloheximide addition (Swisher and Parker, 2010). These data implied that when

overexpressed, Pbp1 forms foci-like or string-like structures, perhaps determined by the carbon sources and/or expression levels. Accordingly, I expressed Pbp1 under its own promoter from a plasmid bearing a centromere and origin of replication (CEN/ARS) in WT cells, which resulted in ~2 fold expression of Pbp1 compared to WT. However, 2-fold expression of Pbp1 did not change its distribution pattern when imaged under fluorescence microscope (Figure 3-4). To further increase the expression level of Pbp1, I swapped the Pbp1 promoter on the above-mentioned plasmid with a stronger TEF1 promoter, but no significant changes were observed (Figure 3-4). Perhaps an even higher expression level needs to be achieved in order for Pbp1 to form exclusive assemblies.

Pbp1 self-associates in cells grown in respiratory growth condition

It has previously been suggested that Pbp1 has the potential to homo-multimerize (Mangus et al., 1998), which could explain its ability to form assemblies (Figure 3-1).

Immunoprecipitation experiments showed Pbp1 with different tags interact with each other

Using diploid cells expressing two different epitope-tagged versions of Pbp1, we examined the ability of Pbp1 to self-interact as assessed by co-immunoprecipitation from cell extracts. Pbp1 was strongly self-associated in extracts from cells grown in SL medium, in contrast to cells grown in SD (Figure 3-5A). Such interactions were also detected following lysis and subsequent mixing of extracts obtained from two haploid strains, each expressing a different tagged version of Pbp1 (Figure 3-5B). These data indicate that not only does Pbp1

have a propensity to self-associate, but that such self-association is highly dynamic. Furthermore, the addition of glucose to cells growing in SL medium gradually reduced the ability of Pbp1 to self-associate (Figure 3-5C). Therefore, the ability of Pbp1 to interact with both itself and Kog1 is dynamic and responsive to cellular metabolic state.

Pbp1 forms pelletable assemblies under respiratory condition

Fractionation experiments showed that in cells grown in SL medium, the majority of Pbp1 protein was present in the pellet fraction, consistent with the idea that it may form large protein assemblies under such conditions (Figure 3-6). However, in cells grown in glucose, substantial amounts of Pbp1 were present in the soluble fraction, in addition to the pellet fraction (Figure 3-6). To summarize, I observed a strong correlation between the appearance of non-uniform Pbp1-containing substructures as visualized by fluorescence microscopy and the presence of Pbp1 protein in the pellet fraction following centrifugation. Taken together, these observations indicate that at normal expression levels and physiological temperatures, Pbp1 does not form foci-like granules and is instead present in the form of pelletable assemblies during respiratory growth, which may play a role in the negative regulation of TORC1.

A C-terminal low-complexity (LC) region of Pbp1 phase separates and forms labile fibrils of cross-β structure *in vitro*

Sequence analysis revealed two low complexity regions on Pbp1

I next tried to identify regions of Pbp1 which were required for self-association and perhaps the inhibition of TORC1. Sequence analysis of Pbp1 revealed two characteristically special regions downstream of the putative RNA-binding domains. These two regions are of low-complexity (LC) and intrinsically disordered (Figure 3-7), which are features of proteins that have a tendency to self-assemble or aggregate (Han et al., 2012; Molliex et al., 2015).

Purifying Pbp1 fragments containing the low complexity regions

To determine whether these two low-complexity (LC) regions contribute to the self-association of Pbp1, I designed and made 12 constructs each containing different regions covering these two LC regions (Figure 3-8). In collaboration with Masato Kato, Ph.D. in the McKnight lab in the Department of Biochemistry at UT Southwestern Medical Center, these 12 fragments were expressed and purified using bacterial expression system. The initial protein solubility test showed that all 12 of these proteins were present in the inclusion body (Figure 3-9). To purify these proteins from the inclusion body, we used a lysis buffer containing 2 M guanidine hydrochloride and successfully obtained these Pbp1 fragments.

The C-terminal LC region of Pbp1 forms fibrils of cross-β structure

Upon examination of all 12 purified Pbp1 fragments using transmission electron microscopy, we observed apparent fibrils formed by a fragment containing the C-terminal LC

region of Pbp1 (a.a. 570-722) (Pbp1_LC hereafter) (Figure 3-8-fragment 4, 3-10). Other fragments either remained soluble, formed very short fibrils, or aggregated (Figure 3-10).

The fibrils form by Pbp1_LC were 10-20 nm in length. X-ray diffraction analysis of Pbp1_LC yielded a characteristic diffraction pattern with circular reflections at 4.7 A and 10 A, indicating that the fibrils are of cross-β structure (Figure 3-11) (Astbury et al., 1935; Geddes et al., 1968; Sunde and Blake, 1997).

The purified Pbp1_LC phase separates into droplets

We further assessed the biochemical features of this C-terminal LC region. Upon lowering the salt concentration to physiological levels, this purified fragment readily phase-separated into droplets *in vitro* (Figure 3-12A), and the droplets were stable within the time observed (24 h). In addition, these Pbp1_LC droplets were sensitive to 1,6-hexanediol, an alcohol commonly used to disrupt weak hydrophobic interactions and disturb phase separation (Lin et al., 2016; Molliex et al., 2015; Ribbeck and Gorlich, 2002; Romero et al., 2007). The droplets exhibited higher sensitivity to 1,6-hexanediol compared to 2,5-hexanediol (Figure 3-12B), which can be a property of proteins that phase separate (Kroschwald et al., 2015; Lin et al., 2016; Shi et al., 2017). Consistent with the phase-separated droplets, the Pbp1_LC fibrils were also more sensitive to 1,6-hexanediol (Figure 3-12C).

The Pbp1_LC fibrils are not SDS-resistant

The prion-like fibers of cross-β structure described broadly throughout the literature are thought to be irreversible and pathological (Harrison et al., 2001; Murakami et al., 2015; Patel et al., 2015; Takeda and Klimov, 2008). To examine the stability of Pbp1_LC fibrils, we applied semi-denaturing detergent agarose gel electrophoresis (SDD-AGE) to compare them with those generated from the yeast Sup35 protein (Wickner, 1994). After 10 min incubation at 37℃ with 0%, 0.5%, 1%, or 2% of SDS, the Sup35 fibers were still completely resistant to even the highest level of SDS tested (2%). By contrast, the Pbp1_LC fibrils were highly labile, and completely disassembled upon incubation at 37°C in the absence of SDS (Figure 3-13). It thus appears that despite sharing cross-β structural properties, the Pbp1_LC must be fundamentally and functionally different from the prion-like, irreversible fibers.

The C-terminal low-complexity (LC) region of Pbp1 is required for inhibition of TORC1

The C-terminal LC region enables Pbp1 to self-associates in vivo

The phase-separated droplets and fibrils form by the purified Pbp1_LC in vitro demonstrated its self-association propensity. To examined whether this C-terminal LC region of Pbp1 enables the self-association of full-length Pbp1 in cells, I expressed a variant of Pbp1 lacking the C-terminal LC region (Pbp1ΔLC) (Figure 3-14A) in diploid cells with two different tags, and assayed self-association using immunoprecipitation. In contrast to full-length Pbp1,

Pbp1ΔLC showed reduced ability to self-associate (Figure 3-14B). Moreover, the Pbp1ΔLC mutant was less concentrated in the pellet after fractionation (Figure 3-14C).

Pbp1ΔLC also exhibited a more uniform distribution pattern throughout the cytosol compared to full-length Pbp1 protein (Figure 3-15). Taken together, these data indicate that the self-association of Pbp1 in cells is mediated by the C-terminal LC region.

The C-terminal LC region is required for TORC1 inhibition

Next, I tried to determine whether this region might be necessary for regulating TORC1 signaling. Upon assessment of its function *in vivo*, this mutant exhibited increased phosphorylation of Atg13 (Figure 3-16A), reduced autophagy (Figure 3-16B), and an increased growth phenotype indistinguishable from *pbp1*Δ cells (Figure 3-16C). These results suggested that the C-terminal LC region, and hence the self-association of Pbp1, is required for TORC1 inhibition.

Methionine residues in the C-terminal LC region of Pbp1 influence stability of phase separation and are critical for inhibition of TORC1

Pbp1 C-terminal LC region has extraordinarily high methionine content

Sequence analysis of the Pbp1 C-terminal LC region revealed an unusually high frequency of methionine residues compared to the rest of the yeast proteome (Figure 3-17A and 3-17B). Pbp1_LC contains 24 methionines in 150 a.a., which is the third highest among

the entire yeast proteome. The protein that contains the highest and second highest number of methionine are Srp54 (32 methionines in 150 a.a.) and Ctr1 (30 methionines in 150 a.a.), respectively.

The methionine residues located near the center of Pbp1 C-terminal LC region are important for autophagy regulation and fibril formation

To test the importance of the methionines in the C-terminal LC region, we constructed a series of C-terminal truncation mutants lacking increasing numbers of methionine residues (Figure 3-18A), and examined their ability to induce autophagy in SL medium (Figure 3-18B).

We observed that a Pbp1 mutant lacking a region containing the last 8 methionines (M_{17}-M_{24}) (Figure 3-18B, mutant (2)) could still induce autophagy, but further deletion of a region that contains M_{11}-M_{16} significantly reduced autophagy (Figure 3-18B), suggesting the importance of this subset of methionines for function.

Simultaneously, I constructed 12 mutants of Pbp1_LC each bearing 2 methionine to serine substitutions (Figure 3-19). By mutating pairs of adjacent methionine residues, we observed differential effects among these mutation pairs on Pbp1_LC fibril formation. The mutant Pbp1_LC harboring $M_{11\text{-}12} \rightarrow$S substitutions exhibited the weakest ability to form fibrils *in vitro,* we observed almost no fibrils under electron microscope (Figure 3-20). The mutants harboring M → S substitutions on immediately upstream and downstream of $M_{11\text{-}12}$ (i.e. $M_{7\text{-}8} \rightarrow$S, $M_{9\text{-}10} \rightarrow$S, or $M_{13\text{-}14} \rightarrow$S) also showed significantly impaired fibril formation ability. Mutations on other methionines showed modest ($M_{1\text{-}2} \rightarrow$S, $M_{3\text{-}4} \rightarrow$S, $M_{5\text{-}6} \rightarrow$S, or $M_{15\text{-}}$

$_{16}$ →S) to no effect (M_{17-18} →S, M_{19-20} →S, M_{21-22} →S, or M_{23-24} →S) on fibril formation (Figure 3-20).

A set of methionine residues in the C-terminal LC region of Pbp1 influence stability of phase separation and are critical for inhibition of TORC1

These two results both indicated that the methionine residues around M_{11-12} could be of the most importance. We therefore mutated M_{11}, M_{12} and immediately upstream and downstream methionine residues to serine, to generate a series of mutants containing 2, 4, 6, or 8 M→S mutations (Figure 3-21A).

Substitution of methionine to serine decreases the stability of Pbp1_LC droplets

All of the mutant combinations tested still phase-separated into droplets (Figure 3-21B). However, variants harboring increasing numbers of methionine mutations significantly decreased the stability of phase separated droplets as the droplets dissolved more readily upon lowering the protein concentration (Figure 3-21C). Using fluorescence recovery after photobleaching (FRAP) assay, we observed that the Pbp1_LC M_{7-14}S droplets were able to recover much faster compared to WT droplets (Figure 3-22A, 3-22B), consistent with their decreased stability. Therefore, the functional WT Pbp1_LC region exhibits slower FRAP and is more solid-like, whereas a non-functional mutant *in vivo* exhibits faster FRAP and is more liquid-like.

Substitution of methionine to serine on full-length Pbp1 decreases autophagy in cells

We then tested the effect of these M → S mutations on the ability of full-length Pbp1 to induce autophagy. Strikingly, increasing the number of M → S substitutions within this region gradually reduced the ability of Pbp1 to induce autophagy in cells. In particular, the M_{7-14}S mutant exhibited severely reduced autophagy (Figure 3-23). Moreover, this mutant protein was less concentrated in the pellet fraction, with a substantial amount instead present in the soluble fraction (Figure 3-23).

To confirm the importance of M_{7-14} on Pbp1's function, I made a Pbp1 variant harboring M → S substitutions on M_{17-24}, which had no effect on fibril formation (Figure 3-24A). In contrast to cells expressing Pbp1 M_{7-14} which had greatly reduced autophagy, Pbp1 M_{17-24} showed a level of autophagy comparable to WT cells (Figure 3-24B).

Taken together, the M → S substitutions within the C-terminal LC region of Pbp1 have a negative effect on Pbp1's function. We observed a strong correlation between the decreased stability of phase-separated droplets *in vitro*, and the decreased ability of the protein to sediment to the pellet and induce autophagy in live cells.

Substitution of methionine to phenylalanine/tyrosine on full-length Pbp1 enhances autophagy

To test whether increasing number of the aromatic amino acids causes Pbp1 to be more prone to self-associate and thereby enhance autophagy induction, I substituted the 8 methionines (M_{7-14}) within the C-terminal LC region of Pbp1 to either phenylalanine or tyrosine (Figure 3-25A). These M → F and M → Y variants caused increased amounts of Pbp1

to sediment to the pellet fraction (Figure 3-25B). By contrast, the M → S variant was observed to destabilize the assemblies as deduced by the presence of increased amounts of Pbp1 in the soluble fraction of cellular lysates. Consistently, cells expressing Pbp1 variants harboring increased number of M → F or M → Y substitutions exhibited increased autophagy compared with WT cells (Figure 3-25C). In particular, the $M_{7\text{-}14}F$ and $M_{7\text{-}14}Y$ mutant exhibited the strongest autophagy.

Discussion

In chapter two, I described Pbp1 as a bona fide negative regulator of TORC1 signaling whose function becomes especially important when cells heavily utilize mitochondria for energy production. The binding between Pbp1 and TORC1 mediated by a.a. 338-442 of Pbp1 is required for this regulation. However, we further identified an unusual, methionine-rich low complexity region of Pbp1 that is also required for the inhibition of TORC1. This LC region readily phase separates to form droplets in vitro. Mutational analysis revealed a specific subset of methionine residues that weaken phase separation. Importantly, these same methionines are critical for inhibition of TORC1 and induction of autophagy in vivo. Taken together, our findings reveal how Pbp1 inhibits TORC1 through an unconventional mechanism involving phase separation. The C-terminal LC region enables Pbp1 to form an intracellular condensate, which is required for inhibiting TORC1 during respiratory growth.

However, since a portion of the protein outside of the C-terminal LC region mediates actual binding to TORC1 (Figure 2-18, 2-19), we propose that an additional mechanism linked

to phase separation of the LC region is required for the inhibition of TORC1, perhaps through modulation of distinct conformational or oligomeric states of TORC1 (Prouteau et al., 2017).

Pbp1 is highly phosphorylated in SL medium

Another key question pertains to the difference between glucose (SD) and lactate (SL) that enables Pbp1 to self-associate and inhibit TORC1. It has been shown that phosphorylation within disordered regions can play a key role in regulating the association of RNA-binding proteins with RNA granules (Lee and Tu, 2015). Both Pbp1 and Ataxin-2 have high serine content (11% and 13% of the overall sequence, respectively).

Using phos-tag gels, I found that the phosphorylation status of Pbp1 varied depending on the carbon sources and nutrients. It became more and more phosphorylated after switching from YPL to SL medium (Figure 3-26A, B). To identify the residues that have different phosphorylation status under non-autophagy- and autophagy-inducing conditions, I compared the phosphorylation changes between Pbp1 variants in SL medium. The phosphorylation of a Pbp1 mutant lacking a.a.299-570 did not change over time in SL medium, indicated that the residues that became phosphorylated in SL are located in this region between the putative RNA-binding domain (LsmAD) and the C-terminal LC region (Figure 3-26C).

Using mass spectrometry, I have identified residues on Pbp1 that are phosphorylated in cells grown in YPL or SL medium, respectively (Figure 3-27, 3-28). To identify the nutrient-specific phosphorylation sites, I compared my data (YPL, SL) with the dataset collected from literature by the BioGrid database (YPD with various treatments) (Figure 3-28). I identified

residues within a.a.299-570 that were selectively phosphorylated in YPD, but not YPL or SL medium, including S442, S451, S453, and S455 (Figure 3-29), as well as residues that were only phosphorylated in SL medium (T429A) (Figure 3-28).

In many studies, phosphorylation of the low complexity domain disrupts phase separation and protein aggregation (Monahan et al., 2017; Murray et al., 2017; Wang et al., 2014). However, in other cases such as the Tau protein, aberrant phosphorylation induces its aggregation and loss of function (Cleveland et al., 1977; Iqbal et al., 1986; Jameson et al., 1980). I first tested whether the 4 serines that are dephosphorylated in lactate culture condition play a role in enhancing Pbp1 self-association. Cells expressing the Pbp1 variant harboring S442, S451, S453, S456 to A substitutions can still induce autophagy after switching to SL medium (Figure 3-30A), ruling out the possibility for these residues to be involved in autophagy regulation. Consistent with the lack of an autophagy deficit, this mutant grew similarly to WT cells in SL medium (Figure 3-30B).

Surprisingly, in YPL medium, this mutant grew faster than WT cells (Figure 3-30C). This phenotype again demonstrated that there are multiple layers of regulation in response to different carbon sources and nutrient availability. Phosphorylation might regulate the protein's ability to inhibit TORC1 perhaps through modulating the binding affinity of Pbp1 to TORC1.

Materials and Methods

Fractionation (total/soluble/pellet)

At the indicated time points, 20 OD of cells were harvested, flash frozen with liquid nitrogen, and stored at -80°C until cell lysis. The cell pellet was resuspended with 250 µl of lysis buffer (150 mM HEPES pH 7.5, 150 mM NaCl, 1 mM EDTA, 0.2% NP-40, 2X protease inhibitor cocktail, 1 mM PMSF, 1 mM DTT). After adding ~100 µl of glass beads, cells were lysed by bead beating 4 times: 30s of beating / 30s of cooling on ice. Cell lysates were clarified by centrifugation at 650 g for 2 min at 4°C. For total protein sample, 100 µl of lysates were taken, mixed with SDS sample dye and boiled for 5 min at 95°C. For soluble and pellet samples, 100 µl of lysates were centrifuged at 100,000 g for 1h at 4°C. The supernatant was transferred to another tube and the pellet was resuspended with 100 µl of 0.2% NP-40 lysis buffer. SDS sample dye was then added to both soluble and pellet samples and boiled for 5 min at 95°C.

Protein expression and purification

All Pbp1 fragments were amplified using PCR from yeast cDNA library and cloned into the multiple cloning sites of the pHis-parallel1 vector (Sheffield et al., 1999). Methionine to serine mutations in the Pbp1 C-terminal LC region were introduced by quickchange site-directed mutagenesis technique and confirmed by sequencing. All proteins were overexpressed in E. coli BL21(DE3) cells with 0.5 mM IPTG at 20°C overnight. Harvested cells were lysed with 0.2 mg/ml lysozyme in a lysis buffer containing 50 mM Tris-HCl pH 7.5, 500 mM NaCl, 20 mM 2-mercaptoethanol, 1% Triton X-100, 2 M guanidine hydrochloride and a protein inhibitor tablet (Sigma) for 30 min on ice, and then sonicated for 2 min (10s on / 30s off). The cell lysate was centrifuged at 35,000 rpm for 1 h. The supernatant was mixed with Ni-NTA

resin (QIAGEN) for 30 min at 4°C. The Ni-NTA resin was packed in a glass column and washed with a washing buffer containing 20 mM Tris-HCl pH 7.5, 500 mM NaCl, 20 mM imidazole, 20 mM 2-mercaptoethanol, 0.1 mM PMSF and 2 M guanidine hydrochloride. The bound proteins were eluted from the resin with an elution buffer containing 20 mM Tris-HCl (pH 7.5), 500 mM NaCl, 200 mM imidazole, 20 mM 2-mercaptoethanol, 0.1 mM PMSF and 2 M guanidine hydrochloride. EDTA was added to a final concentration of 0.5 mM to the eluted protein solutions. The purified proteins were concentrated with Amicon Ultra centrifugal filters (Millipore) to the final concentration of 100-120 mg/ml. The protein solutions were stored at -80°C. The purities of the purified proteins were confirmed by SDS-PAGE, and the concentrations were determined by absorbance at UV_{280}.

Phase-separated droplet formation

Phase-separated droplets of His_6-Pbp1_LC were formed by a quick dilution of the purified protein (90 mg/ml in 6M guanidine HCl) into a gelation buffer containing 20 mM Tris-HCl (pH 7.5), 200 mM NaCl, 20 mM 2-mercaptoethanol, 0.1 mM PMSF and 0.5 mM EDTA to reach the final protein concentration of 1-2 mg/ml. The phase-separated droplet solution was incubated for 30 min to 24 h at room temperature. Images of the droplets were taken using Bio-Rad ZOE Fluorescent Cell Imager with a white light mode.

TEM Image and X-Ray Diffraction

To inspect fibril formation, the purified GFP-Pbp1_LC (200-300 μM) were dialyzed in a gelation buffer for overnight. The dialyzed protein solution was deposited on a surface of a TEM grid (CF-400-Cu from Electron Microscopy Sciences, USA). The surface of the grid was washed three times with 10 μl of distilled water. The grid was subsequently stained for 10 seconds with a 5 μl drop of 2% uranyl acetate. After the uranylacetate solution was blotted, the grid was dried in air. TEM images were obtained with a JEOL 1200EX electron microscope at 120 kV.

For fibril X-ray diffraction, His6-Pbp1_LC was diluted in a gelation buffer at 2 mg/ml. The mixture was incubated for 3 days at 4C°. Polymer pellets were collected by centrifuge at 4000 x g for 30 min. The pellets were resuspended in 0.2 ml milli-Q water and dialyzed in 1 L milli-Q water for 12 h twice. The dialyzed samples were lyophilized for overnight and then exposed to an X-ray beam to obtain cross-β diffraction as described previously (Kato et al., 2012).

Dissolution of phase-separated droplets

Dissolution of phase-separated droplets or fibrils of Pbp1_LC by aliphatic alcohols was monitored by turbidity measurements (absorbance at 395 nm wavelength) with Beckman DU800 spectrophotometer. His6-Pbp1_LC were diluted in the gelation buffer to obtain a final protein concentration of 2 mg/ml (~100 μM).

The phase-separated droplet solution (0.5 ml) was dispensed in plastic cuvettes. 1.6-HD or 2,5-HD (50% w/v in gelation buffer) was added to the cuvettes to obtain the indicated

concentrations and then incubated at room temperature. The OD395 was measured with Beckman DU800 spectrophotometer after 2 min incubation. Plots were calculated from 3 independent experiments.

Semi-denaturing detergent agarose gel electrophoresis (SDD-AGE)

The stability of cross-β polymers were tested by semi-denaturing detergent agarose gel electrophoresis (SDD-AGE) as described previously (Kato et al., 2012). Briefly, the polymers made from His6-tag Pbp1_LC and the amyloid polymers of yeast Sup35NM protein were diluted in a gelation buffer at 0.2 mg/ml and 0.1 mg/ml, respectively, then sonicated briefly to make the polymers short. The short polymers were incubated in the gelation buffer containing indicated concentrations of SDS (0 - 2%) at 37°C for 10 min. The reaction mixtures were loaded onto 1.5% agarose gel to separate polymers and monomers. Proteins were transferred onto a cellulose membrane and analyzed by western blotting with a His-tag antibody.

TEM Image and X-Ray Diffraction

To inspect fibril formation, the purified GFP-Pbp1_LC (200-300 μM) were dialyzed in a gelation buffer for overnight. The dialyzed protein solution was deposited on a surface of a TEM grid (CF-400-Cu from Electron Microscopy Sciences, USA). The surface of the grid was washed three times with 10 μl of distilled water. The grid was subsequently stained for 10 seconds with a 5 μl drop of 2% uranyl acetate. After the uranylacetate solution was blotted, the

grid was dried in air. TEM images were obtained with a JEOL 1200EX electron microscope at 120 kV.

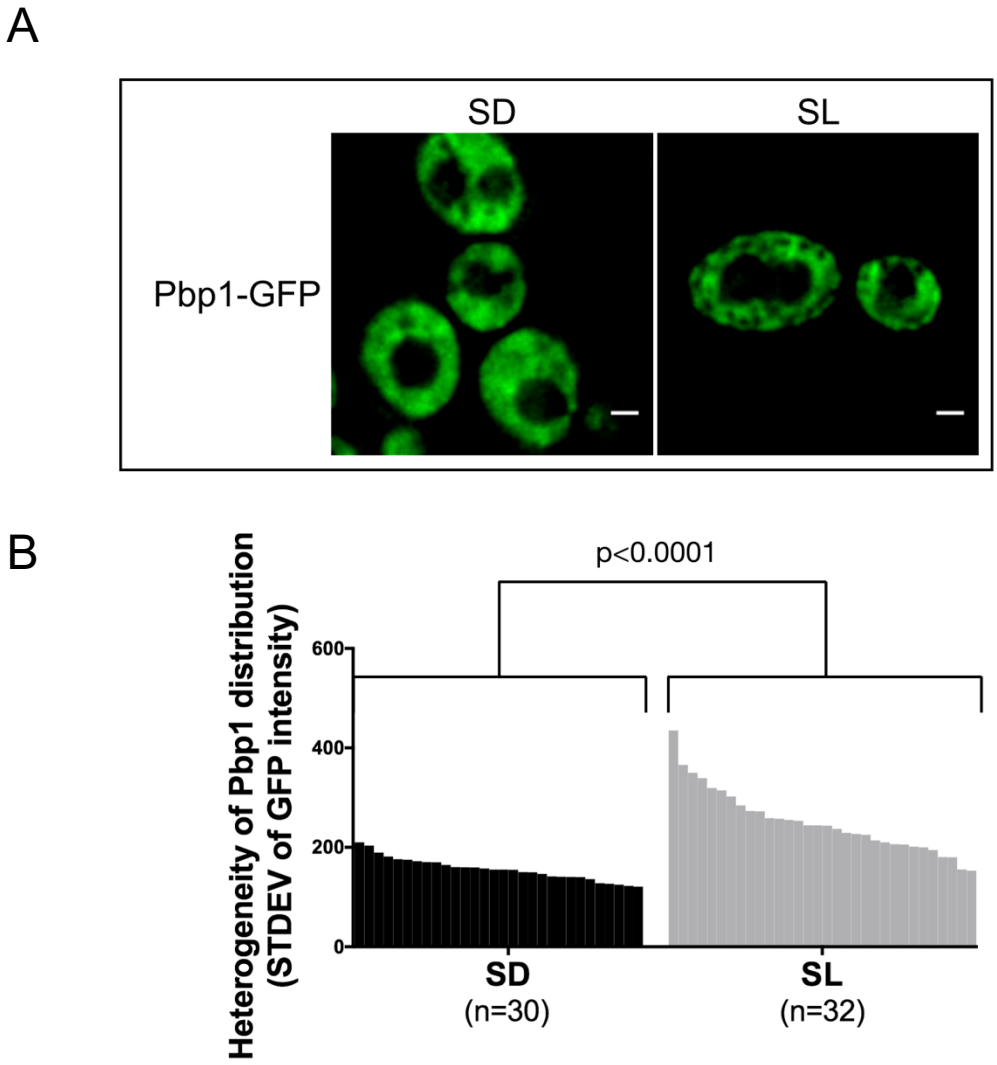

Figure 3-1. Pbp1 distribute heterogeneously in cells grown in SL medium.

(A) Images of Pbp1-GFP in cells growing in SD and SL medium. Images were taken 8 h (SD) or 6h (SL) after switch. Note that Pbp1 was present in the form of non-uniform, nebulous assemblies in SL medium. Scale bar = 1 μm. (B) Pbp1 is distributed more heterogeneously in the cells grown in SL medium ($p<0.0001$ by student's t test). Plot showing the heterogeneity of Pbp1 distribution in individual cells grown in SD or SL. The standard deviation of Pbp1-GFP intensity in individual cells indicates the variability of GFP intensity between regions in a cell.

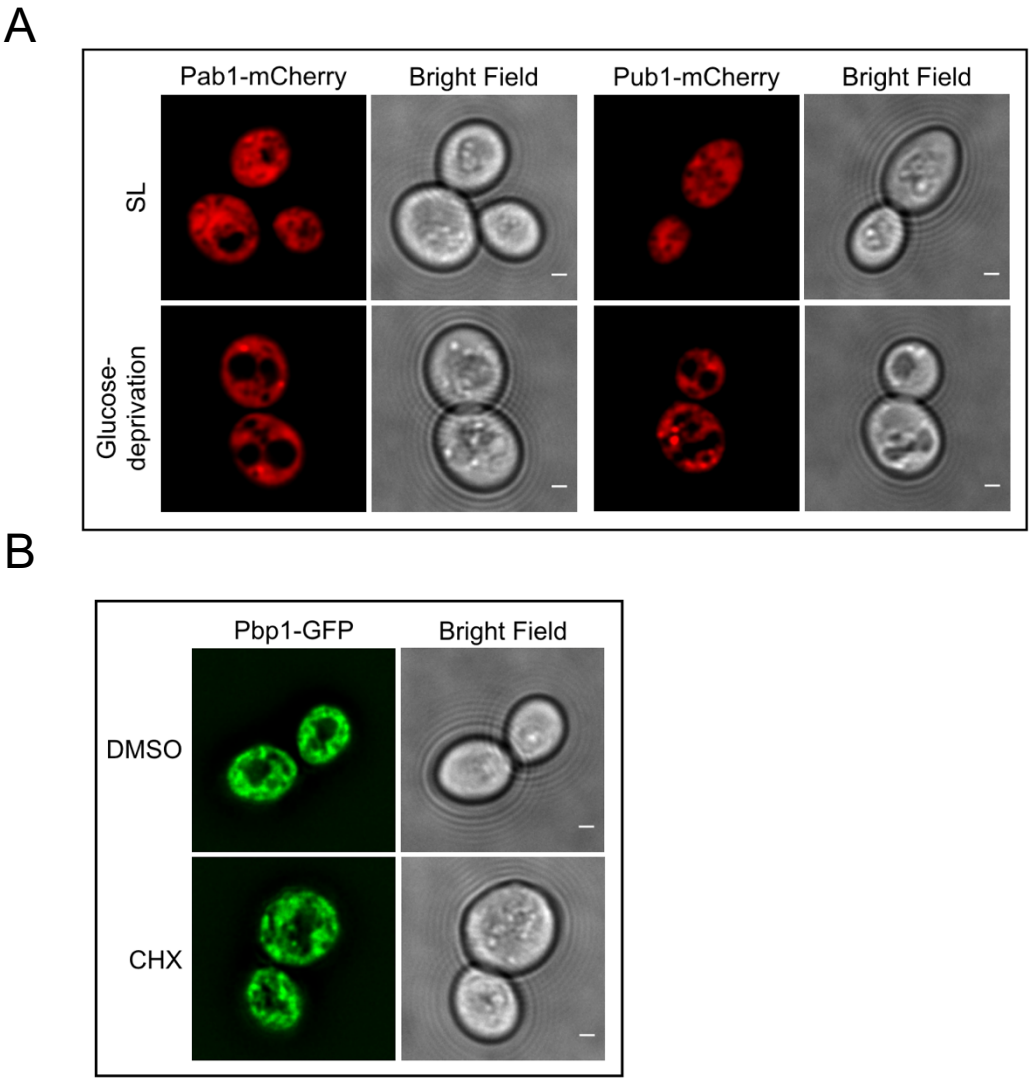

Figure 3-2. Pbp1 and other stress granule-associated proteins do not form foci-like granules when expressed at endogenous levels during respiratory growth.

(A) Images of Pab1-mCherry or Pub1-mCherry expressed at endogenous levels in WT cells. (Top) 6 h after switching from YPL to SL medium. (Bottom) 25 min after switching from SCD to SC medium (glucose deprivation). Scale bar = 1 um. (B) Images of Pbp1-GFP in cells growing in SL medium with DMSO or 25 μg/ml cycloheximide (CHX). Images were taken 1 h after switch. Note that Pbp1 CHX treatment did not change the distribution pattern of Pbp1. Scale bar = 1 um.

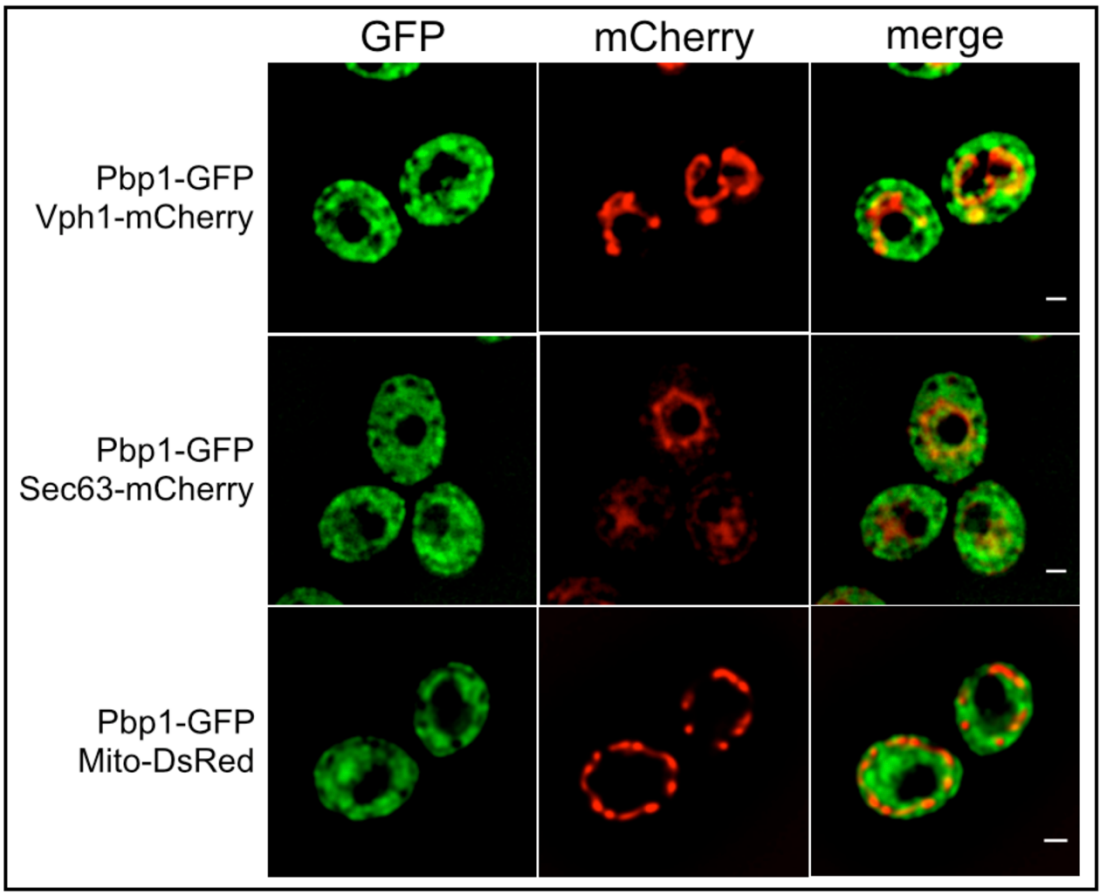

Figure 3-3. Localization of Pbp1 in relation to organelle markers.

Images of cells expressing Pbp1-GFP with either Vph1-mCherry (vacuole), Sec63-mCherry (endoplasm reticulum), or Mito-DsRed (mitochondria) in SL medium. Note that the localization of Pbp1 is completely exclusive of mitochondria, suggesting it may form a condensate surrounding mitochondria. Scale bar = 1 um.

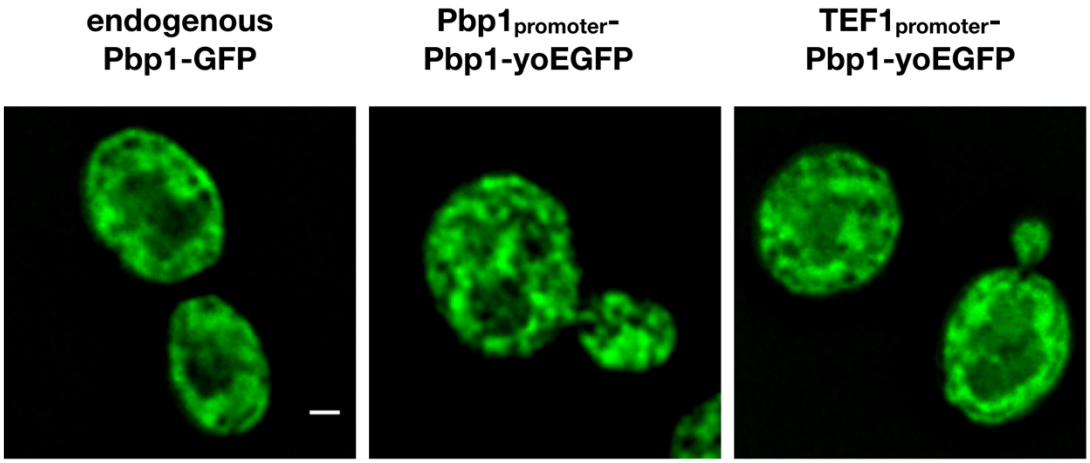

Figure 3-4. Pbp1-yoEGFP showed a clearer pattern of non-homogenous distribution.

Images of endogenous Pbp1-GFP (left), ectopically expressed Pbp1-yoEGFP with Pbp1 promoter (middle), or with Tef1 promoter (right) in WT cells. Images were taken 3 h after switching from YPL to SL medium. Scale bar = 1 um.

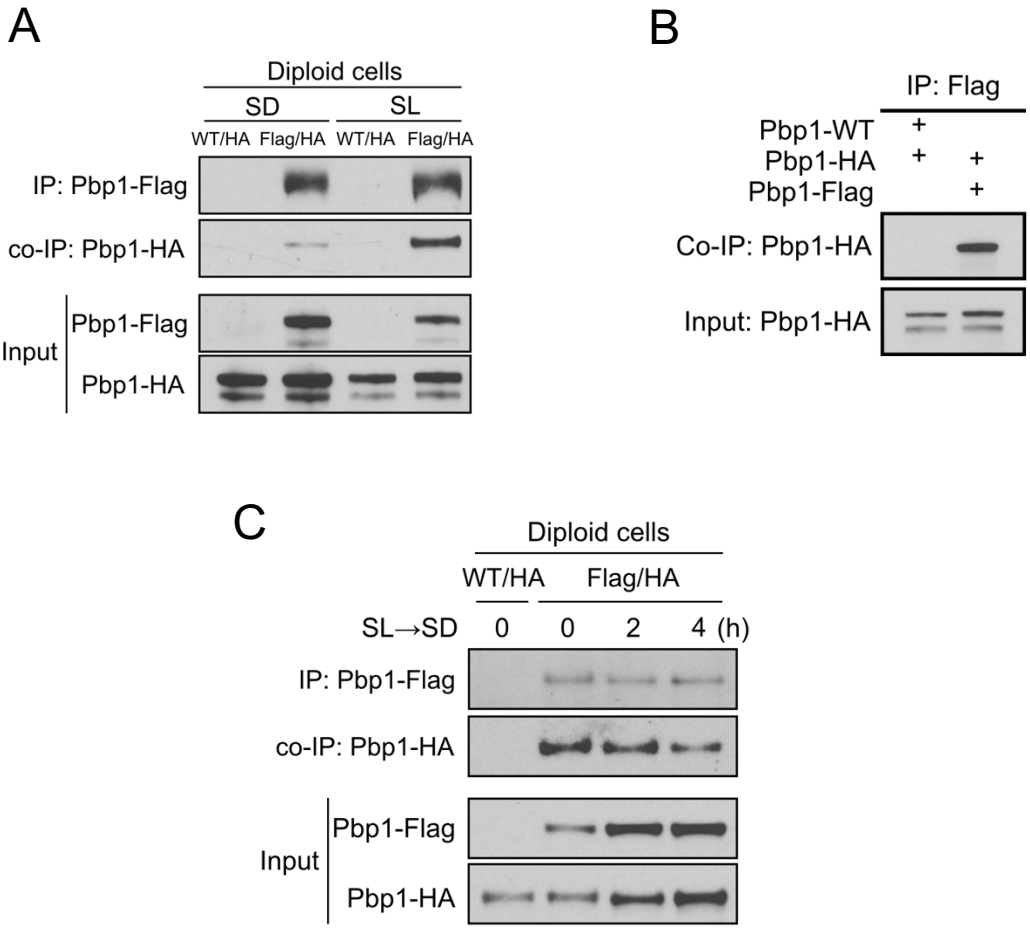

Figure 3-5. Pbp1 self-associates during respiratory growth.

(A) Pbp1 self-associates in cells grown in SL medium. Diploid cells with endogenously Flag- and HA-tagged PBP1 alleles were switched from YPL to SD or SL medium for 6 h. Flag-tagged Pbp1 in cell lysates was precipitated with an anti-Flag antibody. Co-immunoprecipitation of Pbp1-HA was detected by immunoblotting with anti-HA antibody. (B) Pbp1 exhibits a tendency to self-associate. Haploid cells with endogenously tagged Pbp1-Flag or Pbp1-HA were switched from YPL to SL medium for 3 h. Cell lysates were mixed in 1:1 ratio before immunoprecipitation. Immunoprecipitation was performed as described in (A). (C) Pbp1 self-association is decreased after glucose repletion. Diploid cells with endogenously Flag- and HA-tagged PBP1 alleles were switched from YPL to SL for 3 h and then switched back to SD medium for indicated times. Immunoprecipitation was performed as described in (A).

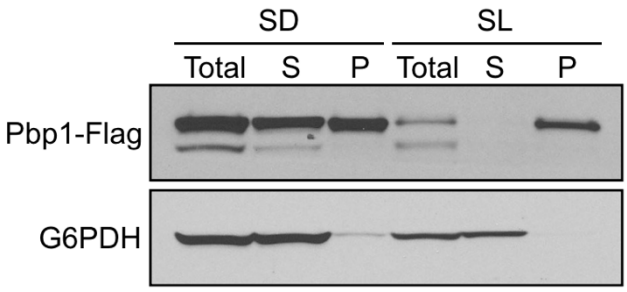

Figure 3-6. Pbp1 self-associates into pelletable assemblies during respiratory growth.

Pbp1 is present primarily in the pellet fraction in cells grown in SL medium. Cells with endogenously tagged Pbp1 grown in YPL were switched to SD or SL medium for 6 h. Lysed cells were centrifuged for 1 h at 100,000g for separating supernatant (S) and pellet (P).

A

```
low complexity regions: SEG 45 3.4 3.75
>Query

                                  1-328  MKGNFRKRDSSTNSRKGGNSDSNYTNGGVP
                                         NQNNSSMFYENPEITRNFDDRQDYLLANSI
                                         GSDVTVTVTSGVKYTGLLVSCNLESTNGID
                                         VVLRFPRVADSGVSDSVDDLAKTLGETLLI
                                         HGEDVAELELKNIDLSLDEKWENSKAQETT
                                         PARTNIEKERVNGESNEVTKFRTDVDISGS
                                         GREIKERKLEKWTPEEGAEHFDINKGKALE
                                         DDSASWDQFAVNEKKFGVKSTFDEHLYTTK
                                         INKDDPNYSKRLQEAERIAKEIESQGTSGN
                                         IHIAEDRGIIIDDSGLDEEDLYSGVDRRGD
                                         ELLAALKSNSKPNSNKGNRYVPPTLRQQ
phhmdpaiisssnsnknenavstdtstpaa    329-507
agapegkppqktsknkkslsskeaqieelk
kfsekfkvpydipkdmlevlkrssstlksn
sslppkpisktpsaktvspttqisagkses
rrsgsnisqgqsstghttrsstslrrrnhg
 sffgaknphtndakrvlfgksfnmfiksk
                                  508-569  EAHDEKKKGDDASENMEPFFIEKPYFTAPT
                                         WLNTIEESYKTFFPDEDTAIQEAQTRFQQR
                                         QL
nsmgnavpgmnpamgmnmggmmgfpmggps    570-700
aspnpmmngfaagsmgmympfqpqpmfyhp
smpqmmpvmgsngaeegggnisphvpagfm
aagpgapmgafgypggipfqgmmgsgpsgm
                    pangsamhshg
                                  701-722  HSRNYHQTSHHGHHNSSTSGHK
```

Low complexity | Non-Low complexity

B

Figure 3-7. Low complexity and intrinsic disorder regions within the Pbp1 protein.

(A) Low complexity sequences analysis identified using the SEG program (Wootton, 1994) (http:// mendel.imp.ac.at/METHODS/seg.server.html) with default parameter – SEG 45 3.4, 3.75. (Left column) low complexity region. (Right column) non-low complexity region. (B) Intrinsic disorder region analysis using IUPRED (http://iupred.enzim.hu/) with "long disorder" parameters (Dosztanyi et al., 2005). Disorder tendency > 0.5 is considered as intrinsic disordered.

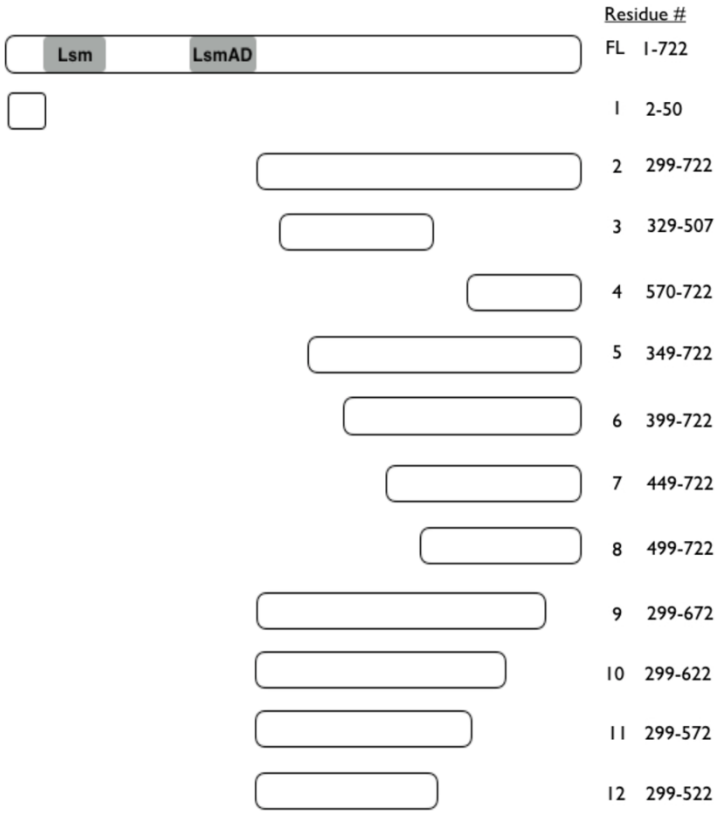

Figure 3-8. Schematic representation of Pbp1 fragments containing low-complexity regions.

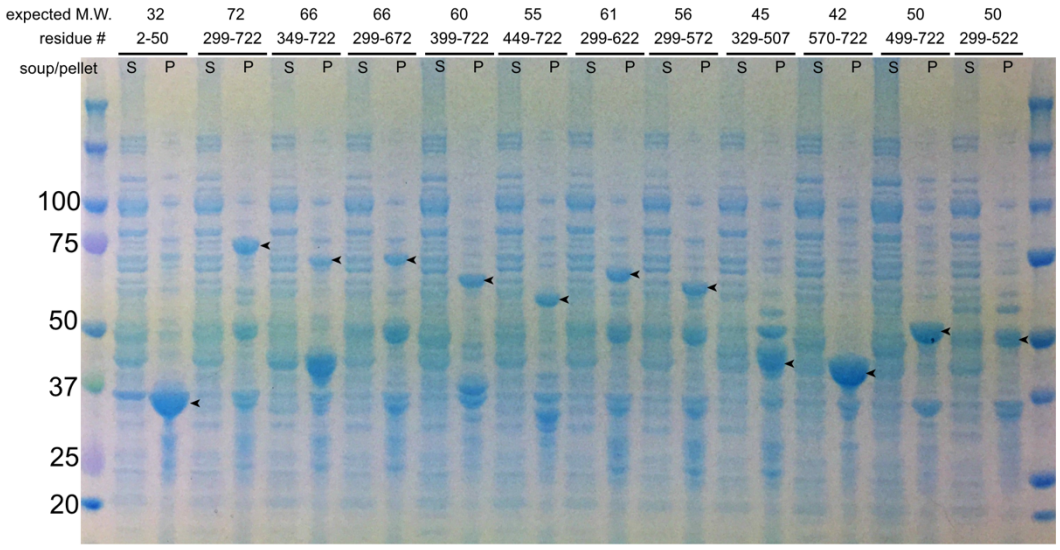

Figure 3-9. Solubility test of Pbp1 mutants covering different fragments of low complexity region.

BL21 cells expressing the indicated Pbp1 mutants were inoculated into 4 ml LB, grown to OD_{600} = 0.6-0.8 at 37℃. Protein expression was induced by 0.1 mM IPTG for 3 h at 37℃. Cell pellets were lysed and sonicated 3 times (1s/time). Supernatant and Pellet were separated by centrifugation followed by SDS-PAGE analysis.

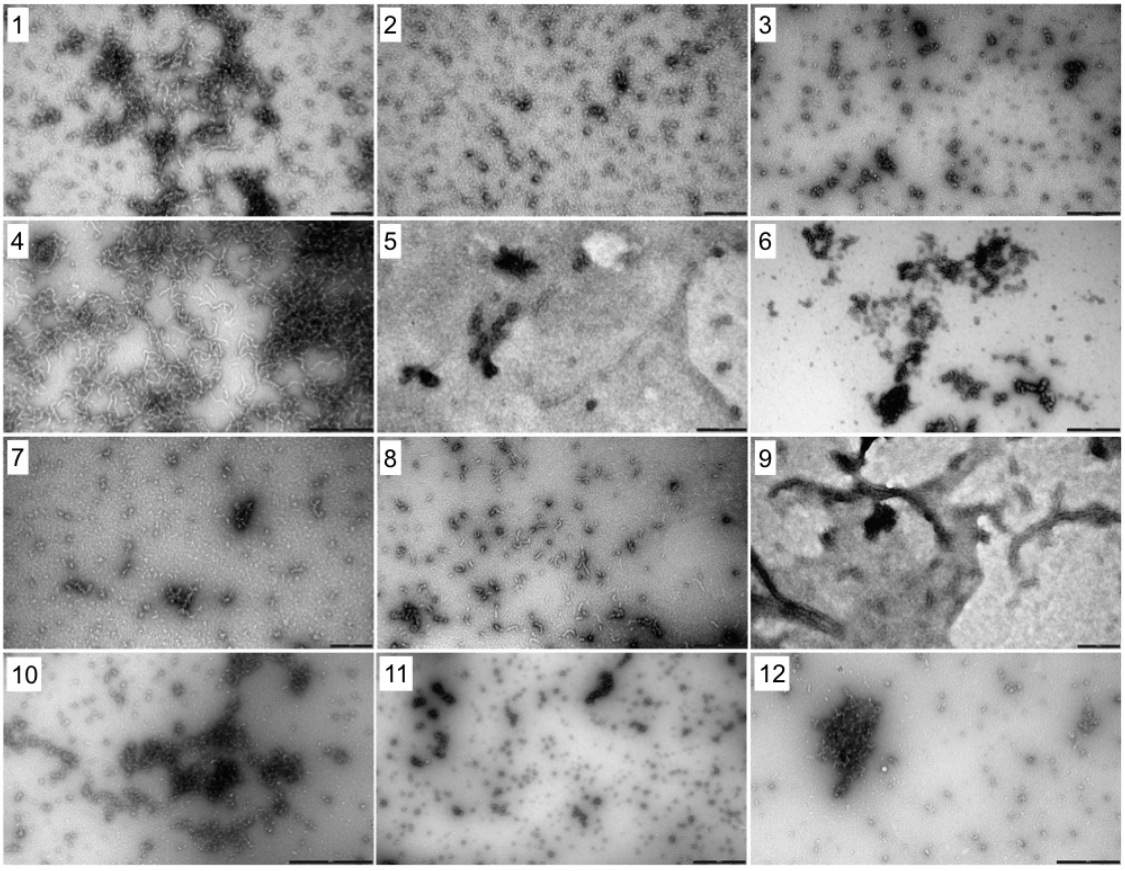

Figure 3-10. Electron micrographs of fibrils formed by GFP-Pbp1 fragments shown in Figure 3-7.

Pbp1 fragment containing the C-terminal low complexity region (a.a. 570-722, fragment #4) formed uniformly similar, polymeric fibrils. Scale bar: 500 nm.

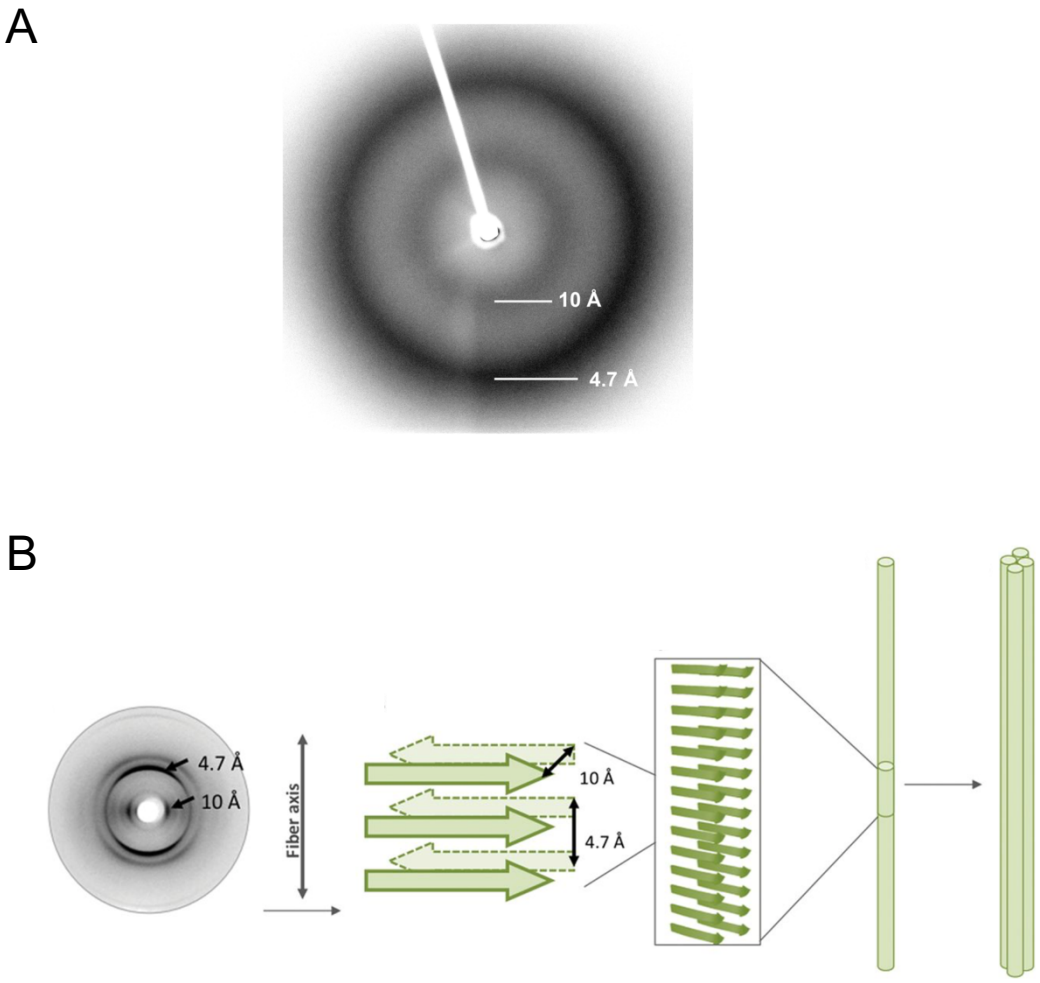

Figure 3-11. X-ray diffraction pattern of Pbp1_LC fibrils revealed its cross-β structure.

(A) X-ray diffraction pattern of His_6-Pbp1_LC polymer fibrils. Clear X-ray reflections were observed at 4.7Å and 10Å, indicative of a cross- β structure. (B) The cross-β diffraction pattern obtained from fibrils arouse from the cross-β structural core of the protofilament. The protofilaments self-associate to form the mature amyloid fibril. Picture modified from (Serpell, 2014).

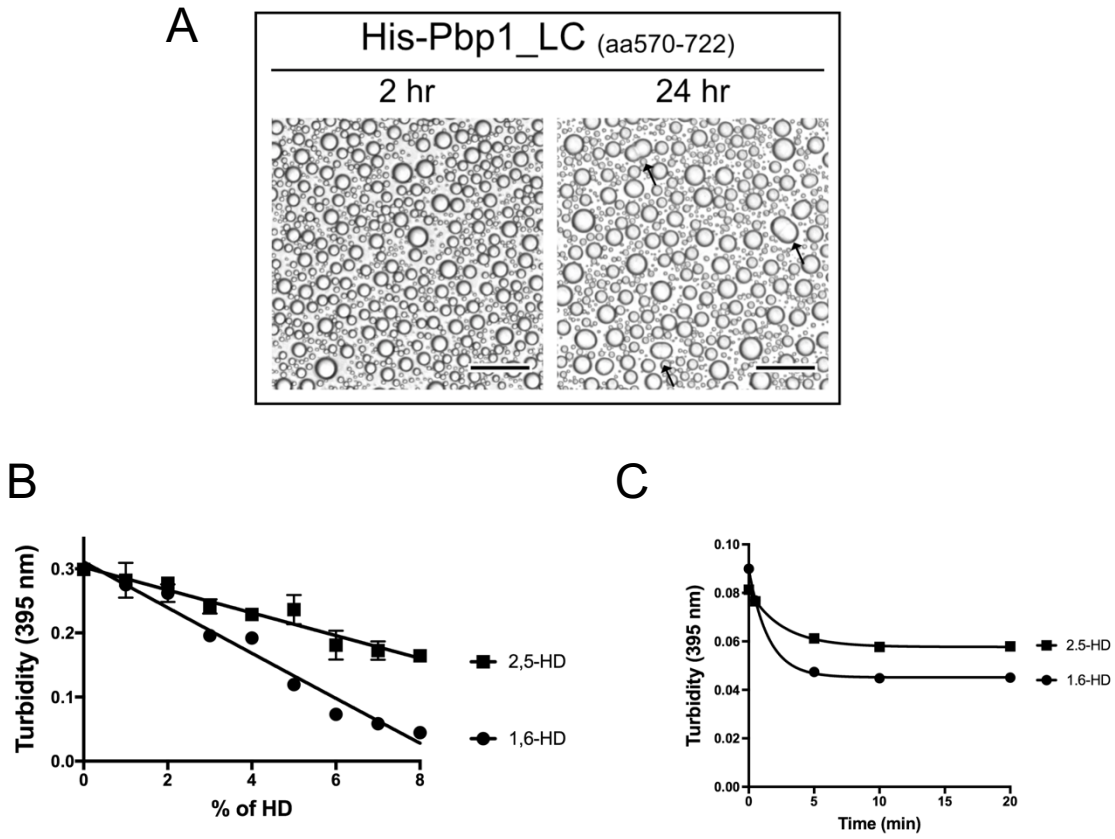

Figure 3-12. Pbp1_LC phase separated into droplets which are sensitive to 1,6-hexanediol.

(A) Phase-separated droplet formation by purified His_6-Pbp1_LC. Images were taken 2 h and 24 h after lowering the salt concentration. Scale bar = 50 um (B) Dissolution of His_6-Pbp1_LC phase-separated droplets by aliphatic alcohols. Turbidity changes of the phase-separated droplet solution containing the indicated concentration of 1,6- or 2,5- hexanediols (HD) were measured by light absorbance at 395 nm. Note that the droplets were more sensitive to 1,6-HD. Data were mean ± s.d. from 3 independent experiments. (C) Dissolution of the Pbp1_LC fibrils by the 1,6- or 2,5-hexanediols (HD). Note that the fibrils were more sensitive to 1,6-HD. Data were mean ± s.d. from 3 independent experiments.

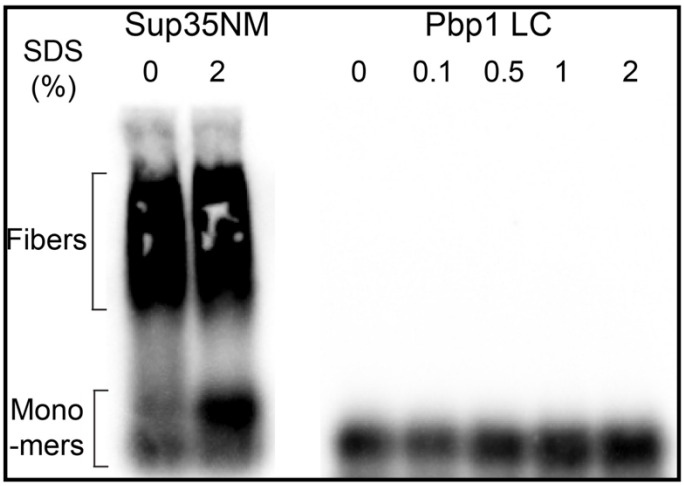

Figure 3-13. Pbp1_LC fibrils are not SDS-resistant

SDD-AGE analysis of yeastSup35 NM amyloid polymers and His_6-Pbp1_LC polymers. SDS exposure did not substantially affect ySup35 NM amyloid polymers whereas Pbp1_LC polymers were fully depolymerized under all conditions.

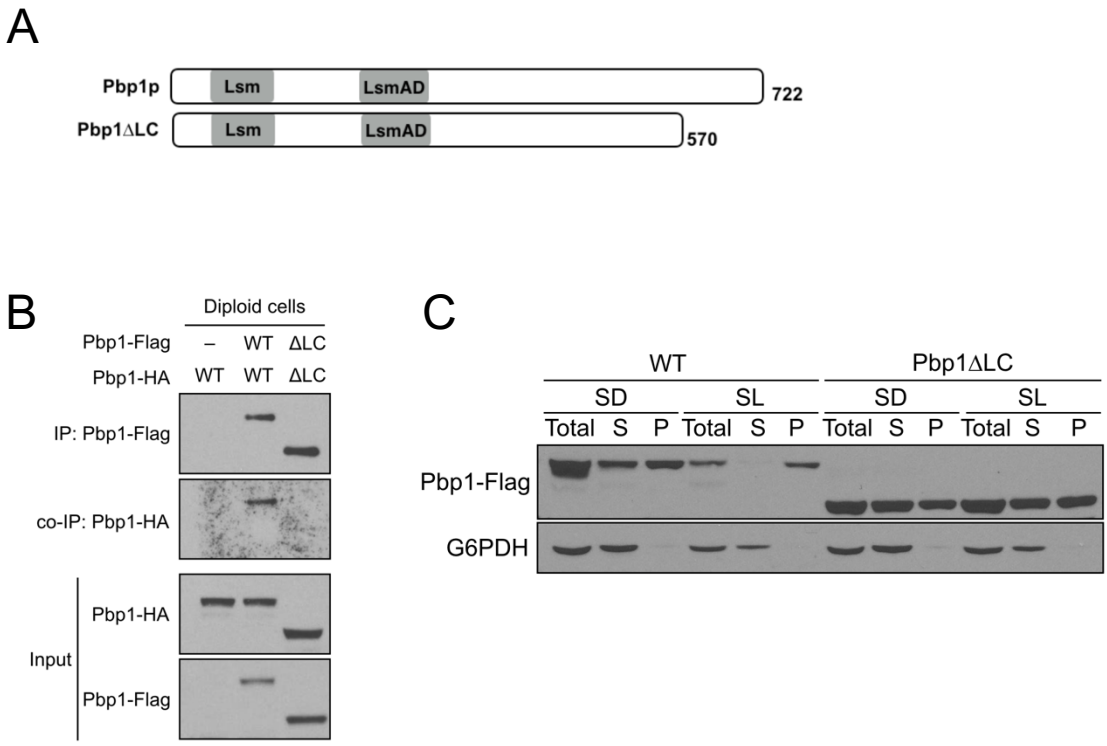

Figure 3-14. The C-terminal LC region enables Pbp1 to self-associate *in vivo*

(A) Schematic of domains present in Pbp1. Pbp1ΔLC lacks the C-terminal LC region, and Pbp1_LC denotes the C-terminal LC region alone. (B) Pbp1ΔLC cannot self-associate in cells grown in SL medium. Diploid cells expressing endogenously Flag- and HA-tagged Pbp1ΔLC alleles were switched from YPL to SL medium for 3 h. Flag-tagged Pbp1ΔLC in cell lysates was precipitated with an anti-Flag antibody. Co-immunoprecipitation of Pbp1ΔLC-HA was detected by immunoblotting with anti-HA antibody. (C) Western blot showing the distribution of Pbp1 WT and Pbp1ΔLC variant in SD or SL medium. Pbp1ΔLC was less concentrated in the pellet fraction in SL medium. Cells were cultured and processed as described in Figure 3-6.

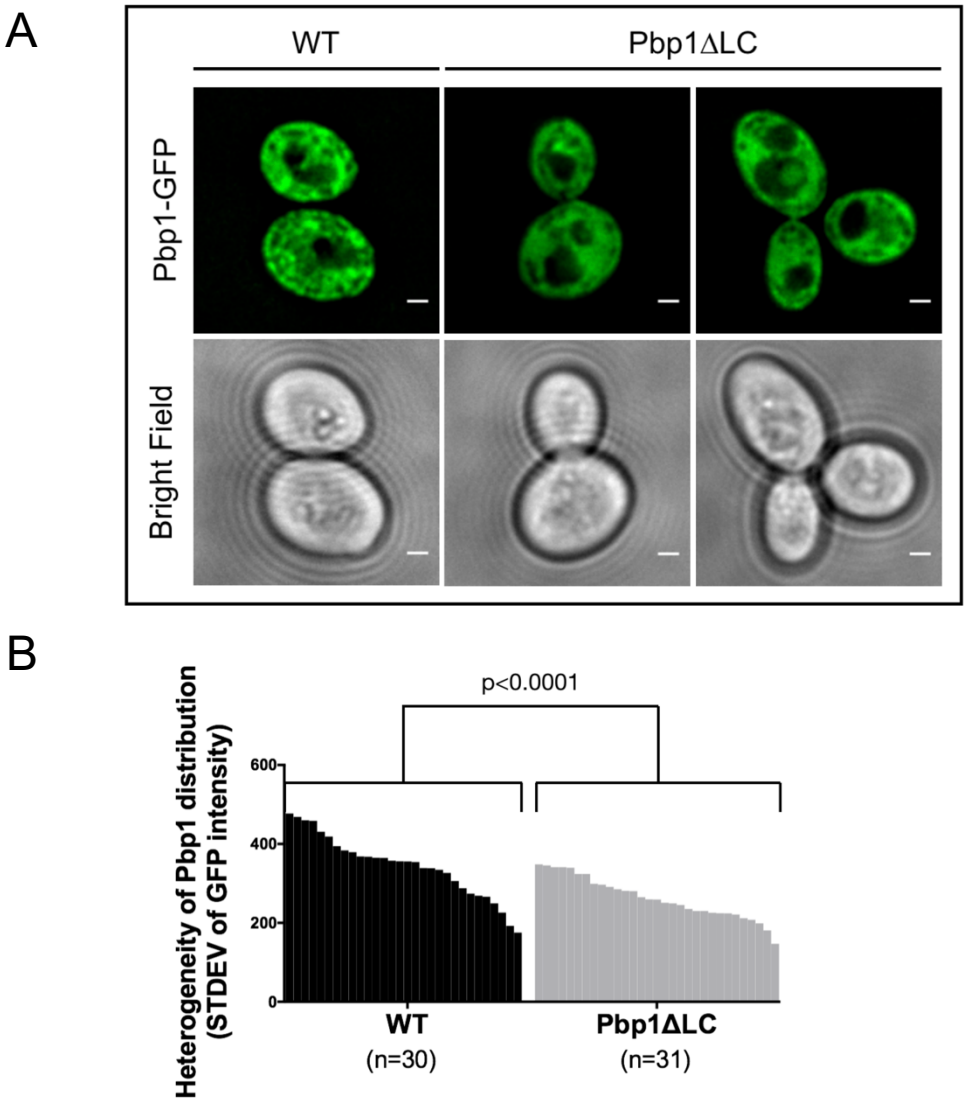

Figure 3-15. Pbp1 mutant lacking the C-terminal LC region exhibited a more uniform distribution pattern throughout the cytoplasm.

Images of cells expressing Pbp1-GFP or Pbp1ΔLC-GFP at endogenous levels in SL medium. Note that Pbp1ΔLC exhibited a more uniform distribution pattern throughout the cytosol ($p<0.0001$ by student's t test). scale bar = 1 μm. Plot showing the heterogeneity of Pbp1 distribution in individual cells expressing either WT or Pbp1ΔLC variant.

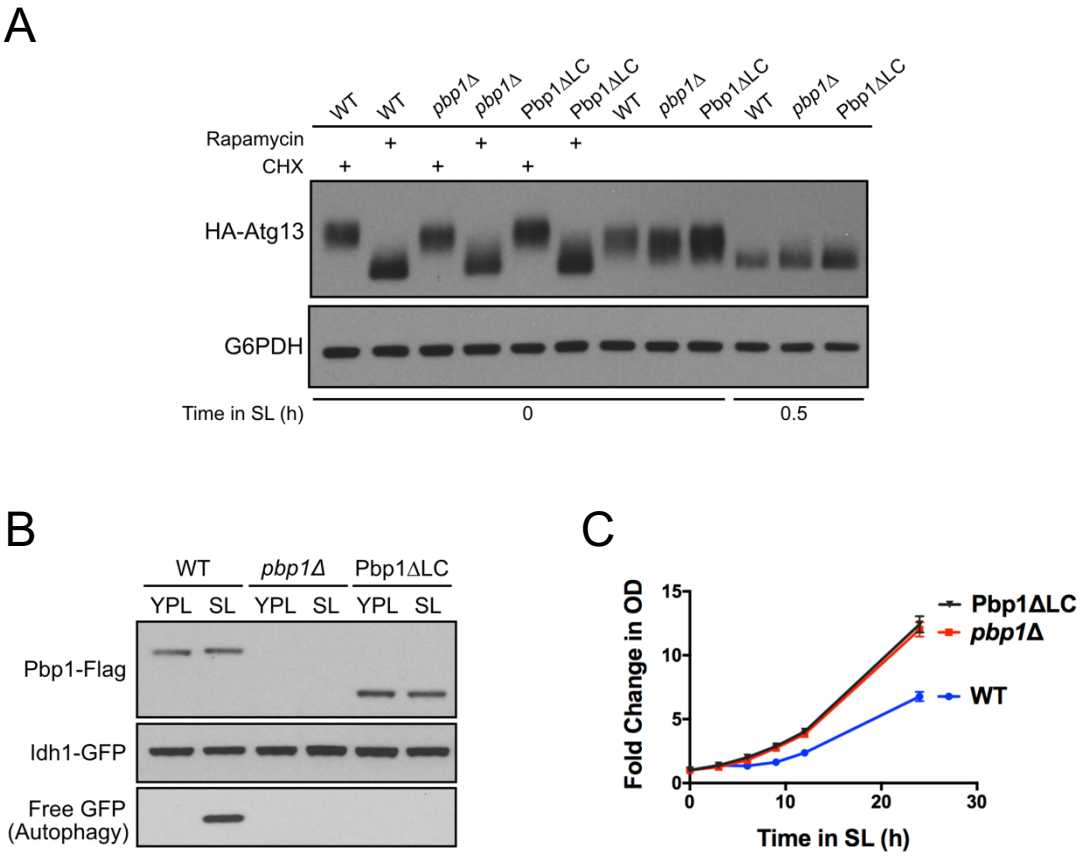

Figure 3-16. The C-terminal LC region is required for inhibition of TORC1.

(A) Cells expressing Pbp1ΔLC exhibited increased phosphorylation of endogenously tagged Atg13 similar to *pbp1*Δ cells. (B) GFP cleavage assay showing cells expressing Pbp1ΔLC completely lost the ability to induce autophagy following switch to SL medium. (C) Growth curves showing cells expressing Pbp1ΔLC exhibited similar growth compared to *pbp1*Δ cells.

A

571
SM1GNAVPGM2NPAM3GM4NM5GGM6M7GFPM8GGPSASPNPM9M10N
GFAAGSM11GM12YM13PFQPQPM14FYHPSM15PQM16M17PVM18GSNGA
EEGGGNISPHVPAGFM19AAGPGAPM20GAFGYPGGIPFQGM21M22GS
GPSGM23PANGSAM24HSHGHSRNYHQTSHHGHHNSSTSGHK
722

B

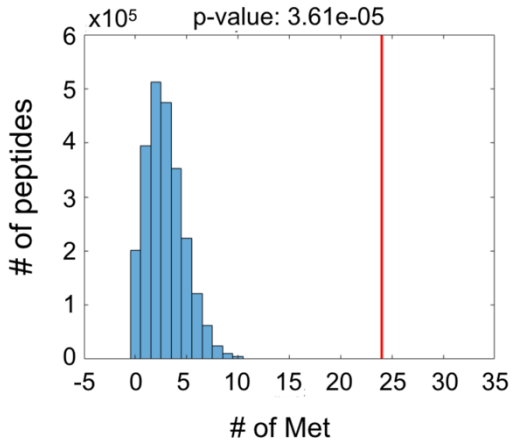

Figure 3-17. Pbp1 C-terminal LC region has high methionine content.

(A) Amino acid sequence of the Pbp1 C-terminal LC region. The 24 methionine residues are numbered and highlighted in blue. The yellow highlighted region denotes the critical methionine residues for function deduced from the experiments below. (B) The C-terminal low complexity region of Pbp1 has unusually high methionine content compared to the rest of the yeast proteome. Plot showing methionine content per 150 amino acids across the yeast proteome. Individual proteins were analyzed using a sliding window of a length of 150 a.a., and the number of methionines was counted for each 150 a.a. window. The number of 150 a.a. peptides (Y-axis) with indicated numbers of methionine residues (X-axis) was plotted. Red line indicates the position of the Pbp1 C-terminal LC region (24 methionines).

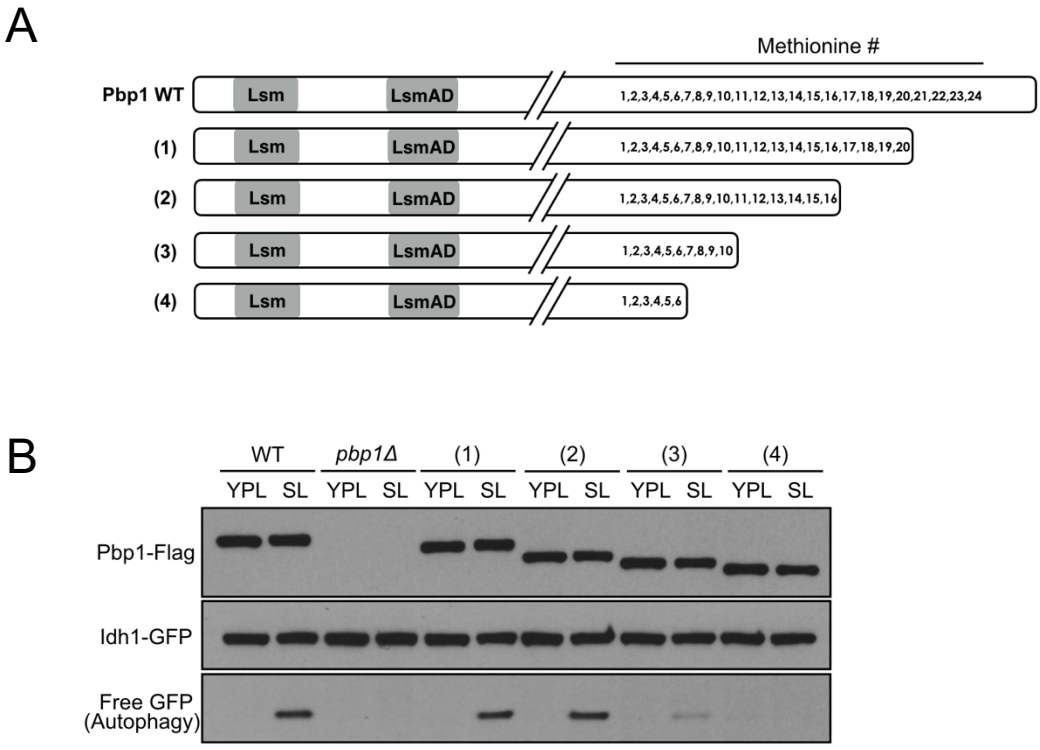

Figure 3-18. Methionine residues in the C-terminal LC region of Pbp1 are critical for its function.

(A) Schematic representation of a series of C-terminal truncation mutants lacking increasing numbers of methionine residues. (B) GFP cleavage assay showing autophagy in cells expressing the mutants depicted in (A). Cells expressing Pbp1 mutants lacking the region containing M_{11} to M_{16} (mutant (3), (4)) showed reduced autophagy.

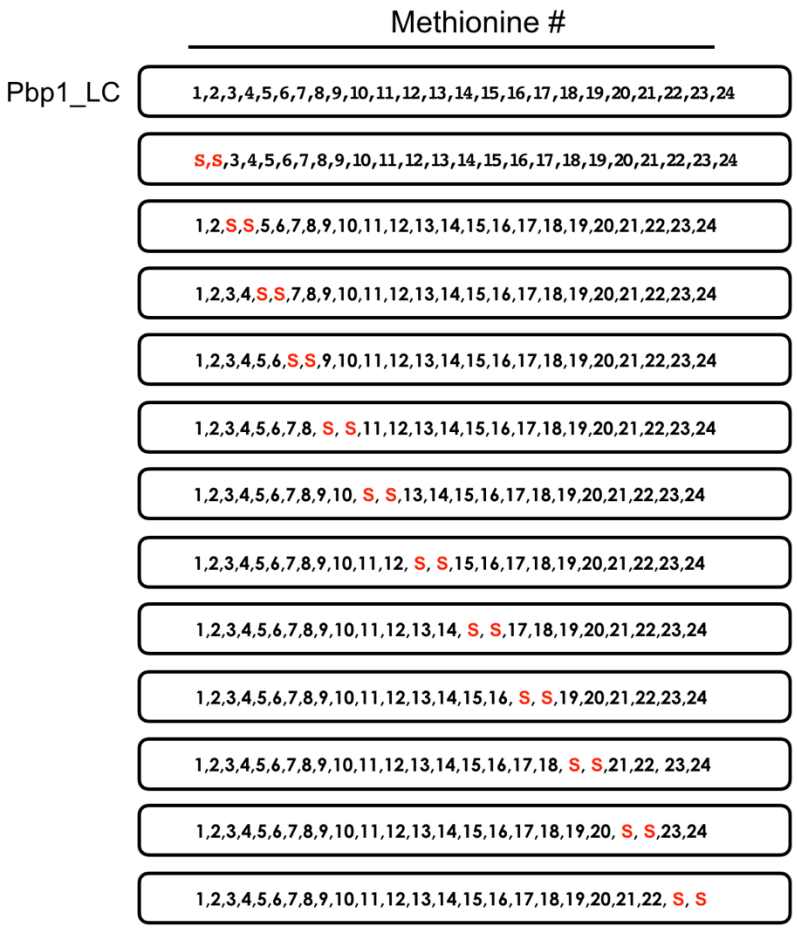

Figure 3-19. Schematic representation of Pbp1_LC variants each harboring two adjacent methionine to serine substitutions.

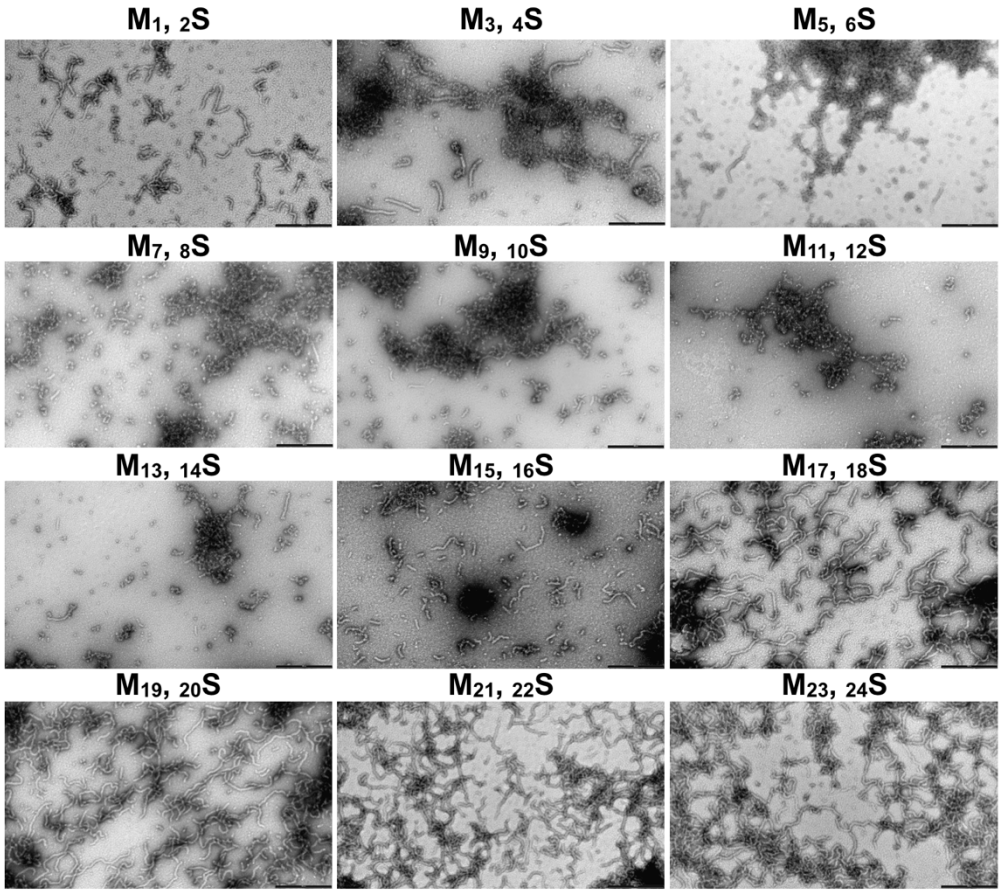

Figure 3-20. Substitution of the methionine residues located in the middle region of Pbp1_LC to serine affects fibril formation.

Electron micrographs of fibrils formed by purified GFP-Pbp1_LC mutants shown in Figure 3-19. The mutants harboring $M_{11,\ 12} \rightarrow S$ showed the most significantly reduced ability to form fibrils. Mutants harboring serine substitutions for any two of the last eight methionine residues ($M_{17,\ 18,\ 19,\ 20,\ 21,\ 22,\ 23,\ 24}$) formed fibrils comparable to WT Pbp1_LC. Scale bar: 500 nm.

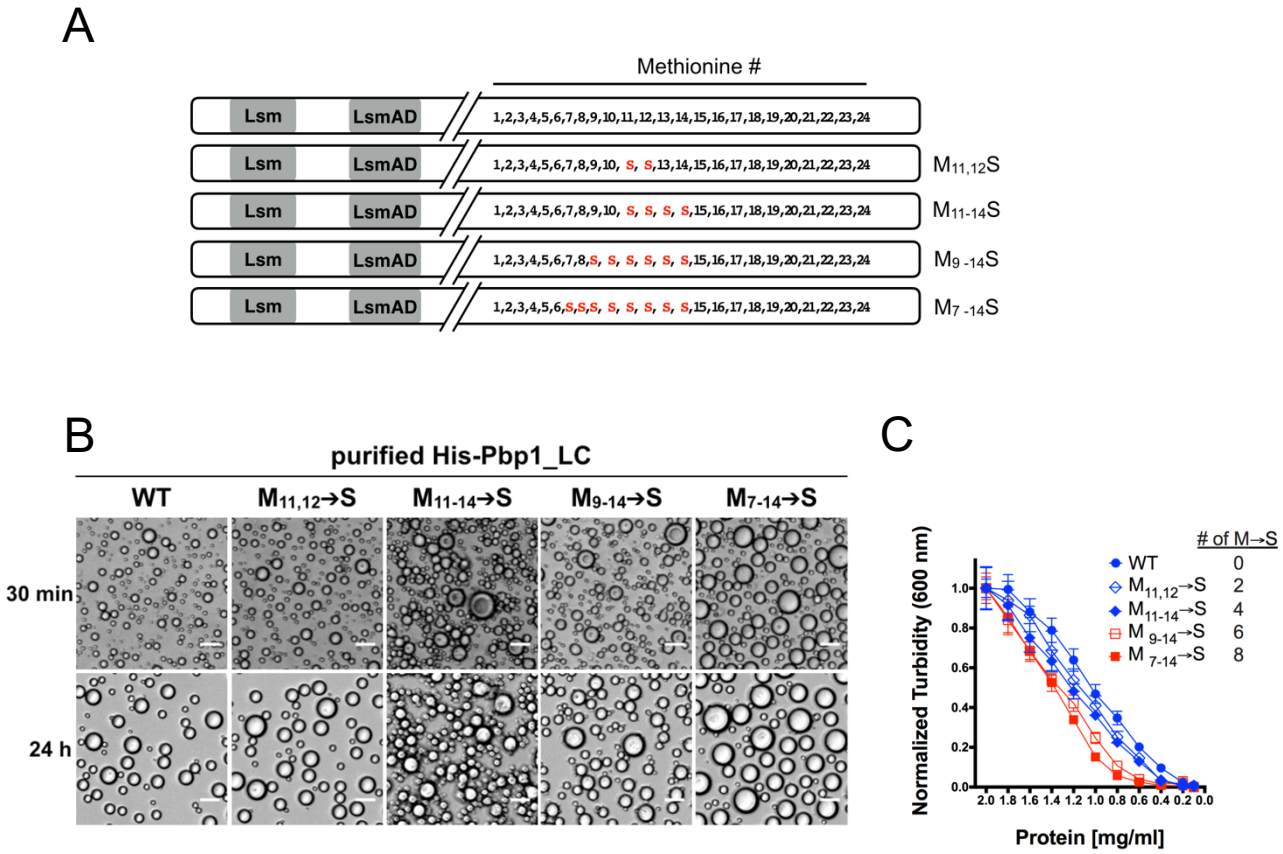

Figure 3-21. Increasing numbers of methionine to serine substitutions reduce the stability of Pbp1_LC droplets.

(A) Schematic representation of Pbp1 variants harboring increasing numbers of methionine to serine substitutions. (B) Phase-separated droplet formation by purified His_6-Pbp1_LC containing indicated methionine to serine mutations. Images were taken 30 min and 24 h after lowering the salt concentration. Scale bar = 10 μm. (C) Dissolution of phase-separated droplets formed from the indicated proteins by dilution. Turbidity was measured by light scattering at 600 nm. Phase-separated droplets formed by the variant bearing 8 methionine mutations dissolved more readily following dilution of the protein concentration. Data were mean ± s.d. from 3 independent experiments.

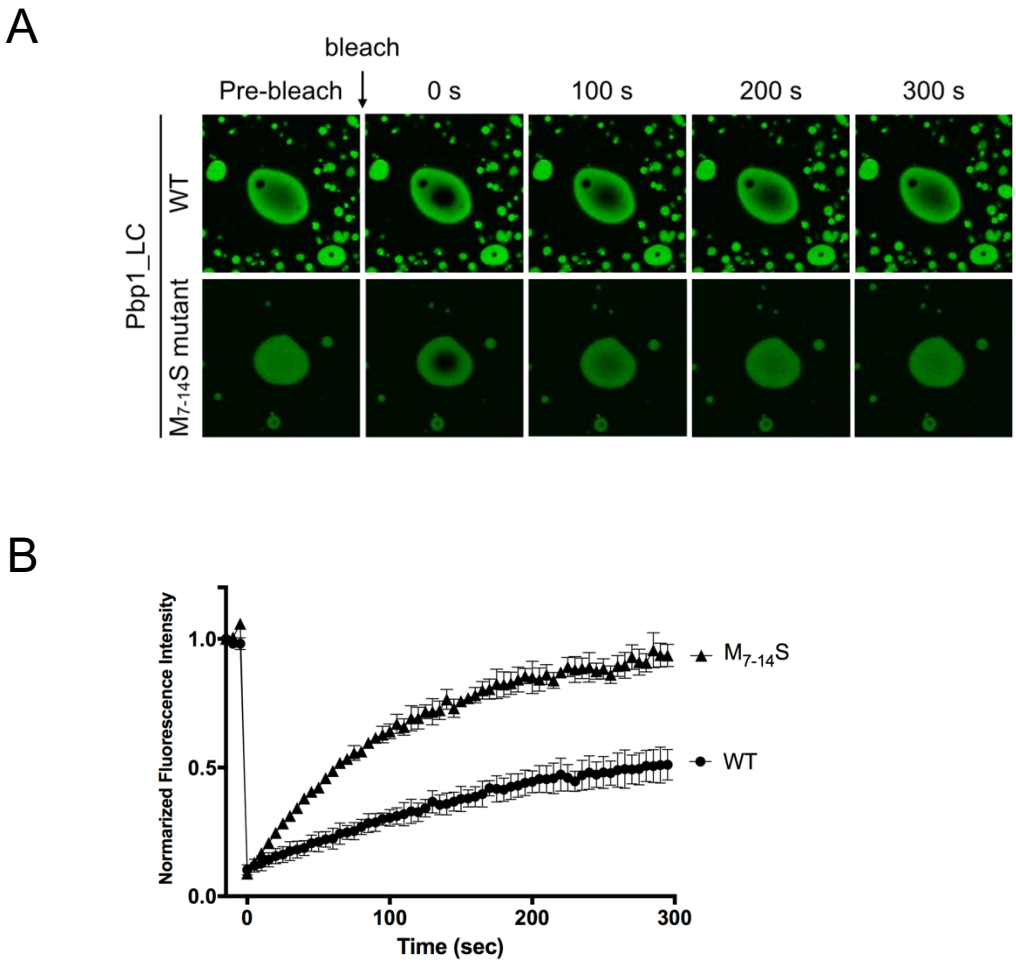

Figure 3-22. Droplets formed by Pbp1_LC harboring methionine to serine substitutions recover faster after photobleaching.

(A) FRAP (fluorescence recovery after photobleaching) analysis of phase-separated droplets formed by purified Pbp1_LC WT or $M_{7\text{-}14} \rightarrow S$ variant. (B) Quantification of FRAP in (A). Note the phase-separated droplets of Pbp1_LC $M_{7\text{-}14} \rightarrow S$ recovered faster compared to WT. Plots are generated from 9 droplets in 3 independent experiments.

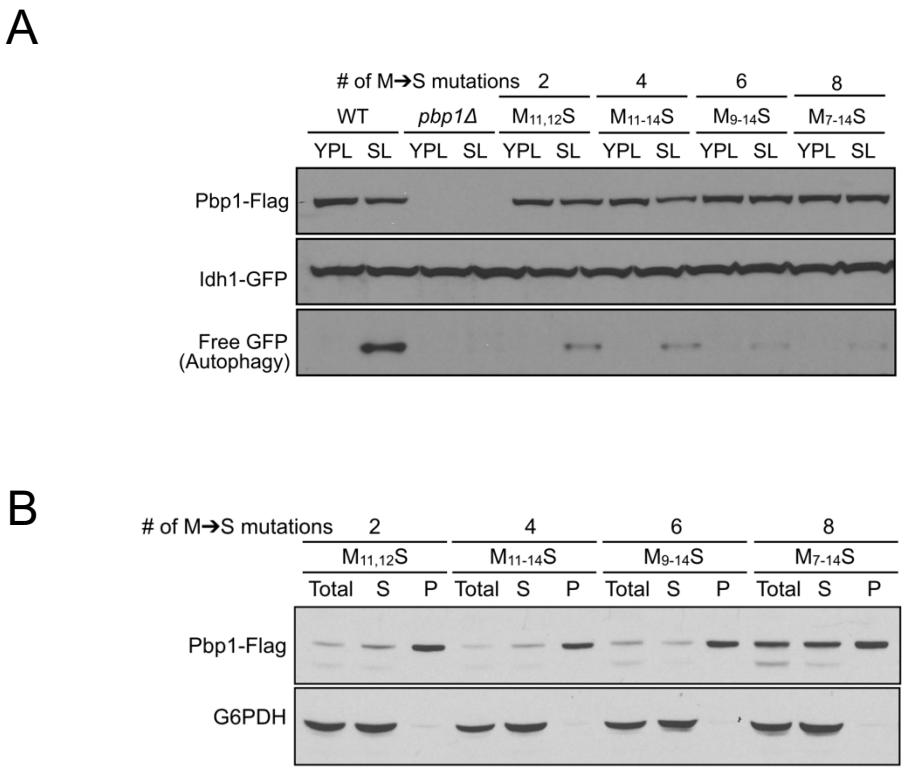

Figure 3-23. Increasing numbers of methionine to serine substitutions decrease the self-association of full-length Pbp1 and autophagy.

(A) GFP cleavage assay showing autophagy in cells expressing Pbp1 mutants with indicated methionine to serine point mutations. Cells expressing Pbp1 with 8 methionine mutations ($M_{7-14} \rightarrow S$) showed severely reduced autophagy. (B) Western blot showing the distribution of Pbp1 mutant proteins with indicated methionine to serine mutations in SL medium. The Pbp1 protein containing 8 methionine mutations ($M_{7-14} \rightarrow S$) was less concentrated in the pellet fraction. Cells were cultured and processed as described in Figure 3-6.

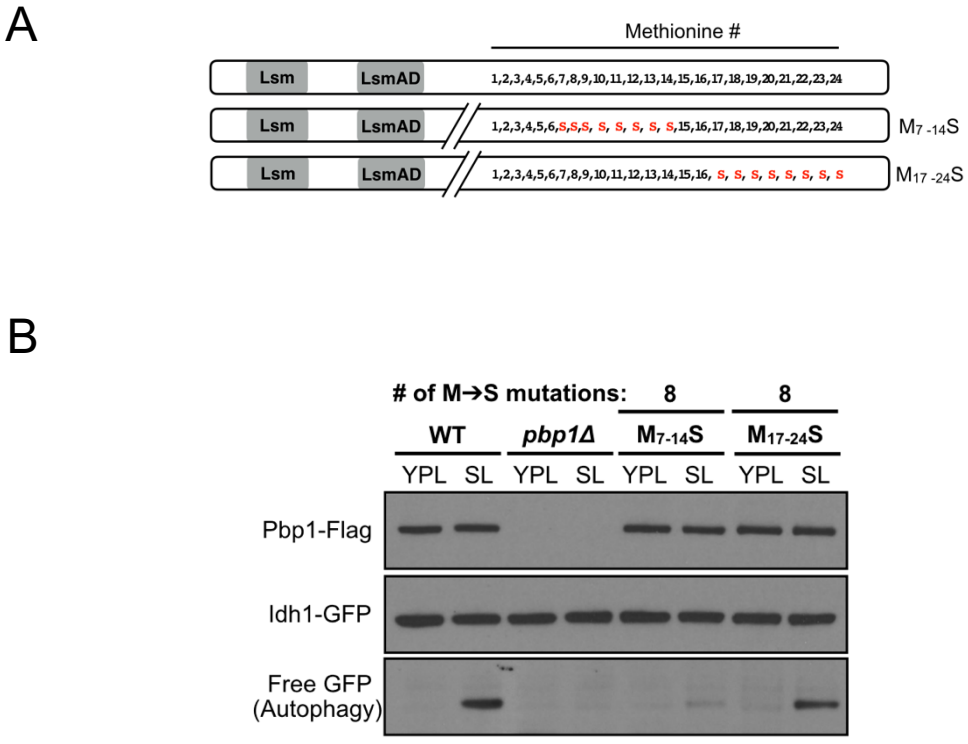

Figure 3-24. M_7-M_{14} residues within Pbp1_LC are important for Pbp1's function *in vivo*.

(A) Schematic representation of Pbp1 variants harboring eight methionine to serine substitutions on M_{7-14} or M_{17-24} (B) GFP cleavage assay that is indicative of mitophagy. Pbp1 $M_{7-14} \rightarrow$ S variant is non-functional for autophagy *in vivo* as indicated by the absence of free GFP, whereas Pbp1 $M_{17-24} \rightarrow$ S is fully capable of inducing autophagy.

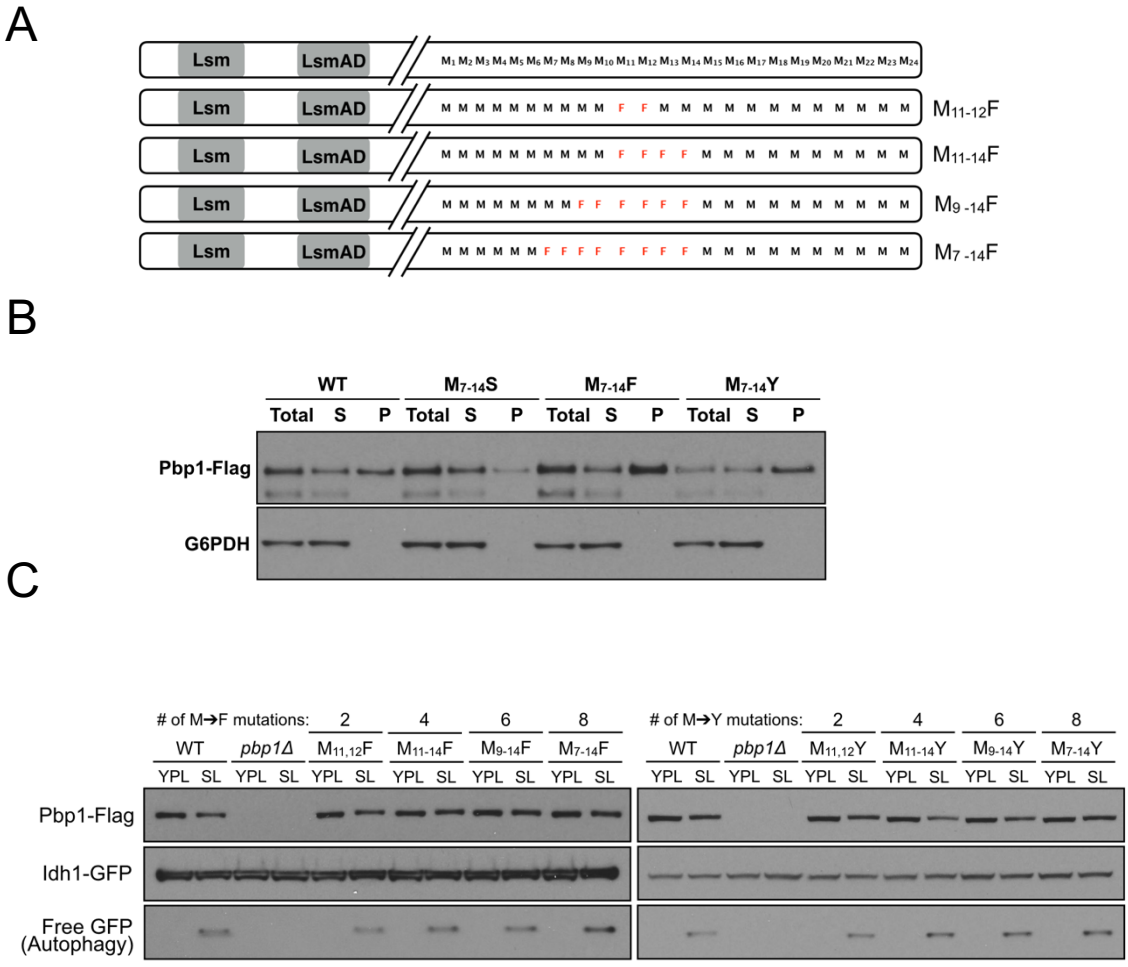

Figure 3-25. Substitution of methionine to phenylalanine/tyrosine enhances self-association of full-length Pbp1 and autophagy.

(A) Schematic representation of Pbp1 variants harboring increasing numbers of methionine to phenylalanine (or tyrosine) substitutions. (B) $M_{17\text{-}24} \rightarrow F$, $M_{17\text{-}24} \rightarrow Y$ variants of Pbp1 are more abundant in pellet fraction compared to WT. Cells were grown and processed as in Figure 3-6. (C) $M_{17\text{-}24} \rightarrow F$, $M_{17\text{-}24} \rightarrow Y$ variants exhibit increased autophagy.

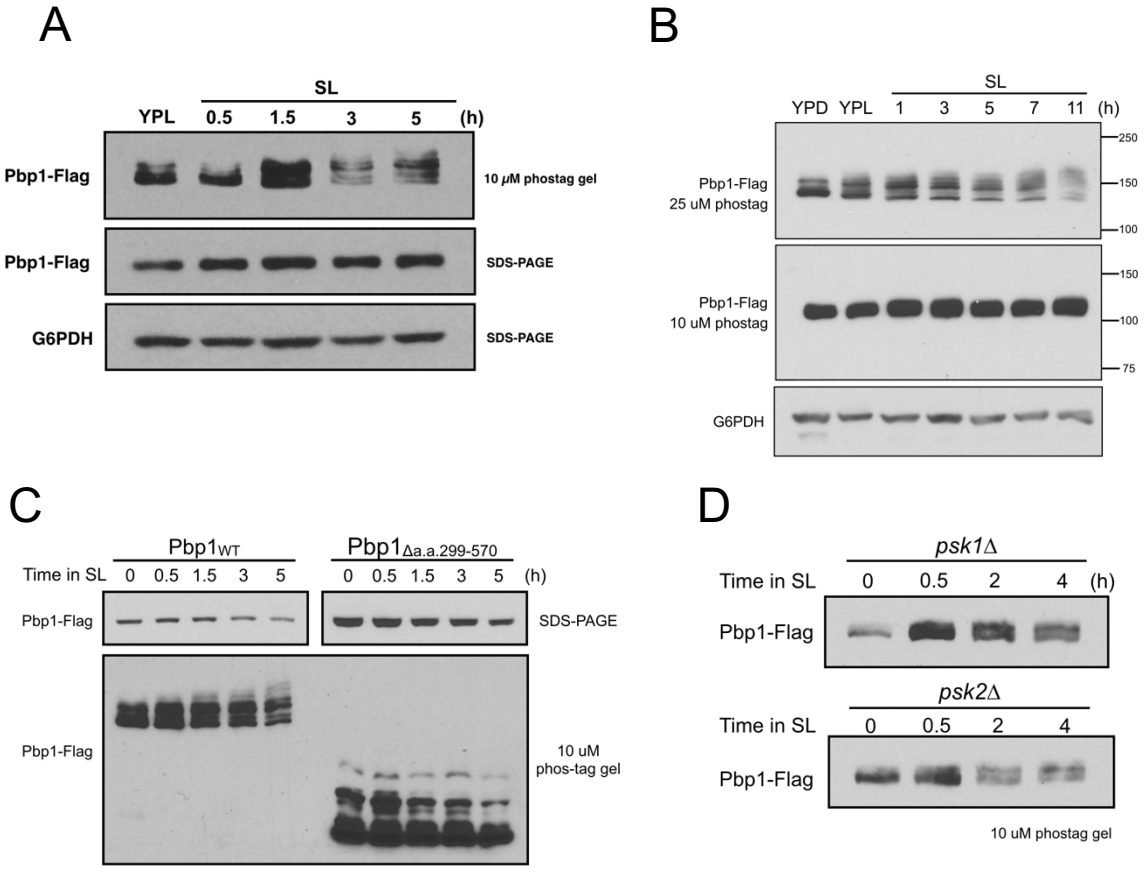

Figure 3-26. Phosphorylation of Pbp1 is gradually increased in SL medium.

Phosphorylation of endogenously tagged Pbp1 at the indicated time points before and after switch to SL medium. Phosphorylated species exhibit reduced migration. (A) Cell extracts were analyzed using SDS-PAGE with or without 10 uM phostag. Note the increase of slower migrating species over time in SL medium. (B) Cell extracts were analyzed using SDS-PAGE with 10 or 25 uM phostag. Higher phostag concentration resulted in further retarded migration, suggesting that Pbp1 is indeed phosphorylated. (C) The migration pattern of a Pbp1 mutant lacking a.a. 299-570 on SDS-PAGE did not change over time in SL medium, suggesting that the residues that became phosphorylated in SL medium are located within a.a. 299-570 of Pbp1. (D) Deletion of *PSK1* or *PSK2* did not affect Pbp1 phosphorylation.

A

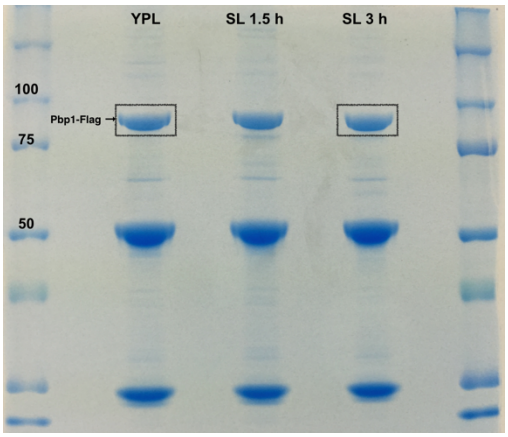

B

MKGNFRKRDS STNSRKGGNS DSNYTNGGVP NQNNSSMFYE NPEITRNFDD RQDYLLANSI GSDVTVTVTS GVKYTGLLVS CNLESTNGID VVLRFPRVAD
SGVSDSVDDL AKTLGETLLI HGEDVAELEL KNIDLSLDEK WENSKAQETT PARTNIEKER VNGESNEVTK FRTDVDISGS GREIKERKLE KWTPEEGAEH
FDINKGKALE DDSASWDQFA VNEKKFGVKS TFDEHLYTTK INKDDPNYSK RLQEAERIAK EIESQGTSGN IHIAEDRGII IDDSGLDEED LYSGVDRRGD
ELLAALKSNS KPNSNKGNRY VPPTLRQQPH HMDPAIISSS NSNKNENAVS TDTSTPAAAG APEGKPPQKT SKNKKSLSSK EAQIEELKKF SEKFKVPYDI
PKDMLEVLKR SSSTLKSNSS LPPKPISKTP SAKTVSPTTQ ISAGKSESRR SGSNISQGQS STGHTTRSST SLRRRNHGSF FGAKNPHTND AKRVLFGKSF
NMFIKSKEAH DEKKKGDDAS ENMEPFFIEK PYFTAPTWLN TIEESYKTFF PDEDTAIQEA QTRFQQRQLN SMGNAVPGMN PAMGMNMGGM MGFPMGGPSA
SPNPMMNGFA AGSMGMYMPF QPQPMFYHPS MPQMMPVMGS NGAEEGGGNI SPHVPAGFMA AGPGAPMGAF GYPGGIPFQG MMGSGPSGMP ANGSAMHSHG
HSRNYHQTSH HGHHNSSTSG HK

C

Protein Size	Protein Coverage	
722 a.a. (78732.09 Da)	531 a.a.	**73.55%**

Figure 3-27. Mass spectrometry analysis of Pbp1 immunoprecipitated from cells grown in YPL or SL medium.

(A) Pbp1-Flag were immunoprecipitated from cells grown in YPL or SL for indicated time and separated using SDS-PAGE. Pbp1-Flag proteins were visualized using Coomassie blue staining, and the target protein bands (Pbp1 pulled down from YPL and SL 3h cell extracts) were cut and phosphorylation on Pbp1 was analyzed using mass spectrometry by Taplin Mass Spectrometry Facility at Harvard Medical School (B) The protein sequence covered by identified peptides of Pbp1. Pbp1 was digested using trypsin. Note that the C-terminal region of Pbp1 was not covered due to lack of trypsin digestion sites. (C) The percentage of Pbp1 sequence covered in this experiment.

A

Residues phosphorylated in YPL

```
1   MKGNFRKRDS STNSRKGGNS DSNYTNGGVP NQNNSSMFYE NPEITRNFDD RQDYLLANSI GSDVTVTVTS
71  GVKYTGLLVS CNLESTNGID VVLRFPRVAD SGVSDSVDDL AKTLGETLLI HGEDVAELEL KNIDLSLDEK
141 WENSKAQETT PARTNIEKER VNGESNEVTK FRTDVDISGS GREIKERKLE KWTPEEGAEH FDINKGKALE
211 DDSASWDQFA VNEKKFGVKS TFDEHLYTTK INKDDPNYSK RLQEAERIAK EIESQGTSGN IHIAEDRGII
281 IDDSGLDEED LYSGVDRRGD ELLAALKSNS KPNSNKGNRY VPPTLRQQPH HMDPAIISSS NSNKNENAVS
351 TDTSTPAAAG APEGKPPQKT SKNKKSLSSK EAQIEELKKF SEKFKVPYDI PKDMLEVLKR SSSTLKSNSS
421 LPPKPISKTP SAKTVSPTTQ ISAGKSESRR SGSNISQGQS STGHTTRSST SLRRRNHGSF FGAKNPHTND
491 AKRVLFGKSF NMFIKSKEAH DEKKKGDDAS ENMEPFFIEK PYFTAPTWLN TIEESYKTFF PDEDTAIQEA
561 QTRFQQRQLN SMGNAVPGMN PAMGMNMGGM MGFPMGGPSA SPNPMMNGFA AGSMGMYMPF QPQPMFYHPS
631 MPQMMPVMGS NGAEEGGGNI SPHVPAGFMA AGPGAPMGAF GYPGGIPFQG MMGSGPSGMP ANGSAMHSHG
701 HSRNYHQTSH HGHHNSSTSG HK
```

B

Residues phosphorylated in SL

```
1   MKGNFRKRDS STNSRKGGNS DSNYTNGGVP NQNNSSMFYE NPEITRNFDD RQDYLLANSI GSDVTVTVTS
71  GVKYTGLLVS CNLESTNGID VVLRFPRVAD SGVSDSVDDL AKTLGETLLI HGEDVAELEL KNIDLSLDEK
141 WENSKAQETT PARTNIEKER VNGESNEVTK FRTDVDISGS GREIKERKLE KWTPEEGAEH FDINKGKALE
211 DDSASWDQFA VNEKKFGVKS TFDEHLYTTK INKDDPNYSK RLQEAERIAK EIESQGTSGN IHIAEDRGII
281 IDDSGLDEED LYSGVDRRGD ELLAALKSNS KPNSNKGNRY VPPTLRQQPH HMDPAIISSS NSNKNENAVS
351 TDTSTPAAAG APEGKPPQKT SKNKKSLSSK EAQIEELKKF SEKFKVPYDI PKDMLEVLKR SSSTLKSNSS
421 LPPKPISKTP SAKTVSPTTQ ISAGKSESRR SGSNISQGQS STGHTTRSST SLRRRNHGSF FGAKNPHTND
491 AKRVLFGKSF NMFIKSKEAH DEKKKGDDAS ENMEPFFIEK PYFTAPTWLN TIEESYKTFF PDEDTAIQEA
561 QTRFQQRQLN SMGNAVPGMN PAMGMNMGGM MGFPMGGPSA SPNPMMNGFA AGSMGMYMPF QPQPMFYHPS
631 MPQMMPVMGS NGAEEGGGNI SPHVPAGFMA AGPGAPMGAF GYPGGIPFQG MMGSGPSGMP ANGSAMHSHG
701 HSRNYHQTSH HGHHNSSTSG HK
```

Figure 3-28. Pbp1 phosphorylation sites identified by mass spectrometry.

(A) Red highlighted are the residues that were phosphorylated in cells grown in YPL medium. (B) Blue highlighted are the residues that were phosphorylated in cells grown in SL medium for 3 h.

Phosphorylation sites collected from literatures

```
1   MKGNFRKRDS STNSRKGGNS DSNYTNGGVP NQNNSSMFYE NPEITRNFDD RQDYLLANSI GSDVTVTVTS
71  GVKYTGLLVS CNLESTNGID VVLRFPRVAD SGVSDSVDDL AKTLGETLLI HGEDVAELEL KNIDLSLDEK
141 WENSKAQETT PARTNIEKER VNGESNEVTK FRTDVDISGS GREIKERKLE KWTPEEGAEH FDINKGKALE
211 DDSASWDQFA VNEKKFGVKS TFDEHLYTTK INKDDPNYSK RLQEAERIAK EIESQGTSGN IHIAEDRGII
281 IDDSGLDEED LYSGVDRRGD ELLAALKSNS KPNSNKGNRY VPPTLRQQPH HMDPAIISSS NSNKNENAVS
351 TDTSTPAAAG APEGKPPQKT SKNKKSLSSK EAQIEELKKF SEKFKVPYDI PKDMLEVLKR SSSTLKSNSS
421 LPPKPISKTP SAKTVSPTTQ ISAGKSESRR SGSNISQGQS STGHTTRSST SLRRRNHGSF FGAKNPHTND
491 AKRVLFGKSF NMFIKSKEAH DEKKKGDDAS ENMEPFFIEK PYFTAPTWLN TIEESYKTFF PDEDTAIQEA
561 QTRFQQRQLN SMGNAVPGMN PAMGMNMGGM MGFPMGGPSA SPNPMMNGFA AGSMGMYMPF QPQPMFYHPS
631 MPQMMPVMGS NGAEEGGGNI SPHVPAGFMA AGPGAPMGAF GYPGGIPFQG MMGSGPSGMP ANGSAMHSHG
701 HSRNYHQTSH HGHHNSSTSG HK
```

Figure 3-29. Pbp1 phosphorylation sites collected from literature.

Orange highlighted are residues reported to be phosphorylated in YPD medium under various treatments. (http://thebiogrid.org/33430/summary/saccharomyces-cerevisiae/pbp1.html)

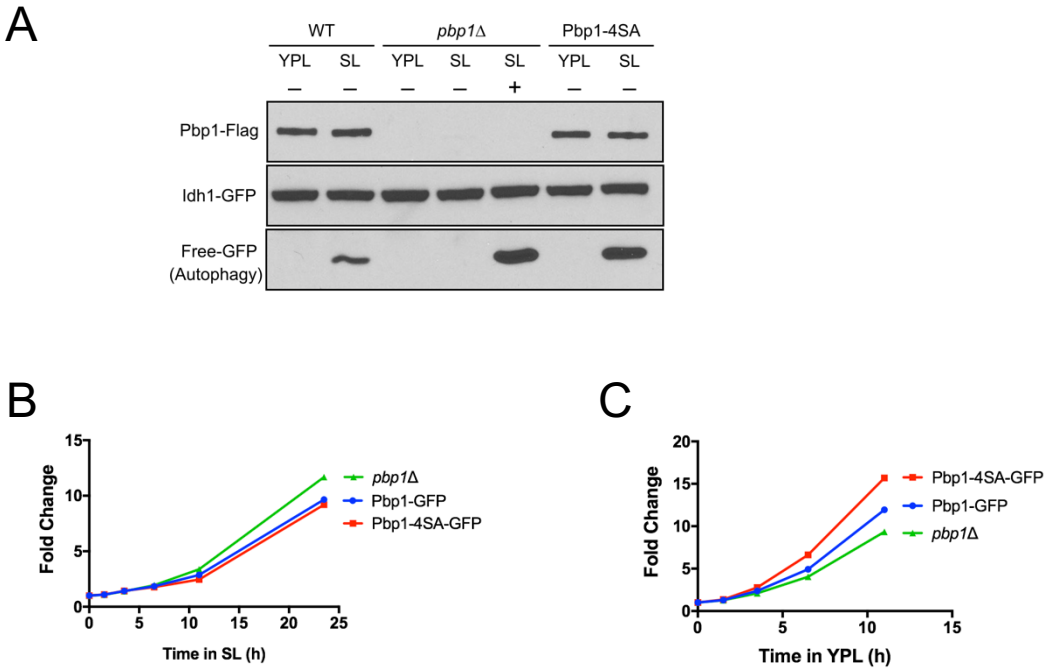

Figure 3-30. Cells expressing Pbp1-4SA variant had normal autophagy and growth in SL medium but exhibited increased growth rate in YPL medium.

(A) GFP cleavage assay reflecting autophagy amounts in cells expressing Pbp1 variant harboring 4 serine to alanine substitutions (S442A, S451A, S453A, S455A)(Pbp1-4SA). Pbp1-4SA is able to induce autophagy in SL medium. (B)(C) Growth of WT (Pbp1-GFP), *pbp1*Δ, and Pbp1-4SA-expressing cells in SL (B) and YPL medium (C). Pbp1-4SA-GFP cells exhibited comparable cell growth to WT in SL medium and increased growth rate in YPL medium. Data were mean ± s.d. from 3 independent experiments.

CHAPTER FOUR :

THE PHYSIOLOGICAL ROLE OF PBP1

PBP1 IS CRITICAL FOR MAINTAINING CELLULAR FITNESS AND MITOCHONDRIAL FUNCTION

Introduction

In response to variable environmental conditions, cells are able to utilize mitochondria in one of two metabolic states. In the presence of fermentable carbon sources, yeast cells utilize mitochondria for biosynthetic purposes useful for the de novo production of purines, pyrimidines, glutamate, glutamine, nicotinamide adenine dinucleotide (NAD^+) and other nitrogenous metabolites (Chen et al., 2017; Laxman et al., 2014). Under conditions of limiting carbon source, yeast mitochondria instead adopt a state of intense respiration wherein molecular oxygen is burned for the purpose of ATP production. Under conditions of intense respiration, the mitochondrial pathways normally used for de novo biosynthetic reactions are compromised. Under such respiratory conditions, the target of rapamycin (TOR) pathway must be carefully regulated between growth and autophagic states (Chen et al., 2017). Autophagy in cells undergoing intense respiration, by allowing for the hydrolysis and re-cycling of pre-existing macromolecules, facilitates production of metabolites that would otherwise be synthesized de novo in the mitochondria of cells growing in a nutrient-rich environment.

In the second paper we submitted (Kato et al., 2018), we report evidence that the methionine residues conspicuous of the LC domain of Pbp1 may represent redox sensors that facilitate a molecular connection between mitochondria and TORC1. These residues are oxidized in both test tube reactions and living cells upon exposure to low concentrations of hydrogen peroxide (H_2O_2). Methionine oxidation is shown to reverse phase separation of the Pbp1_LC. Oxidation is, moreover, relatively protected in a conformationally ordered sub-region of the Pbp1_LC that facilitates assembly of the protein into labile, cross-β polymers. Finally, H_2O_2-mediated melting of Pbp1 phase separated droplets is reversed by enzymatic reduction of methionine oxidation via a coupled, electron reduction circuit dependent upon two methionine sulfoxide reductase enzymes, thioredoxin, thioredoxin reductase, and NADPH.

In this chapter, I will discuss the *in vivo*, mitochondria-related phenotypes resulting from Pbp1 deletion. I will also demonstrate that these mitochondrial dysfunctions were due to dysregulation of TORC1 signaling rather than solely loss of autophagy or mitophagy. After prolonged nutritional stress, mutants lacking Pbp1 developed many aspects of mitochondrial dysfunction and became more sensitive to either hydrogen peroxide or mitochondrial poison Antimycin A or potassium cyanide. Pbp1 methionine mutants that were shown to be resistant to oxidization *in vitro* exhibit gain of function *in vivo*, indicating that Pbp1 functions as a redox sensor that properly synchronizes cell physiology to the metabolic state of mitochondria.

Results

Pbp1 exhibits peri-mitochondrial localization

Both full-length Pbp1 and Pbp1_LC alone localize proximal to mitochondria

In chapter three, I described that I used a mitochondrial DsRed marker to investigate the spatial relationship between Pbp1 and mitochondria. I observed that Pbp1 appeared to be proximal, but exclusive of the mitochondria (Figure 3-3), and this pattern did not change within the time observed (Figure 4-1A). Three-dimensional reconstruction of Pbp1 and mitochondria images further demonstrated the spatial correlation between Pbp1 condensates and mitochondria (Figure 4-1B). Therefore, the C-terminal LC region of Pbp1 may enable the protein to form a nebulous condensate proximal to the mitochondria. In contrast, when the C-terminal LC region was deleted, this Pbp1ΔLC mutant became more uniformly distributed throughout the cytosol (Figure 3-15). When the C-terminal LC region of Pbp1 was expressed alone in cells, I observed that it formed punctate-like structures localized proximal to mitochondria regardless of the culture condition (Figure 4-2). It is worth mentioning that the protein level of Pbp1_LC alone was extremely low, requiring 2 second excitation time under microscope to better visualize its localization compared to < 0.3 seconds for WT. In addition, the punctate-like structures formed by Pbp1_LC-GFP appear very unstable as Pbp1_LC-GFP becomes homogeneous in about 0.5 – 1 min under coverslip or if the cells were pelleted down before imaging.

Taken together, these results suggest that the C-terminal LC region of Pbp1 may enable the protein to form a nebulous condensate proximal to the mitochondria. The LC region alone

seems to be the key for bringing the entire protein proximal to mitochondria. However, sequence analysis did not show any predicted mitochondrial targeting signal in Pbp1_LC. Therefore, how Pbp1_LC localizes near the mitochondria remains to be determined. One possibility is that Pbp1_LC interacts with protein(s) residing in the mitochondrial outer membrane. Immunoprecipitation to identify the interacting proteins of Pbp1_LC may provide useful insights.

Pbp1 is critical for maintaining mitochondrial homeostasis

pbp1Δ cells produced significantly more petites after a prolonged period in stationary phase.

Cells lacking Pbp1 bypass autophagy and continue to grow inappropriately under conditions that require mitochondrial respiration. To investigate the physiological consequences of loss of Pbp1, I grew WT and *pbp1*Δ cells in SL medium to stationary phase as a means of chronic nutritional stress. After a prolonged period in stationary phase, *pbp1*Δ cells exhibited reduced survivability compared to WT (Figure 4-3A). Moreover, *pbp1*Δ cells produced significantly more petites (Figure 4-3B), suggesting that many cells gradually lost mitochondrial respiratory function. It thus appears that mitochondrial dysfunction and cell death may emerge due to loss of Pbp1 following prolonged metabolic or nutritional stress, or as a function of age. Consistent with this idea, the abundance of Pbp1 appears to decrease substantially in replicatively aged cells (Janssens et al., 2015). Pbp1 may therefore sense respiratory status and mitochondrial dysfunction to properly modulate TORC1 signaling.

pbp1Δ cells are more sensitive to mitochondrial respiratory poisons

To investigate whether *pbp1*Δ cells have a different response to mitochondrial stressors due to loss of mitochondrial function, I performed the disc diffusion susceptibility assay. *pbp1*Δ cells showed a larger zone of inhibition induced by both H_2O_2 and Antimycin A, an inhibitor of mitochondrial electron transport chain complex III, compared to that of WT (Figure 4-4). These results suggest that *pbp1*Δ cells became more sensitive to mitochondrial poisons after long term. To further test whether this phenotype is due to loss of autophagy, I conducted the same experiment with an *atg1*Δ mutant which cannot induce autophagy but has normal TORC1 activity. Interestingly, *atg1*Δ showed a zone of inhibition more similar to WT, suggesting that these phenotypes are more due to the dysregulation of TORC1 rather than the loss of autophagy.

pbp1Δ cells showed reduced protein level of Cox2, a component of mitochondrial electron transport chain complex IV

To examine whether deletion of Pbp1 affects the level of mitochondria, I collected cells grown in YPL and various time points in SL medium and detected the protein level of two commonly used mitochondrial markers, Por1 (encoded by nuclear DNA) and Cox2 (encoded by mitochondrial DNA), in the cell extracts. *pbp1*Δ cells have comparable Por1 amounts to WT in both YPL and SL medium (Figure 4-5). Strikingly, *pbp1*Δ cells showed greatly reduced Cox2 level in both media (Figure 4-5). I also observed that WT cells grown in YPL have lower Cox2 level compared to that in SL (Figure 4-5), suggested a negative correlation between Cox2

level and TORC1 activity. Addition of rapamycin to WT cells grown in YPL increased Cox2 level to be comparable to that in SL (Figure 4-5). Therefore, the reduced protein level of Cox2 in *pbp1*Δ cells is likely a result of the hyperactive TORC1 signaling, particularly in the early time points after switching to SL.

The mitochondrial membrane potential in log-phase growing pbp1Δ cells is similar to WT

Since dysfunctional cytochrome c oxidase (complex IV) in the cells was reported to result in a compromised mitochondrial membrane potential (Lee et al., 2001), I examined the mitochondrial membrane potential in both WT and *pbp1*Δ cells by utilizing $DiOC_6$ (3,3'-dihexyloxacarbocyanine iodide), a green fluorescence dye that has been used to detect mitochondrial membrane potential in live cells. *pbp1*Δ cells show an indistinguishable intensity of $DiOC_6$ signal compared to WT at early time points in SL medium (Figure 4-6).

pbp1Δ cells seem to have up-regulated mitochondrial fission-fusion activity

I next tried to examine mitochondrial morphology by imaging GFP-tagged Om45, a mitochondrial outer membrane protein, in *pbp1*Δ cells at various time points after switching from YPL to SL medium. At early time points, *pbp1*Δ mutant cells seemed to have up-regulated mitochondrial fission-fusion activity in SL medium, but the overall difference was not significant (Figure 4-7). Live-cell imaging to continuously monitor the changes in mitochondrial morphology will be a better way to address this question.

Cells expressing Pbp1 variants harboring methionine to phenylalanine/tyrosine substitutions are more resistant to oxidation *in vitro*

Cells expressing Pbp1 M to F/Y mutants are more resistant to H_2O_2 and mitochondrial poisons in vivo

Cells lacking Pbp1 exhibit reduced fitness and survivability following nutritional stress. They also engender more "petite" colonies, indicative of mitochondrial dysfunction (Figure 4-3). In addition to H_2O_2, cells lacking Pbp1 were also hypersensitive to antimycin A, (Figure 4-4). These findings give evidence that Pbp1 senses mitochondrial activity to control the regulatory state of TORC1 in order to promote mitochondrial health.

In chapter three, I have discussed the importance of the methionine residues located in Pbp1 C-terminal LC region in autophagy regulation. To test the importance of these methionines in mitochondrial function, I performed the disc diffusion susceptibility assay on Pbp1 variants harboring methionine to serine, phenylalanine, or tyrosine mutations.

Cells expressing the Pbp1 variant harboring $M_{7\text{-}14}S$ exhibited increased sensitivity to H_2O_2 and antimycin A (Figure 4-8), comparable to cells lacking Pbp1 altogether. In stark contrast, yeast cells expressing the Pbp1 $M_{7\text{-}14}F$ or $M_{7\text{-}14}Y$ variant – compared with WT cells – were equally or slightly more resistant to oxidative or respiratory stress (Figure 4-8).

Pbp1 M to F/Y mutants form stronger condensates that may inhibit TORC1 more potently

Treatment of yeast cells with either H_2O_2, antimycin A, or cyanide each led to the inhibition of autophagy (Figure 4-9A), consistent with observations that TORC1 signaling is

normally activated in response to mitochondrial dysfunction (Khan et al., 2017; Liu and Butow, 2006).

However, expression of the $M_{7\text{-}14}F$ or $M_{7\text{-}14}Y$ variants of Pbp1 reduced the ability of these agents to block autophagy. Since these Pbp1 variants exhibited stronger self-association propensity and induced more autophagy (Figure 3-25), such condensates may inhibit TORC1 more potently owing to their increased resistance to oxidation-induced dissolution (Figure 4-9B).

Taken together, these observations reveal that Pbp1 not only senses H_2O_2 through key methionine residues within its LC domain as a proxy for mitochondrial dysfunction, but is also required to properly modulate TORC1 signaling for the cellular response to mitochondrial respiratory dysfunction.

Materials and Methods

Petite formation

Cells were grown in YPL and then switched to SL as described in chapter two. Cell growth in SL was constantly measured to monitor entry into stationary phase. After reaching stationary phase, ~350 cells were plated onto YPD plate at indicated time points, and grown at 30°C for 50 h. Cell size was analyzed using ImageJ.

Disc diffusion assay

Cells were grown in YPL and then switched to SL as described in chapter two. Cell growth in SL was constantly measured to monitor entry into stationary phase. At stationary phase, 5 OD of cells were plated onto SL plate. Grade 1 filter paper with 1 cm in diameter (Whatman) was placed onto the SL plate and 10 μl of H_2O_2 (1 M) or Antimycin A (200 μg/ml) was soaked into the filter paper. Cells were grown at 30°C for 48 h.

GFP cleavage assay with mitochondrial poisons

A mitochondrial matrix protein, Idh1, was tagged with GFP. When mitophagy is induced, this protein accumulates in the vacuole and is degraded. The more stable GFP is detected by immunoblotting with anti-GFP monoclonal antibody (Roche, clone 7.1 and 13.1) as semi-quantitative evidence for mitophagy (Kanki et al., 2009). Cells were collected at 6 h after switching from YPL to SL. H_2O_2, Antimycin A, or KCN were added to the SL medium at time 0 at indicated concentration.

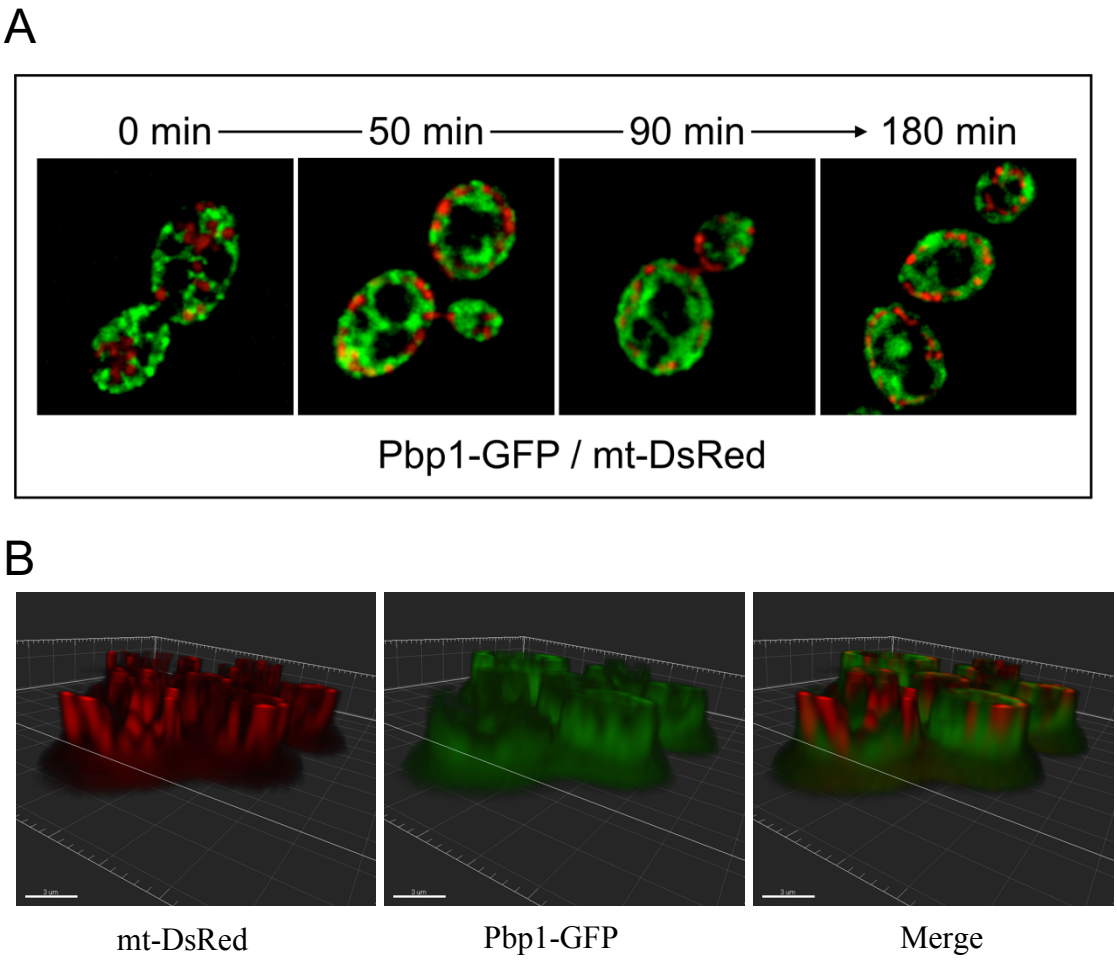

Figure 4-1. Pbp1 exhibits peri-mitochondrial localization.

(A) Images of Pbp1-GFP and mitochondria (Mito-DsRed) in cells switching from YPL to SL medium for the indicated time. Note that the localization of Pbp1 and mitochondria remain the same throughout the time overserved. (B) Three-dimensional reconstruction of Pbp1 and mitochondria images taken in the cells grown in SL medium.

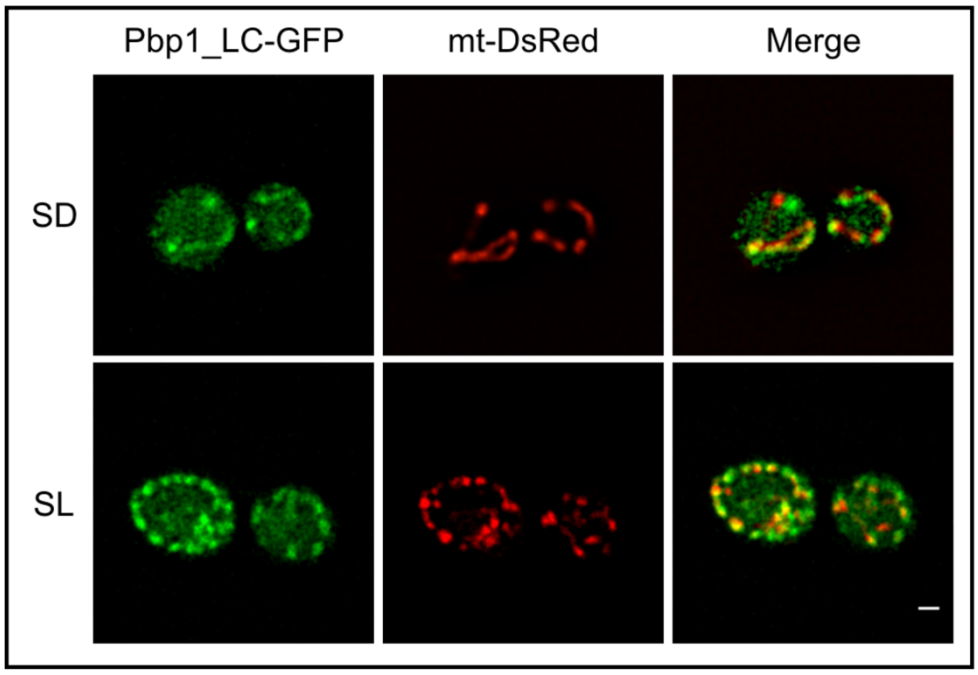

Figure 4-2. Pbp1_LC alone forms punctate-like structures and localizes proximal to mitochondria regardless of the culture medium.

Images of cells expressing Pbp1_LC-GFP at endogenous levels and the mitochondria-targeted RFP reporter (mt-DsRed) in SD and SL medium. Note that Pbp1_LC formed punctate-like structures that appear peri-mitochondrial in both media. Scale bar = 1 μm.

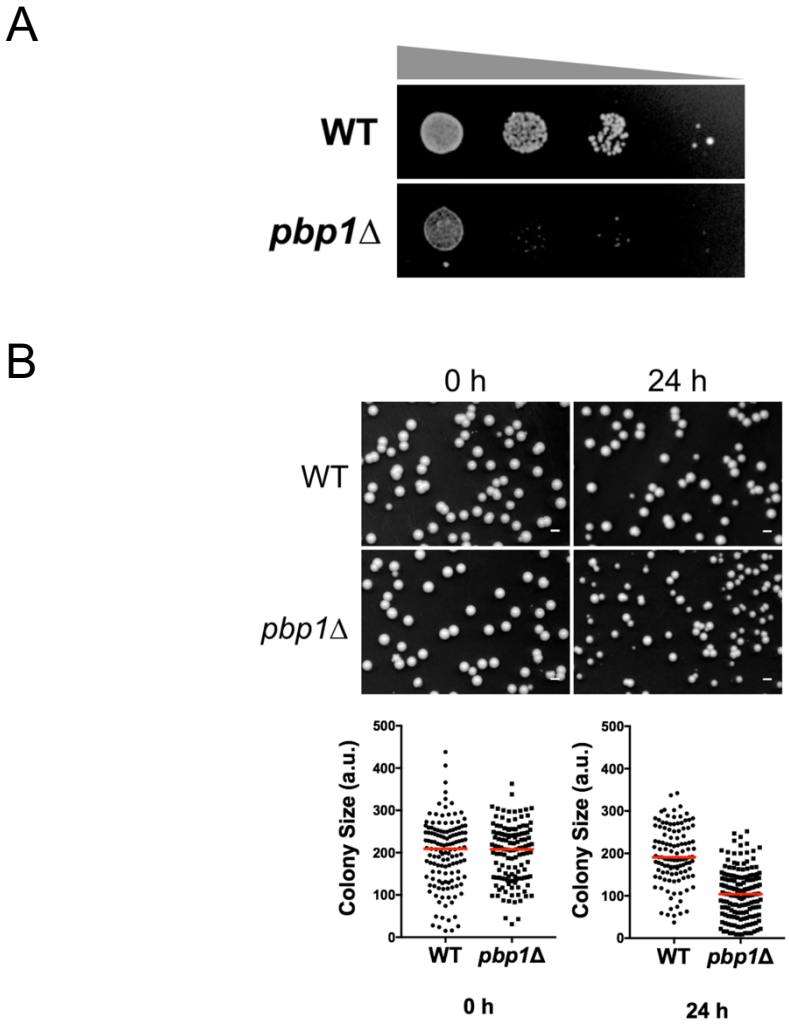

Figure 4-3. Pbp1 is important for maintaining cellular fitness and mitochondrial function.

(A) Spotting assay on SL plates showing the survivability of WT and *pbp1*Δ cells at 24 h after stationary phase. Note that *pbp1*Δ cells exhibited reduced survivability compared to WT. (B) *pbp1*Δ cells produced significantly more petites after a prolonged period in stationary phase. Cells were switched from YPL to SL medium, and grown to stationary phase. ~350 cells were plated onto YPD at indicated time points after entering stationary phase. Colony sizes were analyzed using ImageJ. Scale bar = 0.2 cm.

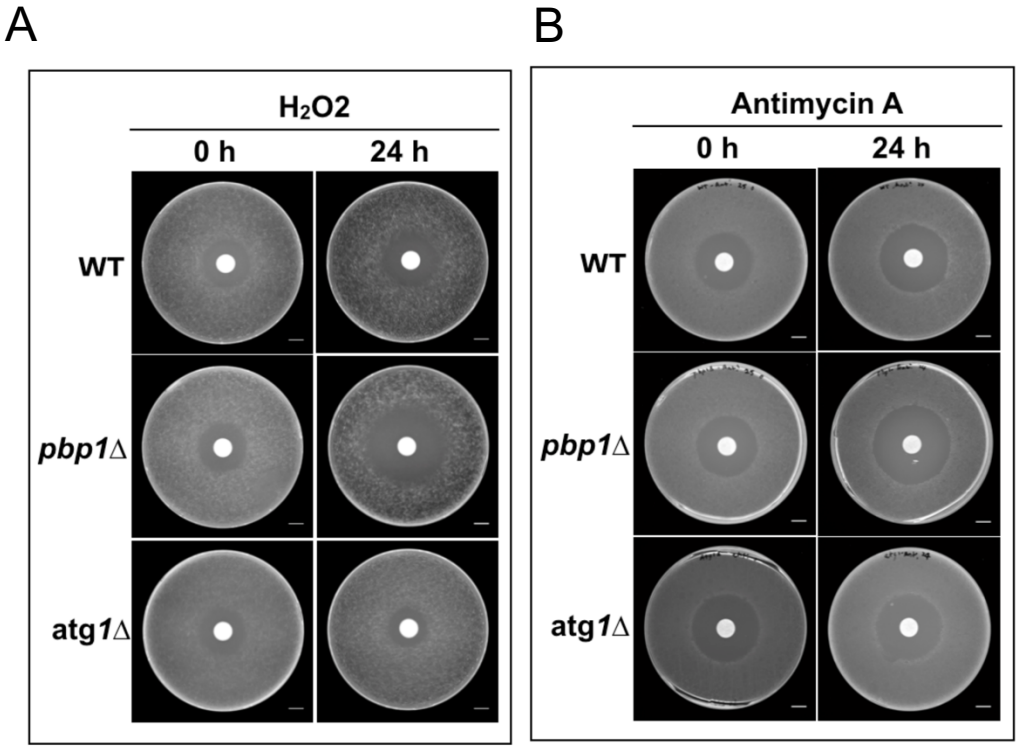

Figure 4-4. *pbp1*Δ cells are more sensitive to mitochondrial poisons.

Disc diffusion assay on SL plates showing the sensitivity of WT, *pbp1*Δ and *atg1*Δ cells to H_2O_2 (A) and Complex III inhibitor Antimycin A (B) at 0 h and 24 h after stationary phase. The indicated strains were grown in SL medium to stationary phase and then spread onto SL plates. A filter disc containing H_2O_2 or antimycin A was placed on top of the lawn, which was allowed to grow at 30°C for 48 h. Note that *pbp1*Δ cells were more sensitive to both mitochondrial poisons whereas *atg1*Δ cells were more similar to WT.

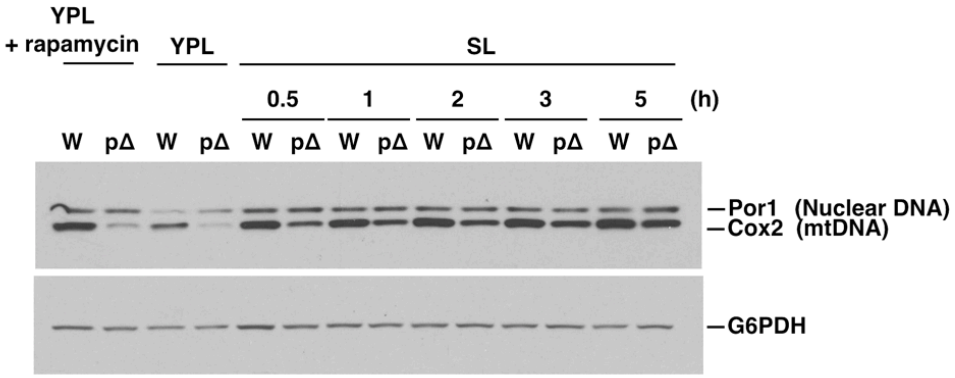

Figure 4-5. *pbp1*Δ cells have reduced Cox2 protein level.

Western Blot showing Por1 and Cox2 protein level in WT and *pbp1*Δ cells in YPL medium with or without rapamycin (200 ng/ml) and SL medium at indicated time points. pΔ: *pbp1*Δ.

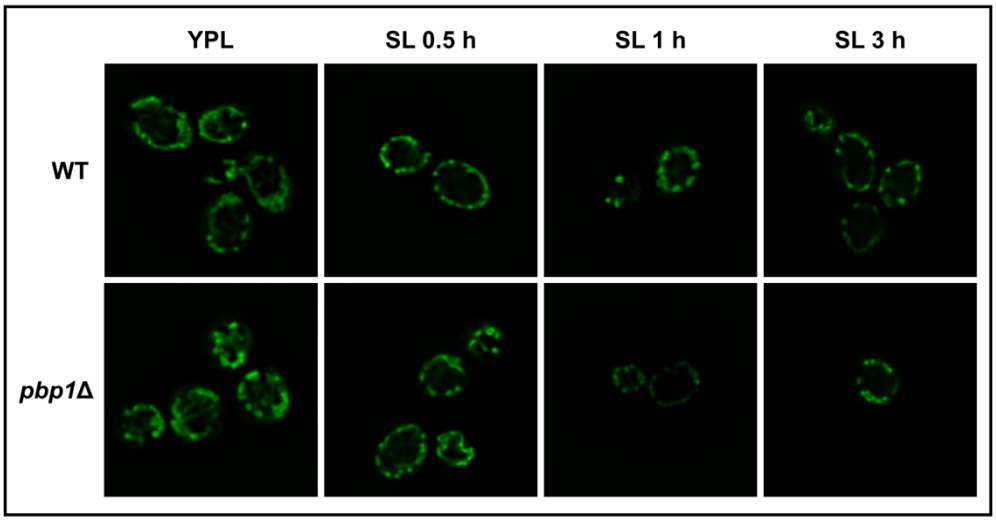

Figure 4-6. *pbp1*Δ cells have normal mitochondrial membrane potential in both YPL and SL medium.

Images of WT and *pbp1*Δ cells in YPL and SL medium stained with $DiOC_6$ as a measurement of mitochondrial membrane potential.

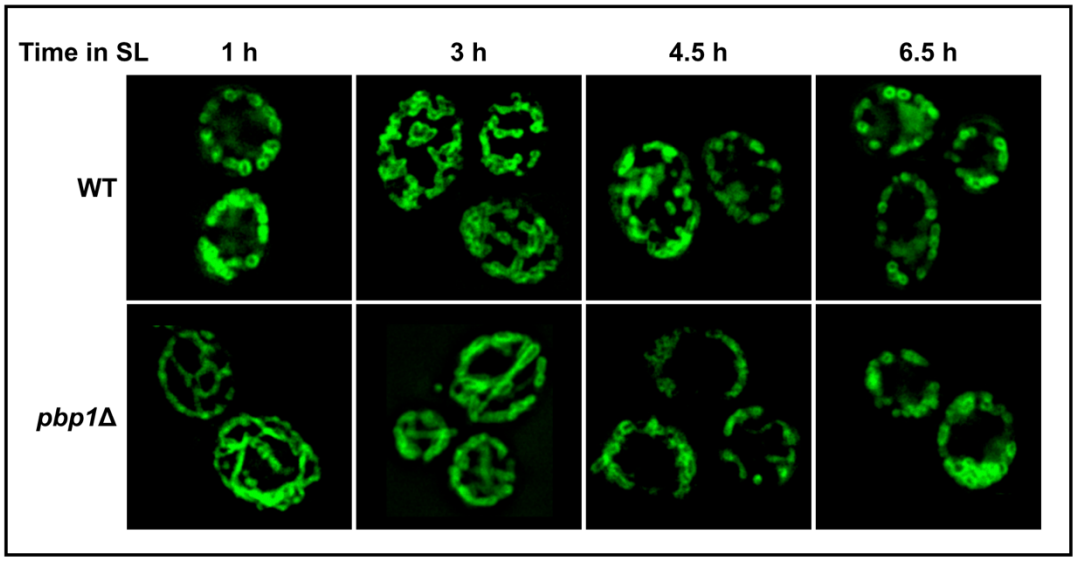

Figure 4-7. *pbp1*Δ cells seem to have up-regulated mitochondrial fission-fusion activity in early time points in SL medium.

Images of Om45-GFP (mitochondrial outer membrane) in WT and *pbp1*Δ cells in SL medium.

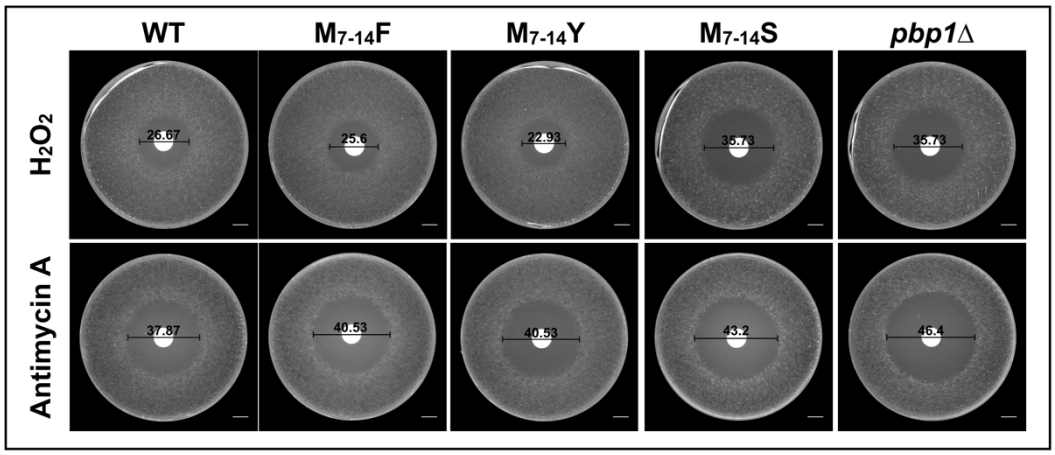

Figure 4-8. Cells expressing Pbp1 variants harboring methionine to phenylalanine or tyrosine mutations are more resistant to H_2O_2 or Antimycin A.

Loss of function variants of Pbp1 exhibit increased sensitivity to H_2O_2 and complex III inhibitor antimycin A. Strains expressing the indicated variants of Pbp1 were grown in SL medium to stationary phase and then spread onto SL plates. A filter disc containing H_2O_2 or antimycin A was placed on top of the lawn, which was allowed to grow at 30°C for 48 h. The numbers indicate the diameters (mm) of inhibition zones.

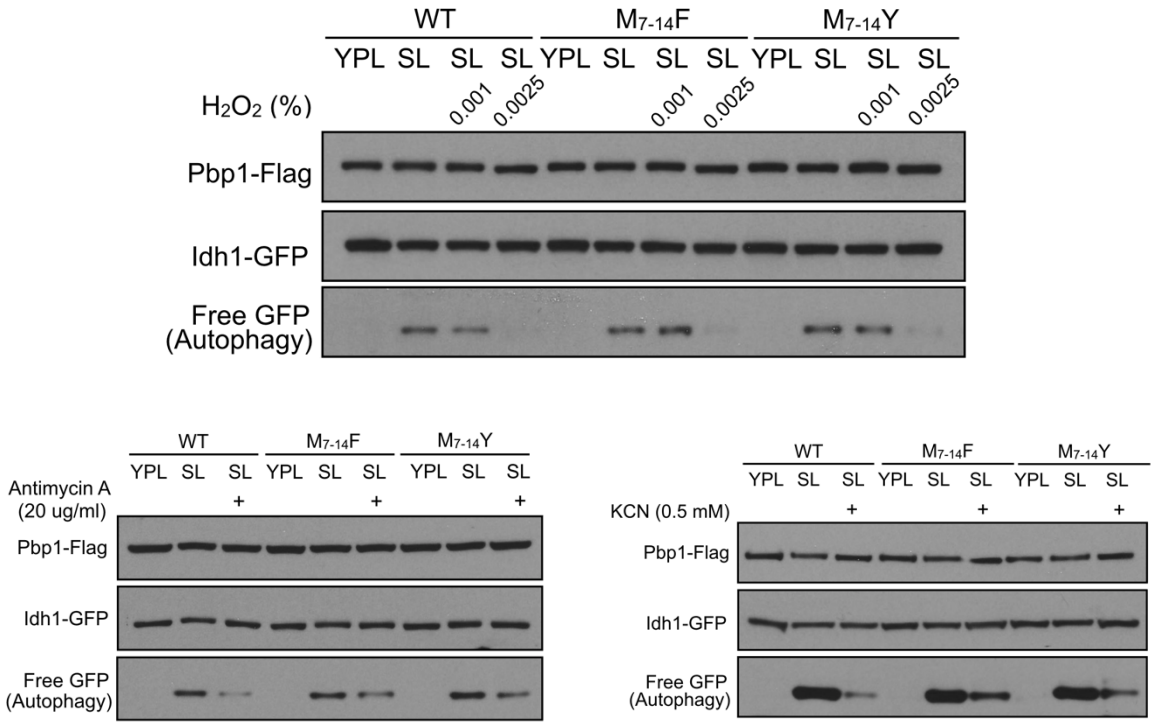

Figure 4-9. Cells expressing gain-of-function Pbp1 variants are more resistant to inhibition of autophagy by respiratory blockers.

(A) Modest concentrations of H_2O_2 inhibit autophagy. Cells expressing the indicated variants of full-length Pbp1-Flag were switched from YPL to SL medium for 6 h in the presence or absence of the indicated concentrations of H_2O_2. Autophagy was assayed by the GFP-cleavage assay. (B) Cells expressing gain-of-function $M_{7-14}F$, $M_{7-14}Y$ variants of Pbp1 are more resistant to inhibition of autophagy by respiratory blockers. Autophagy in the indicated strains was induced and assayed as described in chapter two, but in the presence or absence of the indicated concentrations of antimycin A or potassium cyanide. Note that both agents were less effective in blocking autophagy in strains expressing $M_{7-14}F$, $M_{7-14}Y$, consistent with the idea that they form more stable condensates which can more potently inhibit TORC1.

CHAPTER FIVE :

DISCUSSION AND CONCLUDING REMARKS

IDENTIFICATION OF THE FUNCTION OF PBP1 AND ITS MECHANISM OF ACTION

Pbp1 is a bona fide negative regulator of TORC1 signaling

In this study, we show that Pbp1 is a bona fide negative regulator of TORC1 signaling whose function becomes especially important when cells heavily utilize mitochondria for energy production. Loss of Pbp1function most prominently results in phenotypes associated with hyperactive TORC1 signaling, which include the inhibition of autophagy and increased anabolic metabolism due to promoting the biosynthetic functions of mitochondria (Chen et al., 2017). There has been a lack of clarity regarding the normal physiological function of Pbp1. Previous studies have implicated the protein in various aspects of RNA processing and as a component of stress granules (Buchan et al., 2008; Mangus et al., 1998; Swisher and Parker, 2010). However, during respiratory growth under physiological temperatures and expression levels, we find no evidence that Pbp1 forms discrete, punctate-like bodies that are typically associated with stress granules. Instead, it forms a more disperse condensate whose properties are dependent on the metabolic state.

When cells are growing in lactate, Pbp1 is almost exclusively in the pellet fraction and exhibits a more non-uniform localization throughout the cytosol. With the ability to associate with Kog1, this form of Pbp1 appears to be capable of inhibiting the TORC1 complex.

However, we further identified an unusual, methionine-rich low complexity region of Pbp1 that is also required for the inhibition of TORC1. This LC region readily phase separates to form droplets in vitro. Mutational analysis revealed a specific subset of methionine residues that weaken phase separation. Importantly, these same methionines are critical for inhibition of TORC1 and induction of autophagy *in vivo*. Taken together, our findings reveal how Pbp1 inhibits TORC1 through an unconventional mechanism involving phase separation. The C-terminal LC region enables Pbp1 to form an intracellular condensate, which is required for inhibiting TORC1 during respiratory growth. TORC1 still appears present at vacuoles in SL medium, but at reduced amounts compared to *pbp1*Δ cells (Figure 2-14), which is potentially consistent with a physical sequestration model of inhibition (Takahara and Maeda, 2012). However, since a portion of the protein outside of the C-terminal LC region mediates actual binding to TORC1 (Figure 2-18 and 2-19), we propose that an additional mechanism linked to phase separation of the LC region is required for the inhibition of TORC1, perhaps through modulation of distinct conformational or oligomeric states of TORC1 (Prouteau et al., 2017).

Pbp1 informs the function of mammalian ataxin-2

Ataxin-2 is the mammalian ortholog of yeast Pbp1. Polyglutamine expansions in ataxin-2 are linked to both ALS and spinocerebellar ataxia. However, just like yeast Pbp1, the normal physiological function of ataxin-2 remains unclear (Alves-Cruzeiro et al., 2016; Carmo-Silva et al., 2017; Lastres-Becker et al., 2008). Mutants lacking ataxin-2 have been constructed in multiple species and exhibit several phenotypes consistent with those reported here for Pbp1 as a negative regulator of TORC1. These include increased ribosomal protein amounts (Fittschen et al., 2015), and increased body size of dietary-restricted animals that is accompanied by more rapid animal development (Bar et al., 2016). In addition, ataxin-2 has been reported to cross-talk with disease-associated proteins such as C9orf72 and Gr2b (growth factor receptor bound protein 2), pointing to putative functions in autophagy and nutrient signaling (Drost et al., 2013; Sellier et al., 2016). Consistent with results herein, a recent report also demonstrates that a C-terminal intrinsically disordered region of ataxin-2 mediates the formation of RNP granules in Drosophila cells (Bakthavachalu et al., 2018). Our findings on the function and consequences of loss of Pbp1 in yeast suggest that compromising ataxin-2 function in neurons might result in mitochondrial dysfunction, energetic crisis, and eventually apoptosis, hallmarks that have all been linked to neurodegenerative disease (Nixon, 2013; Tatton and Olanow, 1999).

Pbp1 utilizes its methionine-rich low-complexity regions to respond to cellular redox states and regulate TORC1 signaling

Lastly, why might an intracellular condensate be required to regulate TORC1 specifically during respiratory growth? In addition to ATP synthesis, the mitochondria also play a key role in the biosynthesis of nitrogen-containing amino acids, which is promoted by activation of TORC1 (Chen et al., 2017; Laxman et al., 2014). An increased reliance on mitochondria for ATP synthesis leads to an increased dependency on inhibitors of TORC1 to toggle the mitochondria between ATP and biosynthesis modes in tune with the metabolic state or demands of the cell. Since cells lacking Pbp1 begin to exhibit mitochondrial dysfunction and reduced survivability following prolonged nutritional stress or as a function of age under respiratory conditions, we propose that Pbp1 specifically senses some aspect of mitochondrial activity or dysfunction to adjust TORC1 for purposes of sustaining mitochondrial health.

In the collaborative study, we show precisely how the methionine-rich LC region of Pbp1 senses hydrogen peroxide as a signal of mitochondrial dysfunction to subsequently modulate TORC1 signaling for metabolic adaptation (Kato et al., 2018). Unlike other LC domains studied to date, phase separated Pbp1 is solubilized upon exposure to low concentrations of hydrogen peroxide (H_2O_2). This phenomenon of liquid-like droplet dissolution was found to parallel H_2O_2-mediated oxidation of methionine residues as visualized by changes in Pbp1 protein migration on SDS polyacrylamide gels. Enzymatic reduction of the oxidized methionine residues, via two methionine sulfoxide reductase enzymes, thioredoxin, thioredoxin reductase and NADPH, allows reformation of liquid-like droplets. We thus offer that the LC region of Pbp1 utilizes methionine residues, instead

of tyrosine and/or phenylalanine residues prototypic of other LC domains, so that it can be converted back-and-forth between soluble and labile polymeric states in response to redox state.

In closing, our findings have revealed an unanticipated spatial organization and regulation of signaling and metabolism within the cell necessitated by mitochondrial respiration (Figure 5-1).

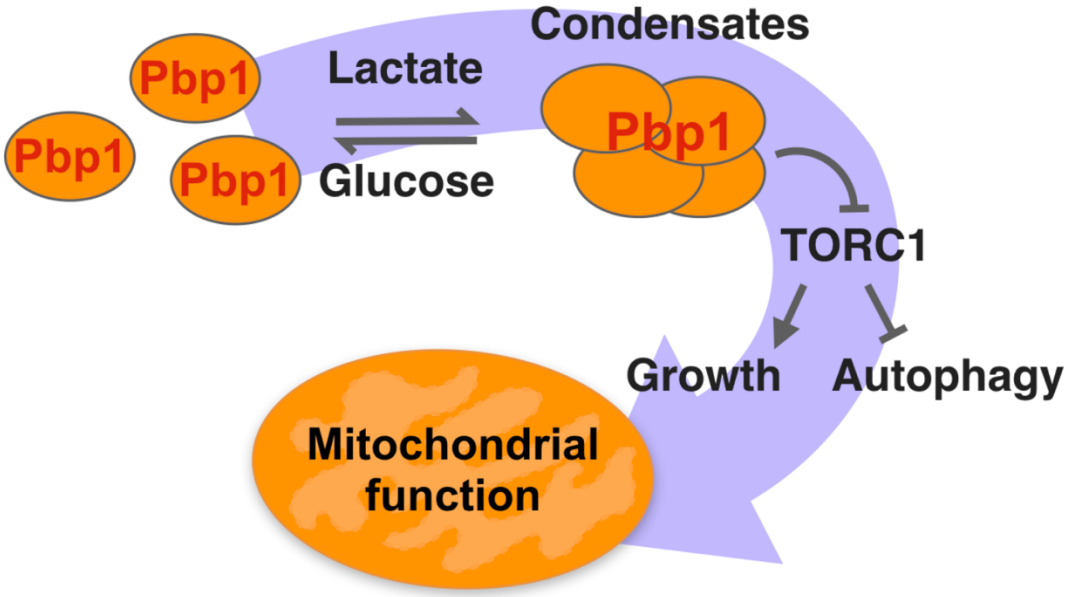

Figure 5-1. Pbp1 regulates TORC1 activity under respiratory condition through forming condensates in response to cellular redox states.

Pbp1 is a bona fide negative regulator of TOR. It functions through forming condensates that seem to surround the mitochondria. This regulation is especially critical when cells are utilizing mitochondria. Loss of function mutations profoundly alter metabolism and signaling. We proposed that these condensates might help the cell sense mitochondria-derived peroxide as a means to regulate TOR activity properly to help cells sustain mitochondrial health.

BIBLIOGRAPHY

Alves-Cruzeiro, J.M., Mendonca, L., Pereira de Almeida, L., and Nobrega, C. (2016). Motor Dysfunctions and Neuropathology in Mouse Models of Spinocerebellar Ataxia Type 2: A Comprehensive Review. Front Neurosci *10*, 572.

Ashburner, M., Ball, C.A., Blake, J.A., Botstein, D., Butler, H., Cherry, J.M., Davis, A.P., Dolinski, K., Dwight, S.S., Eppig, J.T.*, et al.* (2000). Gene ontology: tool for the unification of biology. The Gene Ontology Consortium. Nat Genet *25*, 25-29.

Astbury, W.T., Dickinson, S., and Bailey, K. (1935). The X-ray interpretation of denaturation and the structure of the seed globulins. Biochem J *29*, 2351-2360 2351.

Bakthavachalu, B., Huelsmeier, J., Sudhakaran, I.P., Hillebrand, J., Singh, A., Petrauskas, A., Thiagarajan, D., Sankaranarayanan, M., Mizoue, L., Anderson, E.N.*, et al.* (2018). RNP-Granule Assembly via Ataxin-2 Disordered Domains Is Required for Long-Term Memory and Neurodegeneration. Neuron *98*, 754-766 e754.

Banani, S.F., Lee, H.O., Hyman, A.A., and Rosen, M.K. (2017). Biomolecular condensates: organizers of cellular biochemistry. Nat Rev Mol Cell Biol *18*, 285-298.

Bar, D.Z., Charar, C., Dorfman, J., Yadid, T., Tafforeau, L., Lafontaine, D.L., and Gruenbaum, Y. (2016). Cell size and fat content of dietary-restricted Caenorhabditis elegans are regulated by ATX-2, an mTOR repressor. Proc Natl Acad Sci U S A *113*, E4620-4629.

Bar-Peled, L., Chantranupong, L., Cherniack, A.D., Chen, W.W., Ottina, K.A., Grabiner, B.C., Spear, E.D., Carter, S.L., Meyerson, M., and Sabatini, D.M. (2013). A Tumor suppressor complex with GAP activity for the Rag GTPases that signal amino acid sufficiency to mTORC1. Science *340*, 1100-1106.

Binda, M., Peli-Gulli, M.P., Bonfils, G., Panchaud, N., Urban, J., Sturgill, T.W., Loewith, R., and De Virgilio, C. (2009). The Vam6 GEF controls TORC1 by activating the EGO complex. Mol Cell *35*, 563-573.

Boguski, M.S., and McCormick, F. (1993). Proteins regulating Ras and its relatives. Nature *366*, 643-654.

Boland, B., Kumar, A., Lee, S., Platt, F.M., Wegiel, J., Yu, W.H., and Nixon, R.A. (2008). Autophagy induction and autophagosome clearance in neurons: relationship to autophagic pathology in Alzheimer's disease. J Neurosci *28*, 6926-6937.

Boyle, E.I., Weng, S., Gollub, J., Jin, H., Botstein, D., Cherry, J.M., and Sherlock, G. (2004). GO::TermFinder--open source software for accessing Gene Ontology information and finding significantly enriched Gene Ontology terms associated with a list of genes. Bioinformatics *20*, 3710-3715.

Buchan, J.R., Muhlrad, D., and Parker, R. (2008). P bodies promote stress granule assembly in Saccharomyces cerevisiae. J Cell Biol *183*, 441-455.

Carlson, M. (1999). Glucose repression in yeast. Curr Opin Microbiol *2*, 202-207.

Carmo-Silva, S., Nobrega, C., Pereira de Almeida, L., and Cavadas, C. (2017). Unraveling the Role of Ataxin-2 in Metabolism. Trends Endocrinol Metab *28*, 309-318.

Chen, J., Sutter, B.M., Shi, L., and Tu, B.P. (2017). GATOR1 regulates nitrogenic cataplerotic reactions of the mitochondrial TCA cycle. Nat Chem Biol *13*, 1179-1186.

Cleveland, D.W., Hwo, S.Y., and Kirschner, M.W. (1977). Physical and chemical properties of purified tau factor and the role of tau in microtubule assembly. J Mol Biol *116*, 227-247.

Cuervo, A.M. (2004). Autophagy: in sickness and in health. Trends Cell Biol *14*, 70-77.

DeMille, D., Badal, B.D., Evans, J.B., Mathis, A.D., Anderson, J.F., and Grose, J.H. (2015). PAS kinase is activated by direct SNF1-dependent phosphorylation and mediates inhibition of TORC1 through the phosphorylation and activation of Pbp1. Mol Biol Cell *26*, 569-582.

Dosztanyi, Z., Csizmok, V., Tompa, P., and Simon, I. (2005). IUPred: web server for the prediction of intrinsically unstructured regions of proteins based on estimated energy content. Bioinformatics *21*, 3433-3434.

Drost, J., Nonis, D., Eich, F., Leske, O., Damrath, E., Brunt, E.R., Lastres-Becker, I., Heumann, R., Nowock, J., and Auburger, G. (2013). Ataxin-2 modulates the levels of Grb2 and SRC but not ras signaling. J Mol Neurosci *51*, 68-81.

Elden, A.C., Kim, H.J., Hart, M.P., Chen-Plotkin, A.S., Johnson, B.S., Fang, X., Armakola, M., Geser, F., Greene, R., Lu, M.M*., et al.* (2010). Ataxin-2 intermediate-length polyglutamine expansions are associated with increased risk for ALS. Nature *466*, 1069-1075.

Fittschen, M., Lastres-Becker, I., Halbach, M.V., Damrath, E., Gispert, S., Azizov, M., Walter, M., Muller, S., and Auburger, G. (2015). Genetic ablation of ataxin-2 increases several global translation factors in their transcript abundance but decreases translation rate. Neurogenetics *16*, 181-192.

Gancedo, J.M. (1998). Yeast carbon catabolite repression. Microbiol Mol Biol Rev *62*, 334-361.

Gao, M., and Kaiser, C.A. (2006). A conserved GTPase-containing complex is required for intracellular sorting of the general amino-acid permease in yeast. Nat Cell Biol *8*, 657-667.

Geddes, A.J., Parker, K.D., Atkins, E.D., and Beighton, E. (1968). "Cross-beta" conformation in proteins. J Mol Biol *32*, 343-358.

Han, T.W., Kato, M., Xie, S., Wu, L.C., Mirzaei, H., Pei, J., Chen, M., Xie, Y., Allen, J., Xiao, G.*, et al.* (2012). Cell-free formation of RNA granules: bound RNAs identify features and components of cellular assemblies. Cell *149*, 768-779.

Harding, T.M., Morano, K.A., Scott, S.V., and Klionsky, D.J. (1995). Isolation and characterization of yeast mutants in the cytoplasm to vacuole protein targeting pathway. J Cell Biol *131*, 591-602.

Harrison, P.M., Chan, H.S., Prusiner, S.B., and Cohen, F.E. (2001). Conformational propagation with prion-like characteristics in a simple model of protein folding. Protein Sci *10*, 819-835.

Hetz, C., Thielen, P., Matus, S., Nassif, M., Court, F., Kiffin, R., Martinez, G., Cuervo, A.M., Brown, R.H., and Glimcher, L.H. (2009). XBP-1 deficiency in the nervous system protects against amyotrophic lateral sclerosis by increasing autophagy. Genes Dev *23*, 2294-2306.

Hirose, E., Nakashima, N., Sekiguchi, T., and Nishimoto, T. (1998). RagA is a functional homologue of S. cerevisiae Gtr1p involved in the Ran/Gsp1-GTPase pathway. J Cell Sci *111 (Pt 1)*, 11-21.

Iqbal, K., Grundke-Iqbal, I., Zaidi, T., Merz, P.A., Wen, G.Y., Shaikh, S.S., Wisniewski, H.M., Alafuzoff, I., and Winblad, B. (1986). Defective brain microtubule assembly in Alzheimer's disease. Lancet *2*, 421-426.

Jameson, L., Frey, T., Zeeberg, B., Dalldorf, F., and Caplow, M. (1980). Inhibition of microtubule assembly by phosphorylation of microtubule-associated proteins. Biochemistry *19*, 2472-2479.

Janssens, G.E., Meinema, A.C., Gonzalez, J., Wolters, J.C., Schmidt, A., Guryev, V., Bischoff, R., Wit, E.C., Veenhoff, L.M., and Heinemann, M. (2015). Protein biogenesis machinery is a driver of replicative aging in yeast. Elife *4*, e08527.

Johansen, T., and Lamark, T. (2011). Selective autophagy mediated by autophagic adapter proteins. Autophagy *7*, 279-296.

Kanki, T., Kang, D., and Klionsky, D.J. (2009). Monitoring mitophagy in yeast: the Om45-GFP processing assay. Autophagy *5*, 1186-1189.

Kato, M., Han, T.W., Xie, S., Shi, K., Du, X., Wu, L.C., Mirzaei, H., Goldsmith, E.J., Longgood, J., Pei, J.*, et al.* (2012). Cell-free formation of RNA granules: low complexity sequence domains form dynamic fibers within hydrogels. Cell *149*, 753-767.

Kato, M., Yang, Y.S., Sutter, B.M., McKnight, S.L., and Tu, B.P. (2018). Redox State Controls Phase Separation of the Methionine-rich Low Complexity Domain of Yeast Ataxin-2.

Khan, N.A., Nikkanen, J., Yatsuga, S., Jackson, C., Wang, L., Pradhan, S., Kivela, R., Pessia, A., Velagapudi, V., and Suomalainen, A. (2017). mTORC1 Regulates Mitochondrial Integrated Stress Response and Mitochondrial Myopathy Progression. Cell Metab *26*, 419-428 e415.

Klionsky, D.J. (2007). Autophagy: from phenomenology to molecular understanding in less than a decade. Nat Rev Mol Cell Biol *8*, 931-937.

Klionsky, D.J., Cregg, J.M., Dunn, W.A., Jr., Emr, S.D., Sakai, Y., Sandoval, I.V., Sibirny, A., Subramani, S., Thumm, M., Veenhuis, M.*, et al.* (2003). A unified nomenclature for yeast autophagy-related genes. Dev Cell *5*, 539-545.

Kroschwald, S., Maharana, S., Mateju, D., Malinovska, L., Nuske, E., Poser, I., Richter, D., and Alberti, S. (2015). Promiscuous interactions and protein disaggregases determine the material state of stress-inducible RNP granules. Elife *4*, e06807.

Lastres-Becker, I., Rub, U., and Auburger, G. (2008). Spinocerebellar ataxia 2 (SCA2). Cerebellum *7*, 115-124.

Laxman, S., Sutter, B.M., Shi, L., and Tu, B.P. (2014). Npr2 inhibits TORC1 to prevent inappropriate utilization of glutamine for biosynthesis of nitrogen-containing metabolites. Sci Signal *7*, ra120.

Laxman, S., Sutter, B.M., Wu, X., Kumar, S., Guo, X., Trudgian, D.C., Mirzaei, H., and Tu, B.P. (2013). Sulfur amino acids regulate translational capacity and metabolic homeostasis through modulation of tRNA thiolation. Cell *154*, 416-429.

Lee, C.D., and Tu, B.P. (2015). Glucose-Regulated Phosphorylation of the PUF Protein Puf3 Regulates the Translational Fate of Its Bound mRNAs and Association with RNA Granules. Cell Rep *11*, 1638-1650.

Lee, I., Bender, E., Arnold, S., and Kadenbach, B. (2001). New control of mitochondrial membrane potential and ROS formation--a hypothesis. Biol Chem *382*, 1629-1636.

Lee, S., Lim, W.A., and Thorn, K.S. (2013). Improved blue, green, and red fluorescent protein tagging vectors for S. cerevisiae. PLoS One *8*, e67902.

Levine, B., and Klionsky, D.J. (2004). Development by self-digestion: molecular mechanisms and biological functions of autophagy. Dev Cell *6*, 463-477.

Levine, B., and Kroemer, G. (2008). Autophagy in the pathogenesis of disease. Cell *132*, 27-42.

Lin, Y., Currie, S.L., and Rosen, M.K. (2017). Intrinsically disordered sequences enable modulation of protein phase separation through distributed tyrosine motifs. J Biol Chem *292*, 19110-19120.

Lin, Y., Mori, E., Kato, M., Xiang, S., Wu, L., Kwon, I., and McKnight, S.L. (2016). Toxic PR Poly-Dipeptides Encoded by the C9orf72 Repeat Expansion Target LC Domain Polymers. Cell *167*, 789-802 e712.

Lin, Y., Protter, D.S., Rosen, M.K., and Parker, R. (2015). Formation and Maturation of Phase-Separated Liquid Droplets by RNA-Binding Proteins. Mol Cell *60*, 208-219.

Liu, Z., and Butow, R.A. (2006). Mitochondrial retrograde signaling. Annu Rev Genet *40*, 159-185.

Loewith, R., and Hall, M.N. (2011). Target of rapamycin (TOR) in nutrient signaling and growth control. Genetics *189*, 1177-1201.

Loewith, R., Jacinto, E., Wullschleger, S., Lorberg, A., Crespo, J.L., Bonenfant, D., Oppliger, W., Jenoe, P., and Hall, M.N. (2002). Two TOR complexes, only one of which is rapamycin sensitive, have distinct roles in cell growth control. Mol Cell *10*, 457-468.

Longtine, M.S., McKenzie, A., 3rd, Demarini, D.J., Shah, N.G., Wach, A., Brachat, A., Philippsen, P., and Pringle, J.R. (1998). Additional modules for versatile and economical PCR-based gene deletion and modification in Saccharomyces cerevisiae. Yeast *14*, 953-961.

Mangus, D.A., Amrani, N., and Jacobson, A. (1998). Pbp1p, a factor interacting with Saccharomyces cerevisiae poly(A)-binding protein, regulates polyadenylation. Mol Cell Biol *18*, 7383-7396.

Mangus, D.A., Evans, M.C., Agrin, N.S., Smith, M., Gongidi, P., and Jacobson, A. (2004a). Positive and negative regulation of poly(A) nuclease. Mol Cell Biol *24*, 5521-5533.

Mangus, D.A., Smith, M.M., McSweeney, J.M., and Jacobson, A. (2004b). Identification of factors regulating poly(A) tail synthesis and maturation. Mol Cell Biol *24*, 4196-4206.

Meijer, W.H., van der Klei, I.J., Veenhuis, M., and Kiel, J.A. (2007). ATG genes involved in non-selective autophagy are conserved from yeast to man, but the selective Cvt and pexophagy pathways also require organism-specific genes. Autophagy *3*, 106-116.

Metcalf, D.J., Garcia-Arencibia, M., Hochfeld, W.E., and Rubinsztein, D.C. (2012). Autophagy and misfolded proteins in neurodegeneration. Exp Neurol *238*, 22-28.

Mizushima, N., and Klionsky, D.J. (2007). Protein turnover via autophagy: implications for metabolism. Annu Rev Nutr *27*, 19-40.

Mizushima, N., Levine, B., Cuervo, A.M., and Klionsky, D.J. (2008). Autophagy fights disease through cellular self-digestion. Nature *451*, 1069-1075.

Molliex, A., Temirov, J., Lee, J., Coughlin, M., Kanagaraj, A.P., Kim, H.J., Mittag, T., and Taylor, J.P. (2015). Phase separation by low complexity domains promotes stress granule assembly and drives pathological fibrillization. Cell *163*, 123-133.

Monahan, Z., Ryan, V.H., Janke, A.M., Burke, K.A., Rhoads, S.N., Zerze, G.H., O'Meally, R., Dignon, G.L., Conicella, A.E., Zheng, W.*, et al.* (2017). Phosphorylation of the FUS low-complexity domain disrupts phase separation, aggregation, and toxicity. Embo J *36*, 2951-2967.

Murakami, T., Qamar, S., Lin, J.Q., Schierle, G.S., Rees, E., Miyashita, A., Costa, A.R., Dodd, R.B., Chan, F.T., Michel, C.H., *et al.* (2015). ALS/FTD Mutation-Induced Phase Transition of FUS Liquid Droplets and Reversible Hydrogels into Irreversible Hydrogels Impairs RNP Granule Function. Neuron *88*, 678-690.

Murray, D.T., Kato, M., Lin, Y., Thurber, K.R., Hung, I., McKnight, S.L., and Tycko, R. (2017). Structure of FUS Protein Fibrils and Its Relevance to Self-Assembly and Phase Separation of Low-Complexity Domains. Cell *171*, 615-627 e616.

Nakashima, N., Noguchi, E., and Nishimoto, T. (1999). Saccharomyces cerevisiae putative G protein, Gtr1p, which forms complexes with itself and a novel protein designated as Gtr2p, negatively regulates the Ran/Gsp1p G protein cycle through Gtr2p. Genetics *152*, 853-867.

Nakatogawa, H., Suzuki, K., Kamada, Y., and Ohsumi, Y. (2009). Dynamics and diversity in autophagy mechanisms: lessons from yeast. Nat Rev Mol Cell Biol *10*, 458-467.

Nixon, R.A. (2013). The role of autophagy in neurodegenerative disease. Nat Med *19*, 983-997.

Noda, T., Matsuura, A., Wada, Y., and Ohsumi, Y. (1995). Novel system for monitoring autophagy in the yeast Saccharomyces cerevisiae. Biochem Biophys Res Commun *210*, 126-132.

Nonhoff, U., Ralser, M., Welzel, F., Piccini, I., Balzereit, D., Yaspo, M.L., Lehrach, H., and Krobitsch, S. (2007). Ataxin-2 interacts with the DEAD/H-box RNA helicase DDX6 and interferes with P-bodies and stress granules. Mol Biol Cell *18*, 1385-1396.

Panchaud, N., Peli-Gulli, M.P., and De Virgilio, C. (2013). Amino acid deprivation inhibits TORC1 through a GTPase-activating protein complex for the Rag family GTPase Gtr1. Sci Signal *6*, ra42.

Patel, A., Lee, H.O., Jawerth, L., Maharana, S., Jahnel, M., Hein, M.Y., Stoynov, S., Mahamid, J., Saha, S., Franzmann, T.M., *et al.* (2015). A Liquid-to-Solid Phase Transition of the ALS Protein FUS Accelerated by Disease Mutation. Cell *162*, 1066-1077.

Prouteau, M., Desfosses, A., Sieben, C., Bourgoint, C., Lydia Mozaffari, N., Demurtas, D., Mitra, A.K., Guichard, P., Manley, S., and Loewith, R. (2017). TORC1 organized in inhibited domains (TOROIDs) regulate TORC1 activity. Nature *550*, 265-269.

Ralser, M., Albrecht, M., Nonhoff, U., Lengauer, T., Lehrach, H., and Krobitsch, S. (2005). An integrative approach to gain insights into the cellular function of human ataxin-2. J Mol Biol *346*, 203-214.

Ravikumar, B., Vacher, C., Berger, Z., Davies, J.E., Luo, S., Oroz, L.G., Scaravilli, F., Easton, D.F., Duden, R., O'Kane, C.J., *et al.* (2004). Inhibition of mTOR induces autophagy and reduces toxicity of polyglutamine expansions in fly and mouse models of Huntington disease. Nat Genet *36*, 585-595.

Reinke, A., Anderson, S., McCaffery, J.M., Yates, J., 3rd, Aronova, S., Chu, S., Fairclough, S., Iverson, C., Wedaman, K.P., and Powers, T. (2004). TOR complex 1 includes a novel component, Tco89p (YPL180w), and cooperates with Ssd1p to maintain cellular integrity in Saccharomyces cerevisiae. J Biol Chem *279*, 14752-14762.

Ribbeck, K., and Gorlich, D. (2002). The permeability barrier of nuclear pore complexes appears to operate via hydrophobic exclusion. Embo J *21*, 2664-2671.

Romero, C.M., Paez, M.S., Miranda, J.A., Hernandez, D.J., and Oviedo, L.E. (2007). Effect of temperature on the surface tension of diluted aqueous solutions of 1,2-hexanediol, 1,5-hexanediol, 1,6-hexanediol and 2,5-hexanediol (vol 258, pg 67, 2007). Fluid Phase Equilibr *260*, 359-359.

Rubinsztein, D.C., Gestwicki, J.E., Murphy, L.O., and Klionsky, D.J. (2007). Potential therapeutic applications of autophagy. Nat Rev Drug Discov *6*, 304-312.

Sarkar, S., Krishna, G., Imarisio, S., Saiki, S., O'Kane, C.J., and Rubinsztein, D.C. (2008). A rational mechanism for combination treatment of Huntington's disease using lithium and rapamycin. Hum Mol Genet *17*, 170-178.

Schurmann, A., Brauers, A., Massmann, S., Becker, W., and Joost, H.G. (1995). Cloning of a novel family of mammalian GTP-binding proteins (RagA, RagBs, RagB1) with remote similarity to the Ras-related GTPases. J Biol Chem *270*, 28982-28988.

Sekiguchi, T., Hirose, E., Nakashima, N., Ii, M., and Nishimoto, T. (2001). Novel G proteins, Rag C and Rag D, interact with GTP-binding proteins, Rag A and Rag B. J Biol Chem *276*, 7246-7257.

Sellier, C., Campanari, M.L., Julie Corbier, C., Gaucherot, A., Kolb-Cheynel, I., Oulad-Abdelghani, M., Ruffenach, F., Page, A., Ciura, S., Kabashi, E., *et al.* (2016). Loss of C9ORF72 impairs autophagy and synergizes with polyQ Ataxin-2 to induce motor neuron dysfunction and cell death. Embo J *35*, 1276-1297.

Sengupta, S., Peterson, T.R., and Sabatini, D.M. (2010). Regulation of the mTOR complex 1 pathway by nutrients, growth factors, and stress. Mol Cell *40*, 310-322.

Serpell, L. (2014). Amyloid structure. Essays Biochem *56*, 1-10.

Sheffield, P., Garrard, S., and Derewenda, Z. (1999). Overcoming expression and purification problems of RhoGDI using a family of "parallel" expression vectors. Protein Expr Purif *15*, 34-39.

Shi, K.Y., Mori, E., Nizami, Z.F., Lin, Y., Kato, M., Xiang, S., Wu, L.C., Ding, M., Yu, Y., Gall, J.G.*, et al.* (2017). Toxic PRn poly-dipeptides encoded by the C9orf72 repeat expansion block nuclear import and export. Proc Natl Acad Sci U S A *114*, E1111-E1117.

Shintani, T., and Klionsky, D.J. (2004). Autophagy in health and disease: a double-edged sword. Science *306*, 990-995.

Stolz, A., Ernst, A., and Dikic, I. (2014). Cargo recognition and trafficking in selective autophagy. Nat Cell Biol *16*, 495-501.

Sunde, M., and Blake, C. (1997). The structure of amyloid fibrils by electron microscopy and X-ray diffraction. Adv Protein Chem *50*, 123-159.

Sutter, B.M., Wu, X., Laxman, S., and Tu, B.P. (2013). Methionine inhibits autophagy and promotes growth by inducing the SAM-responsive methylation of PP2A. Cell *154*, 403-415.

Swisher, K.D., and Parker, R. (2010). Localization to, and effects of Pbp1, Pbp4, Lsm12, Dhh1, and Pab1 on stress granules in Saccharomyces cerevisiae. PLoS One *5*, e10006.

Takahara, T., Hara, K., Yonezawa, K., Sorimachi, H., and Maeda, T. (2006). Nutrient-dependent multimerization of the mammalian target of rapamycin through the N-terminal HEAT repeat region. J Biol Chem *281*, 28605-28614.

Takahara, T., and Maeda, T. (2012). Transient sequestration of TORC1 into stress granules during heat stress. Mol Cell *47*, 242-252.

Takeda, T., and Klimov, D.K. (2008). Temperature-induced dissociation of Abeta monomers from amyloid fibril. Biophys J *95*, 1758-1772.

Takeshige, K., Baba, M., Tsuboi, S., Noda, T., and Ohsumi, Y. (1992). Autophagy in yeast demonstrated with proteinase-deficient mutants and conditions for its induction. J Cell Biol *119*, 301-311.

Tatton, W.G., and Olanow, C.W. (1999). Apoptosis in neurodegenerative diseases: the role of mitochondria. Biochim Biophys Acta *1410*, 195-213.

Thumm, M., Egner, R., Koch, B., Schlumpberger, M., Straub, M., Veenhuis, M., and Wolf, D.H. (1994). Isolation of autophagocytosis mutants of Saccharomyces cerevisiae. FEBS Lett *349*, 275-280.

Tsukada, M., and Ohsumi, Y. (1993). Isolation and characterization of autophagy-defective mutants of Saccharomyces cerevisiae. FEBS Lett *333*, 169-174.

Vilchez, D., Saez, I., and Dillin, A. (2014). The role of protein clearance mechanisms in organismal ageing and age-related diseases. Nat Commun *5*, 5659.

Wang, J., Choi, J.M., Holehouse, A.S., Lee, H.O., Zhang, X., Jahnel, M., Maharana, S., Lemaitre, R., Pozniakovsky, A., Drechsel, D.*, et al.* (2018). A Molecular Grammar Governing the Driving Forces for Phase Separation of Prion-like RNA Binding Proteins. Cell *174*, 688-699 e616.

Wang, J.T., Smith, J., Chen, B.C., Schmidt, H., Rasoloson, D., Paix, A., Lambrus, B.G., Calidas, D., Betzig, E., and Seydoux, G. (2014). Regulation of RNA granule dynamics by phosphorylation of serine-rich, intrinsically disordered proteins in C. elegans. Elife *3*, e04591.

Wedaman, K.P., Reinke, A., Anderson, S., Yates, J., 3rd, McCaffery, J.M., and Powers, T. (2003). Tor kinases are in distinct membrane-associated protein complexes in Saccharomyces cerevisiae. Mol Biol Cell *14*, 1204-1220.

Wickner, R.B. (1994). [URE3] as an altered URE2 protein: evidence for a prion analog in Saccharomyces cerevisiae. Science *264*, 566-569.

Williams, A., Jahreiss, L., Sarkar, S., Saiki, S., Menzies, F.M., Ravikumar, B., and Rubinsztein, D.C. (2006). Aggregate-prone proteins are cleared from the cytosol by autophagy: therapeutic implications. Curr Top Dev Biol *76*, 89-101.

Wootton, J.C. (1994). Non-globular domains in protein sequences: automated segmentation using complexity measures. Comput Chem *18*, 269-285.

Wu, X., and Tu, B.P. (2011). Selective regulation of autophagy by the Iml1-Npr2-Npr3 complex in the absence of nitrogen starvation. Mol Biol Cell *22*, 4124-4133.

Xiang, S., Kato, M., Wu, L.C., Lin, Y., Ding, M., Zhang, Y., Yu, Y., and McKnight, S.L. (2015). The LC Domain of hnRNPA2 Adopts Similar Conformations in Hydrogel Polymers, Liquid-like Droplets, and Nuclei. Cell *163*, 829-839.

Xie, Z., and Klionsky, D.J. (2007). Autophagosome formation: core machinery and adaptations. Nat Cell Biol *9*, 1102-1109.

Zhang, X., Li, L., Chen, S., Yang, D., Wang, Y., Zhang, X., Wang, Z., and Le, W. (2011). Rapamycin treatment augments motor neuron degeneration in SOD1(G93A) mouse model of amyotrophic lateral sclerosis. Autophagy *7*, 412-425.